UNIVERSITÀ
DEGLI STUDI
FIRENZE

DOTTORATO DI RICERCA

INTERNATIONAL DOCTORATE IN STRUCTURAL BIOLOGY

CICLO XXXIV

COORDINATOR Prof. Lucia Banci

Production, structural and functional characterization of proteins involved in iron-sulfur cluster biogenesis and trafficking

Settore Scientifico Disciplinare CHIM/03

PhD student

Dott. Sara Matteucci

Tutor

Prof. Lucia Banci

Coordinator

Prof. Lucia Banci

November 2018 – October 2021

This thesis has been approved by the University of Florence, the University of Frankfurt and the Utrecht University

Universiteit Utrecht

INDEX

INTRODUCTION

1. INTRODUCTION

1.1. The role of iron in biological system

Out of the more than 100 chemical elements known to scientists today, only a relatively small number of them are present in the human body: oxygen, carbon, hydrogen and nitrogen constitute the majority of the body; while a few other elements are present at trace level.[1] Some of these are metal ions, such as copper, zinc, iron and manganese, which are essential for life[2]. Essential metal ions can also be toxic if present in excess or at reduced level[3]. Metals are involved in a wide range of biochemical processes in all living organism, they are the "key" players in electron transfer, oxygen transport and numerous catalytic reactions. The use of metals in living organism is mainly related to red-ox reactions and to the ability to catalyze essential functions such as hydrolysis.

Metals are involved also in a large amount of proteins, called metalloproteins. It is a generic term for the proteins that required metals to carry out their function. In metalloproteins, metal ions are usually coordinated by oxygen, sulfur, or nitrogen centers belonging to amino acid residues in the protein. The presence of the metal ion in metalloproteins allows them to take part in diverse biological processes.[4]

One of the most abundant essential trace elements in human body is iron. Nevertheless, it is necessary for our survival[5,6]. Organisms encode a large number of iron-containing proteins that are extensively involved in the respiratory chain. The bulk of iron is bound to hemoglobin in red blood cells, where it is necessary for oxygen transport in the blood. In addition to hemoglobin, other important proteins are the myoglobin and the cytochromes, which transfer electrons. Other class of iron bound proteins are those binding iron-sulfur clusters.[7] Fe-S cluster proteins utilize a group of ancient cofactors composed of iron and sulfur in different and interchangeable stoichiometry, which are usually ligated to cysteines of associated proteins.[8]

1.2. Type and function of ISCs

Iron sulfur clusters (ISCs) are ubiquitous protein cofactors highly conserved from bacteria to human.[9] Fe-S clusters are found in a variety of metalloproteins, such as the ferredoxins, as well as NADH dehydrogenase, hydrogenases and cytochrome C reductase. Fe-S clusters (ISCs) are best known for their role in the oxidation-reduction reactions of electron transport chain.[10]

In eukaryotic organism, the most common Fe-S clusters are composed by iron ions and inorganic sulfide (S^{2-}) ions. Also the rubredoxins, which contain only one iron atom per molecule and no inorganic sulfide, are classified as iron-sulfur proteins[11] (Fig. 1).

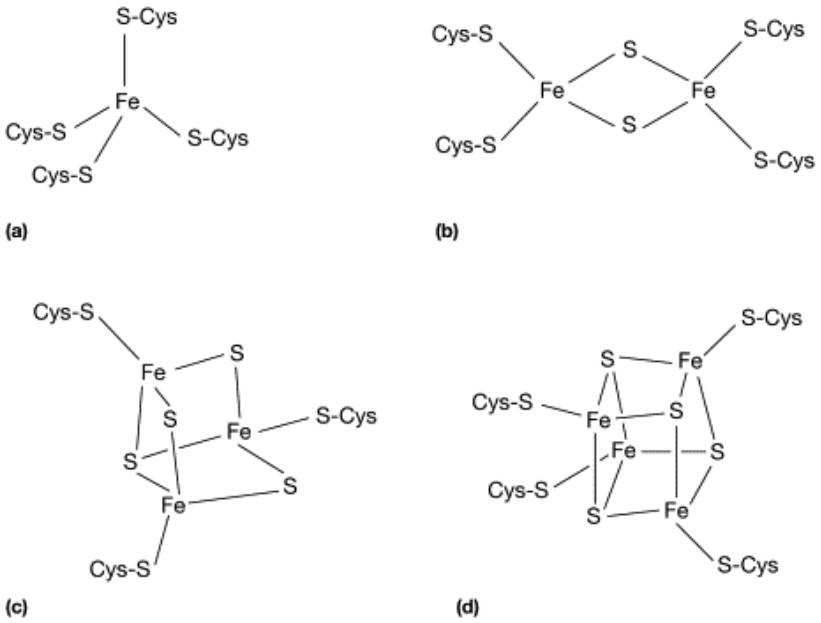

Fig. 1 – (a) rubredoxin cluster (b) [2Fe-2S] (c) [3Fe-4S] (d) [4Fe-4S]

The simplest and most common types of biological Fe–S clusters are [2Fe–2S], [3Fe–4S], and [4Fe–4S]. In each of them, the iron ions are coordinated by bridging sulfide ions (two or three) with the four-iron coordination completed by protein donor atoms, which in the majority of cases are cysteine. While this essentially always the case for the [4Fe-4S] clusters, in the case of [2Fe-2S] the coordinating residues can also be histidines (Rieske proteins). The [3Fe-4S] clusters have a geometry similar to that of [4Fe–4S] clusters, with one iron missing. In any type of cluster, only one electron is exchanged. The [2Fe-2S] clusters typically cycle between an oxidized diferric state ($2Fe^{3+}$) and a one electron reduced state (Fe^{2+} - Fe^{3+}) and the biological importance of iron is largely attributable to its chemical properties as a transition metal.[12] Among these classes of iron–sulfur clusters, the [4Fe–4S] clusters are the most versatile because they can exist in three different oxidation states: 3^+, 2^+, and 1^+. However, in any given protein, only one of the two oxidation–reduction pairs is used.

The $[4Fe–4S]^{2+}$ cluster contains two Fe^{2+} and two Fe^{3+} ions, which are manifest as two $Fe^{2.5+}$–$Fe^{2.5+}$ mixed-valence pairs due to valence delocalization. As a result of magnetic coupling between the two $Fe^{2.5+}$–$Fe^{2.5+}$ mixed-valence pairs, the net spin is zero and hence $[4Fe–4S]^{2+}$ clusters are diamagnetic. In the reduced state, the $[4Fe–4S]^{1+}$ cluster contains three Fe^{2+} ions and one Fe^{3+} ion, which are manifest as an equal-valence Fe^{2+}–Fe^{2+} pair and a mixed-valence $Fe^{2.5+}$–$Fe^{2.5+}$ pair. The paramagnetic coupling between the equal-valence Fe^{2+}–Fe^{2+} pair and the mixed-valence $Fe^{2.5+}$–$Fe^{2.5+}$ pair, the net spin is 1/2 and hence the $[4Fe–4S]^{1+}$ clusters are paramagnetic.

1.3. Biogenesis of ISCs

The most extensive studies about the biosynthesis of the ISCs, were focused on bacteria (*Escherichia Coli* and *Azetobacter vinelandii*) and on yeast *Saccharomyces cerevisiae*. Three different system were identified for the biogenesis of bacteria Fe-S proteins: the NIF system, for specific maturation of nitrogenase in azototrophic bacteria; the ISC assembly and the SUF system, that are present in parallel in some bacteria.[13] The biosynthesis of Fe-S clusters in eukaryotes takes place in mitochondria and as a model organism, the yeast *Saccharomyces cerevisiae* has been used. Thus, the mitochondrial ISC machinery for biosynthesis of cellular Fe-S cluster appears to be conserved in eukaryotes from bacteria. Three distinct protein machinery are required for the biogenesis: the ISC assembly machinery in mitochondria, the ISC export machinery and the cytosolic ISC assembly machinery (CIA machinery)[7]. The mitochondrial ISC machinery is required for the generation of all cellular Fe-S proteins, while the ISC export and the CIA machinery are involved in the maturation of cytosolic ISC proteins.

1.3.1. Mitochondrial ISC assembly machinery

The basic principle of mitochondrial Fe/S protein maturation is the synthesis of the Fe/S cluster on a scaffold protein before the cluster is transferred to apo proteins. The ISC biogenesis in mitochondria is comprised of two main steps, and the central component is the scaffold protein IscU on which *de novo* assembly of a Fe-S cluster takes place[14]. It has three cysteine residues, which are necessary for the [2Fe-2S] binding; however, the molecular mechanism is not yet fully understood. The cluster is transferred to glutaredoxin GLRX5[15], followed by the formation of mitochondrial [2Fe-2S] proteins, the synthesis of [4Fe-4S] clusters and their target-specific insertion into the recipient apo proteins. The GLRX5, BOLA3, and NFU1 proteins are part of a ISC assembly pathway leading to the synthesis of a [4Fe-4S] cluster on NFU1[16]. The [2Fe-2S] GLRX5-BOLA3 complex transfers its cluster to monomeric apo NFU1 to form, in the presence of a reductant, a [4Fe-4S] cluster bound to dimeric NFU1. However, the actual more reliable model is that a [ISCA1- ISCA2-IBA57] complex converts [2Fe-2S] clusters, received by GLRX5, into a [4Fe-4S] cluster[17]. According to this model, it has been demonstrated that GLRX5 can transfer a [2Fe-2S] cluster to a heterodimeric complex formed by human ISCA1 and ISCA2 through a cluster mediated protein-protein interaction event[18], and that this complex acts as the assembler of [4Fe-4S] cluster by a reductive coupling process of two [2Fe-2S]-GLRX5 donated clusters. The ISCA1 protein is the key player of the [4Fe-4S] protein maturation process because of its ability to interact with both NFU1 and ISCA2, in a ternary complex[19]. The ISC late acting factors are NFU1 and BOLA3 proteins, but it is still largely undefined. (Fig. 2)

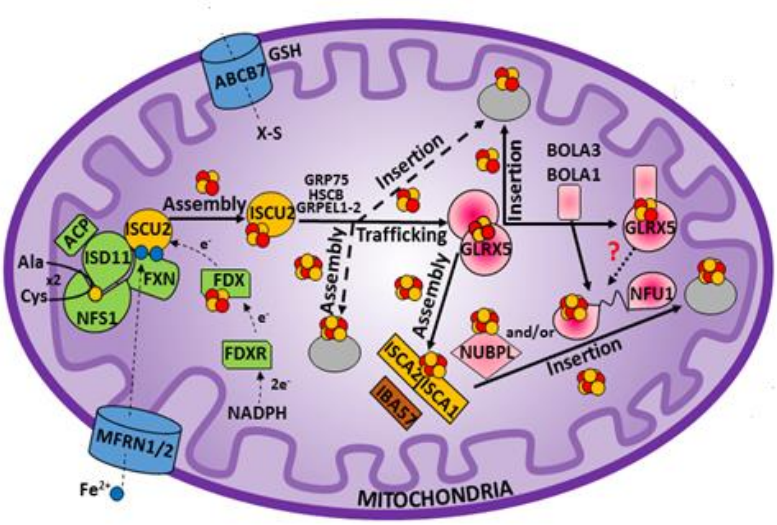

Fig. 2 – The mitochondrial ISC machinery.

(Reprinted from Metallomics, Vol. 10, 2018)

1.3.2. ISC export machinery

The biogenesis of Fe-S clusters in cytosol is performed by the CIA machinery, whose detailed mechanism of action and complete set of components are still not well defined. Two different models have been proposed for the iron and sulfur pooling in the cytosol. In the first model, mitochondria export in the cytosol a still unknown [2Fe-2S]-binding compound via the ISC export machinery, composed by the ABCB7 membrane transporter, and by GSH. The ATP-binding cassette (ABC) transporter of the mitochondrial inner membrane performs an essential function only in the generation of cytosolic Fe-S proteins by mediating export of Fe-S cluster unknown precursors synthesized.[20] It has been demonstrated, *in vivo*, that the transporter depletion is associated with defects in cellular iron homeostasis resulting in cytosolic iron deficiency and a concomitant iron accumulation in mitochondria.

The GSH can form *in vitro* a stable tetra-GSH-coordinated [2Fe-2S] cluster complex ($(GS)_4$-[2Fe-2S])[21], that is a viable substrate candidate for the mitochondrial ABCB7 export protein[22]. However, this model needs further experimental confirmations.

In the second model, an inorganic sulfur species that is generated in mitochondria by cysteine desulfurase is exported in the cytosol via the ABCB7 transporter[23]. In this model, Fe(II) ions are delivered by the poly(C)-binding proteins (PCBPs) family.[24] Philpott's group recently demonstrated that the αCP1 member of the PCBPs family (also known as PCBP1) coordinates iron(II) in complex with BolA2, a protein involved in the cytosolic Fe-S biogenesis[25]. *In vivo* and *in vitro* experiments indicated that

PCBP1–Fe–GSH–BolA2 serves as an intermediate complex that is required for the assembly of [2Fe–2S] clusters on BolA2–GLRX3[26], thereby linking the ferrous iron and Fe–S cluster distribution systems in cells. However, still this argument needs to be addressed in order to better define the mechanism of action of the interaction.

1.3.3. Cytosolic ISC assembly machinery

The cytosolic Fe-S protein assembly machinery is structured in main two steps, the early one, necessary for Fe-S cluster assembly, and the last one, responsible for cluster transfer and insertion into target cytosolic and nuclear proteins (Fig. 3). The process has been mostly characterized in yeast, where the first component to be identified was the essential and highly conserved nucleotide triphosphatases (NTPases) CFD1 and NBP35 proteins[2728]. These two proteins form a CFD1-NBP35 heterocomplex, that performs a scaffold function in the early step of the CIA machinery by *de novo* assembling [4Fe-4S] clusters[29,30]. This process is assisted by an electron transfer chain composed by Tah18 and Dre2 proteins[31].

The mechanism for the maturation of the [4Fe−4S] clusters at both N- and C-terminal motifs of the two human NTPases NUBP1 and NUBP2 is still elusive[18]. The human glutaredoxin-3 protein (GLRX3) is a possible player of the CIA machinery responsible for the maturation of the [4Fe−4S] clusters on NUBP1-NUBP2[32,33]. GLRX3 protein consists of three domains: one N-terminal thioredoxin domain and two monothiol glutaredoxin domains, each able to bind a glutathione-coordinated $[2Fe{-}2S]^{2+}$ cluster, via protein dimerization. It has been demonstrated that GLRX3 *de facto* acts as a [2Fe–2S] cluster chaperone in the cytosol, transferring its two [2Fe–2S] clusters to apo anamorsin *in vitro*[25,34] and *in vivo*[35]. Recently, it was showed that GLRX3 transfers its two [2Fe–2S] clusters also to NUBP1, and, in the presence of GSH, the two [2Fe–2S] clusters are converted into a [4Fe−4S] cluster[33].

The late-acting step of the CIA machinery involves the transfer and insertion of the newly assembled [4Fe - 4S] cluster from the NUBP1-NUBP2 scaffold complex into apo target Fe-S proteins. In yeast, depletion of all four early-acting CIA factors (CDF1, NBP35, Tah18, Dre2) impairs Fe - S cluster incorporation into Nar1 *in vivo*[31,36]. Assuming that all the *in vivo* findings on yeast hold in human cells, the most reliable model is that NUBP1-NUBP2 complex could be responsible of the maturation process of NARFL ([4Fe-4S] insertion in the C-terminal cluster-binding site). However, this model needs further experimental confirmations.

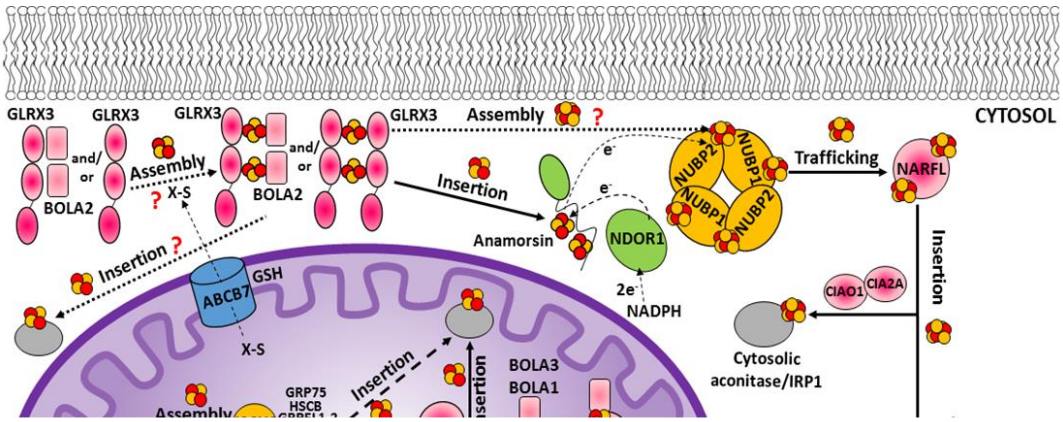

Fig. 3 – The integrated ISC export and cytosolic ISC machineries.

(Reprinted from Metallomics, Vol. 10, 2018)

1.4. Aim and topics of the research

My research activity was characterized by expression, purification, and structural characterization of recombinant human proteins involved in the iron-sulfur cluster biogenesis. During the three years of my PhD course, several cytoplasmic proteins involved in CIA machinery were chosen in order to understand at the molecular level their functional role in the pathways responsible for the Fe-S clusters incorporation into cytoplasmic targets. The aim of my project is to characterize iron-sulfur proteins and to perform cluster transfer experiments in order to obtain information about iron-sulfur cluster biogenesis in the cytosol.

The CIA machinery is organized in two steps and the protein anamorsin was shown to be a crucial member of the early step. My goal was to define the role of anamorsin as electron donor in the CIA maturation pathway, as its yeast homologous (Dre2) does[31]. In previous paper, it has been demonstrated that holo GLRX3 acts as clusters chaperone to NUBP1[33], a model protein, and the [4Fe-4S] clusters were formed through the reductive coupling of the 2[2Fe-2S]-GLRX3 by GSH. My research was focused on demonstrating that GSH can be replaced by anamorsin and to define how anamorsin and GLRX3, a physical and functional protein partner, interact each other.

The eukaryotic anamorsin protein are composed of two structurally independent domains fused by an unfolded linker of 51 residues. The N-terminal S-adenosyl methionine (SAM) methyl transferase-like domain comprising 172 residues is connected to the largely unstructured C-terminal domain of 90 residues named cytokine-induced apoptosis inhibitor 1 (CIAPIN1), which contains two highly conserved cysteine-rich motifs (M1 and M2 motifs) able to independently bind Fe-S clusters. In literature, there is

a debate concerning the cluster type bound to M2 motif, while it is generally accepted that M1 motif binds a [2Fe-2S] cluster[37]. The second topic of my research was to clarify the type of Fe-S clusters bound to human anamorsin.

By biochemical and spectroscopic approaches, it has been shown that the complex formed by Tah18 and Dre2 in yeast is part of an electron transfer chain required for assembly of Fe-S clusters[31]. Complementation studies showed that the human proteins NDOR1 and CIAPIN1 are able to substitute for yeast Tah18 and Dre2, respectively. One electron transfer reaction was observed to occur from the hydroquinone state of the FMN moiety of NDOR1 to the oxidized [2Fe-2S] cluster bound to the first motif of anamorsin[38]. The anamorsin-NDOR1 complex can efficiently supply electrons to cytosolic targets; however, the target is not identified yet. The NUBP1-NUBP2 complex, which is located at the early stages of the CIA machinery similarly to the anamorsin-NDOR1 complex, is the best candidate to receive electrons from the anamorsin-NDOR1 complex.

The structure of NUBP1-NUBP2 heterocomplex and how their clusters are assembled is still elusive. A possible player of the CIA machinery responsible for the maturation of the [4Fe−4S] clusters on NUBP1-NUBP2 is the cytosolic monothiol glutaredoxin GLRX3[32], which is, indeed, a crucial component for the assembly of cytosolic Fe−S proteins. GLRX3 is implicated in the maturation of anamorsin[34] and NUBP1 clusters[33], so I investigated the ability of human GLRX3 to act as a cluster chaperone for NUBP1-NUBP2, in order to clarify the assembly machinery in the cytosol.

At the same time, it was possible to characterize the structure of the human complex. I*n vitro* and *in vivo* studies on the yeast homologous heterocomplex suggested the presence of bridging [4Fe-4S] clusters in a heterodimer/tetramer structural organization[29], but the structure has not been defined yet. In my project, the main goal was to demonstrate the presence of that cluster because it is probably a transient cluster, and the most reliable model is that NUBP1-NUBP2 complex could be responsible of the maturation process of NARFL protein[36], donating the bridging cluster. The structure of that complex could help in understanding of next step of CIA machinery.

In order to shed light on the first part of the cytosolic iron-sulfur cluster biogenesis, it has been proposed a new pathway in which the iron was pooled in the cytosol. In eukaryotic cells, the delivery of Fe(II) ions is facilitated by the PCBP proteins family[24]. Structurally, PCBPs contain three conserved RNA-binding domains, termed heterogeneous nuclear ribonucleoprotein K homology (KH) domains[39], which have specific roles in interactions with RNA and proteins, in fact *in vivo* studies suggested that PCBP1 coordinates iron(II) in complex with BolA2[35], a protein involved in the biogenesis together with GLRX3. *In vivo* and *in vitro* experiments indicate that PCBP1–Fe–GSH–BolA2 serves as an intermediate complex

required for the assembly of [2Fe–2S] clusters on BolA2–GLRX3, thereby linking the ferrous iron and Fe–S distribution systems in cells. This suggestion needs structural confirmations and my work was focused on that the characterization of PCBP1–Fe–GSH–BolA2 system, in order to define the mechanism of action of the proposed alternative CIA pathway.

MATERIALS AND METHODS

2. MATERIALS AND METHODS

2.1. Bioinformatics approach

The initial part of every research project is chosen a protein target, on which to base the project. In my first part of PhD, the bioinformatics have become an integral part of research and development. It is an interdisciplinary research area at the interface between the biological and computational science, it has an essential role both in deciphering genomic, transcriptomic and proteomic data and in organizing information gathered from traditional biology.

Genome browsing is the first and crucial step for the expression and characterization of a recombinant protein. In this step, bioinformatics tools are necessary in order to analyze the nucleotide and the amino acids sequences. A number of data banks are available and provide the scientific community tools for researching gene banks, for the analysis of protein sequences, for the prediction of a variety of proteins properties. Primary databases contain information of DNA and protein sequence:

- BLAST (https://blast.ncbi.nlm.nih.gov) Basic Local Alignment Search Tool is a set of search programs designed to find regions of local similarity between sequences.
- CLUSTAW (https://www.ebi.ac.uk/Tools/msa/clustalw2/) is a general purpose multiple sequence alignment program for DNA or proteins
- EXPASY (https://web.expasy.org/translate/) is a translate tool which allows the translation of a nucleotide (DNA/RNA) sequence to a protein sequence

Secondary database are so called because they contain the results of analysis of the primary resource including information on sequence pattern or motifs.

Once the target protein is chosen, it is subjected to further bioinformatics investigation in order to predict important features like stability, solubility, hydrophobicity, secondary and tertiary structures.

- NCBI (https://www.ncbi.nlm.nih.gov/) This web site integrates information from several database
- PDB (https://www.rcsb.org/) This resource is powered by the Protein Data Bank archive-information about the 3D shapes of proteins, nucleic acids, and complex assemblies
- MODELLER (https://salilab.org/modeller/) is used for homology or comparative modeling of protein three-dimensional structures
- PROTPARAM (https://web.expasy.org/protparam/) is a tool that allows the computation of various physical and chemical parameters for a given protein stored in Swiss-Prot or TrEMBL or for a user entered protein sequence. The computed parameters include the molecular weight,

theoretical pI, amino acid composition, atomic composition, extinction coefficient, estimated half-life, instability index, aliphatic index and grand average of hydropathicity

2.2. Gene cloning

In order to get high yield of soluble proteins, many factors have to be taken in consideration, such as the choice of the vector, of the cloning strategy, and of culture conditions. Gene fusion technology has played an important role in fundamental biological research and it can facilitate purification, enhance protein expression and solubility, chaperone proper folding and reduce protein degradation. The best way to maximize the probability of obtaining a soluble and correctly folded target protein is to proceed with a parallel cloning and expression of it with a high number of fusion partners. Classical cloning, using restriction enzymes, typically cannot be adapted to high-throughput approaches, and Gateway cloning are the recombinant DNA technologies proven to be of importance for structural biology by enabling one to clone, over-express and purify the protein(s) of interest. Gene cloning involves the production *in vitro* of new DNA molecules which contain novel combinations of genes or oligonucleotides and the propagation of such recombinant DNA molecules by the exploitation *in vivo* of the replicative mechanisms of bacteria and other organisms. The developments of genetic engineering techniques have permitted the alteration of the genome of microorganisms so that it produces substances of little intrinsic value but of great medical or economic value to mankind.[40] The host organism is referred as the over-expression host. Gram-negative bacterium Escherichia coli is the most widely used host for the production of proteins. The bacteria has been studied extensively and has led to the better understanding of its genetics. This understanding of cellular physiology of *E. coli* has led to the development of improved genetic tools. Thus, *E. coli* bacterium is been used most abundantly for over-expression of recombinant protein including complex proteins of eukaryotic origin. The recombinant expression of protein in that host relies on the introduction of the exogenous gene encoding the protein of interest in an autonomously replicating DNA molecule called the cloning vector. The gene is introduced downstream to a promoter and ribosome binding sequence; the most commonly used promoter sequence is the bacteriophage T7 transcription promoter. Genes under the control of T7/lac promoter can be transcribed by T7 RNA polymerase, in presence of lactose. Since *E.coli* cells do not produce this type of RNA polymerase, in order to use this promoter system they have to be genetically modified by incorporation of the gene encoding the T7 RNA polymerase, the lac promoter and the lac operator into their genome. The repressor is displaced from the lac operator when lactose or a similar molecule like isopropyl β-D-1-thiogalactopyranoside (IPTG), is added to the culture. IPTG activates gene encoding T7 RNA polymerase and the target protein in the plasmid.

Restriction Enzyme Cloning Approach

Traditionally, molecular cloning is defined as the isolation and amplification of a specific DNA fragment. Most of these fragments are created either by digesting an existing piece of DNA with restriction enzymes or by targeting it via PCR. Short inserts of ~ 100 bp can also be commercially synthesized as complementary single-stranded oligos, which are subsequently annealed to form a double-stranded fragment.[41]

After successful isolation, the DNA of interest is ligated into a vector plasmid, a double-stranded circular piece of DNA that can be propagated in *E. coli*. Vectors used in the laboratory represent a smaller version of naturally occurring plasmids that include several basic features: a replication origin, a drug-resistance gene, and unique restriction sites to facilitate the insertion of DNA fragments. Often, several different restriction sites are clustered together in so-called 'polylinker regions' or 'multiple cloning sites,' making it easier to choose convenient and unique restriction enzyme combinations for a variety of inserts.

The choice of restriction enzymes is critical when designing a cloning strategy. While some sever the double-stranded DNA in one place, creating 'blunt' ends, others leave an overhang of a few bases at the cut site. These complementary 'sticky' ends find one another easily, increasing the efficiency of the ligation reaction and thus the chances for a successful cloning event. Thoughtful combination of restriction enzymes can also help to control the directionality of the insert, which is critical to many applications, but this technology cannot be adapted to high-throughput approaches, due to the complication of selecting compatible and appropriate restriction enzymes for each cloning procedure and to its multistep process. Moreover, all steps must be repeat for every vector final plasmid (Fig. 4)

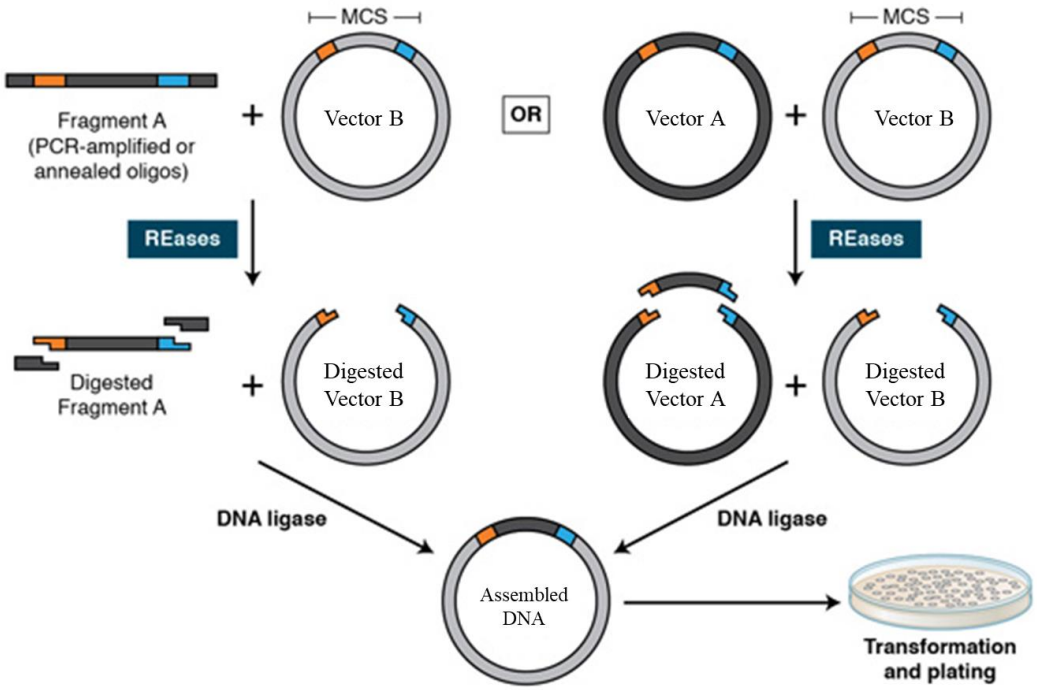

Fig. 4 - Restriction Enzyme Cloning Approach

Gateway Cloning System

The Gateway technology is a cloning method based on the site-specific recombinant of bacteriophage lambda, which facilities the integration of lambda into E.coli chromosome and the switch between the lytic and lysogenic cycle. By this technology, it is possible to clone a target gene into different expression vectors eliminating time-consuming work with restriction enzymes and ligase. (Fig. 5) [42]

Fig. 5 – Gateway cloning technology

The entry vector is obtained via recombination reaction of the pENTR/TOPO vector with our gene; the Topoisomerase I catalyzes the reaction. After isolation of the entry vector, the second step is to generate an expression construct by performing an LR recombination reaction between the entry clone and a Gateway destination vector of choice. This cloning method is faster due to the higher reaction efficiency, moreover, using different destination vectors allows expressing a chosen protein with different fusion tags, which could increase solubility, yield and make the purification step much easier.

However, this method resolves the over-expression of the protein target but not its solubility. A strategy, which is usually adopted to overcome the problems mentioned above, is to use a fusion protein where the protein of interest is fused of another protein or tail, and is expressed as such. The fusion tag is another protein that has high expression level and high solubility when it is expressed in bacterial culture even in minimal medium. The fusion not only helps in solubility to the desired protein but also in some case, helps to fold it properly. Some of the notable examples of fusion proteins are

- hexa-histidine affinity tag
- maltose binding protein (MBP)
- thioredoxin (Trx)
- glutathione S-transferase (GST)

2.3. Protein Expression

After bioinformatics characterization and choice of the cloning strategy, several conditions for the target expression have to be tested in order to obtain a high yield of soluble protein. The variables that affect the expression of a recombinant protein are host strain, growth medium and induction parameters (temperature, induction time or IPTG concentration). The preliminary expression test was performed in a small-volume scale changing:

- expression vectors (containing different fusion tags)
- E.coli strains (e.g. BL21 (DE3) GOLD, Rosetta(DE3), BL21 (DE3) RIPL Codon Plus)
- expression temperature
- IPTG concentration
- time of incubation
- growth medium (LB, M9 medium, MOPS medium)

Expression results are checked on SDS polyacrylamide gels (SDS-PAGE). The kind of this approach allows to explore a large set of expression conditions and to evaluate which one gives the best yiels of soluble protein.

Based on the preliminary results, a second expression test can be performed to better refine the conditions before the scale-up.

2.4. Protein purification

Protein purification is a series of processes intended to isolate the target protein. The step of purification is more important for the characterization of the function, structure and interactions of the protein. Separation of one protein from all others is typically laborious and it exploit differences in protein size or binding affinity. Usually a protein purification protocol contains one or more chromatographic steps. The basic procedure in chromatography is to flow the solution containing the protein through a column packed with various materials. Different proteins interact differently with the column material, and can thus be separated by the time required to pass the column, or the conditions required to elute the protein from the column. Usually proteins are detected as they are coming off the column by their absorbance at 280 nm.

Size Exclusion Chromatography

Chromatography can be used to separate protein in solution or denaturing conditions by using porous gels. This technique is known as size exclusion chromatography. The principle is that smaller molecules have to traverse a larger volume in a porous matrix. Consequentially, proteins of a certain range in size will require a variable volume of eluant (solvent) before being collected at the other end of the column of gel. In the context of protein purification, the eluent is usually pooled in different test tubes. All test tubes containing no measurable trace of the protein to purify are discarded. The remaining solution is thus made of the protein to purify and any other similarly-sized proteins.

Ion Exchange Chromatography

Ion exchange chromatography separates compounds according to the nature and degree of their ionic charge. The column to be used is selected according to its type and strength of charge. Anion exchange resins have a positive charge and are used to retain and separate negatively charged com pounds, while cation exchange resins have a negative charge and are used to separate positively charged molecules. The most weakly charged compounds will elute first, followed by those with successively stronger charges. Because of the nature of the separating mechanism, pH, buffer type, buffer concentration, and temperature

all play important roles in controlling the separation. Ion exchange chromatography is a very powerful tool for use in protein purification and is frequently used in both analytical and preparative separations.

Metal Binding- Affinity Chromatography

A common technique involves engineering a sequence of 6 to 8 histidines into the terminus of the protein. The polyhistidine binds strongly to divalent metal ions such as nickel and cobalt. The protein can be passed through a column containing immobilized nickel ions, which binds the polyhistidine tag. All untagged proteins pass through the column. The protein can be eluted with imidazole, which competes with the polyhistidine tag for binding to the column. After the affinity purification, the fusion tag must be removed from the recombinant protein. Indeed many expression vectors are engineered to express a protease cleavage site between the fusion tag and the protein. Tobacco Etch Virus (TEV), Thrombin or Ubl-specific protease 1 (Ulp1) are some examples of proteases that are normally used for the cleavage of tags.

2.5. Protein characterization

2.5.1. Nuclear Resonance Spectroscopy

Nuclear magnetic resonance (NMR) spectroscopy is the technique that provide structural information of inorganic and biological molecules, such as proteins, DNA and RNA at atomic resolution and it provides a wealth of information about dynamics of proteins molecules[43]. The power of NMR spectroscopy lies in its ability to probe the dynamic properties at multiple sites within the molecule under investigation. Furthermore, NMR can provide information about protein-protein and protein-ligand interactions as well as their quantification in terms of structure, kinetics and thermodynamics[44]. Relaxation in NMR is an important clue about the protein function. NMR experiments are capable of providing information from which a subset of distances between pairs of atoms can be estimated, and the final possible conformations of a protein can be determined by solving a distance constrains, with the aid specialized programs, which perform the structure calculations. NMR spectroscopy is unique among the methods available for three-dimensional structure determination of proteins at atomic resolution due to the fact that the NMR data can be recorded in solution. Since all proteins, except integral membrane proteins, function in solutions, knowledge of the molecular structure determination, NMR applications include investigations of dynamic features of the molecular structures, as well as studies of structural, thermodynamic and kinetic aspects of interactions between proteins and other solution components, which may either be other proteins or low molecular weight ligands[45].

2.5.2. Electron Paramagnetic Resonance

Electron Paramagnetic Resonance (EPR) spectroscopy is a technique for studying chemical species that have one or more unpaired electrons, such as organic or inorganic free radicals or inorganic complexes possessing a transition metal ion. The basic physical concepts of EPR are analogous to those of nuclear magnetic resonance (NMR), but electron spins are excited instead of spins of atomic nuclei. Using only paramagnetic species is a limitation, but also means that EPR is great specific technique. In typical experiment, the sample is placed in a resonant cavity which has a high quality factor Q (high Q to high sensitivity of the EPR method). At a fixed microwave frequency, the magnetic field B_0 is varied until resonance occurs at the value Be given by

$$Be = hv = g\beta B_0$$

In this equation g is the "g-factor" of the unpaired electron and β is the unit magnetic moment of the spinning electron (Bohr magneton). Free radicals have values that are fairly close to f = 2.0023 which characterizes a free electron, while some transition ions, such as cobalt and copper, have g-values which differ significantly from that theoretical value.

The resonant absorption is not infinitely narrow, since unpaired electrons do not only interact with the externally applied field, but also with the magnetic fields in their neighborhood. By observing spectral line width and intensity, it is possible to obtain information about the spin environment. Electron spin exchange between identical and non-identical molecules, chemical exchange between the paramagnetic molecule and its environment, and the interaction of nearby molecules having unpaired spins are some examples of environmental effects, which can influence line width and intensity in the EPR spectrum. Moreover, an observed spectrum can split in several lines referred to as hyperfine structure, arising from the electrons interacting with surrounding nuclear spins. This last property becomes very useful when investigation biological molecules that contain transition metal ions in their structure, since it can be exploited to characterize their coordination environment in dependence of their intrinsic geometry.

2.5.3. Circular Dichroism

Circular dichroism (CD) is an essential analytical technique used to analyze chirality in molecules through their optical activity, it is an excellent method to analyze protein and nuclei acid secondary structure in solution and it can be used to follow the changes in folding ad a function of temperature or denaturant. Proteins adopt unique conformations, optimized to perform specific structural, regulatory, or enzymatic functions. Therefore, the information on the protein structure is paramount to elucidating how proteins function. CD is a phenomenon occurring when asymmetrical molecules interact with circularly polarized light, thus absorbing left and right hand circularly polarized light with different absorption coefficients. In the protein, the major optically active groups are the amide bonds of the peptide backbone, typically disposed in highly ordered arrays such as α-helices or β-pleated sheets. In dependence of the orientation of the peptide bonds in the arrays, given by the symmetry of its disposition, optical transitions are differently split by exciton splitting, thus yielding characteristic spectral profiles for each of the three basic secondary structures of a polypeptide chain. The far-UV (180-250 nm) region probes the peptide backbone chain, whose phi and psi angles rotate depending on the protein conformation. There are two absorption bands which make up the far-UV CD spectrum: a strong p à p* around 190 nm and a weaker but broader *n* à p* transition between 210-220 nm. These two absorption bands give rise to different characteristic bands (Figure 7) that can be deconvoluted to estimate the secondary structure components of the protein under different solution and environmental conditions. While each of the four secondary structure components (a-helical, b-sheet, turn, and unordered) have distinguishing CD spectra, deconvolution is more complex than assigning a band to each component. Secondary structure analyses require curve fitting procedures based on a set of reference spectra with known secondary structure components that is used to estimate the components in the unknown (or sample) spectrum through regression analysis. The aromatic side chain residues and disulfide bonds are also known to contribute to the far-UV spectrum, further complicating estimations. Secondary structure analysis is best used to clarify shifts in CD data. More similar secondary structures, such as b-sheet and turn, can be teased out and structural changes from a majority of sheet to a majority of turn can be confidently confirmed. The near-UV CD spectrum (250-320 nm) reflects the protein tertiary structure, made up of the aromatic amino acid side chains. The three residues, phenylalanine, tyrosine and tryptophan, exhibit fine structure peaks between 255-270 nm, 275-285 nm, and 290-305 nm, respectively. The number and proximity of the aromatic residues will affect the strength of the CD signal, as well as the disulfide bonds, degree of hydrogen bonding, and rigidity of the chromophores in folded conformations. The buffer or solvent the sample is in will also affect the CD spectrum. Solvents used for absorption measurements will typically suffice, however the following conditions should be taken in consideration when choosing a solvent for

CD measurements: (1) solubility, (2) transparency in the wavelength range being probed, (3) optically inactive, and (4) sample stability. Condition 2 is especially important for secondary structures studies in the far-UV, since many solvents absorb strongly below 200 nm, as well as denaturing agents such as guanidinium chloride and urea. The addition of salts to buffers will may also increase absorbance and potentially induce scattering, reducing the S/N. Sugar-based formulation buffers not only absorb highly in the far-UV but also have a CD signal and should be avoided for CD measurements.

In addition to absorption spectroscopy, the technique of circular dichroism (CD) have also been used to study iron-sulfur proteins. CD has been used as a monitor of protein purity and of structural changes due to environmental change (including denaturation), and as a diagnostic of iron-sulfur cluster type. CD is expected to be more sensitive than absorption spectra to changes in the cluster environment. On the one hand, this makes CD an excellent probe of deviations from native protein structure; on the other hand, this can diminish the utility of CD as a diagnostic of cluster type. The CD is good to differ iron-sulfur cluster type, because of the lack of a positive Cotton effect in this spectral region is consistent with a [4Fe–4S] cluster and is quite distinct from the Cotton effect of the vis-CD spectra typically observed for [2Fe–2S] clusters.

RESULTS

In-cellulo Mössbauer and EPR studies bring new evidences to the long-standing debate on the iron-sulfur cluster binding in human anamorsin

3. RESULTS

3.1. *In-cellulo* Mössbauer and EPR studies bring new evidences to the long-standing debate on the iron-sulfur cluster binding in human anamorsin

3.1.1 Introduction

The paper was published on April 2021 on Angewandte Chemie International Edition.

Human anamorsin is a Fe-S cluster binding protein required in the early stages of the Fe-S protein biogenesis in the cytoplasm[1]. Upon its interaction with the diflavin reductase protein NDOR1[1,2] anamorsin works as an electron donor in the electron transfer chain required for the assembly of a [4Fe-4S] cluster on the scaffold complex formed by the two P-loop nucleoside triphosphatases NUBP1 and NUBP2. The latter complex then provides the assembled [4Fe-4S] cluster to all cytosolic and nuclear Fe-S proteins with the help of several other proteins that specifically cooperate in the biogenesis of the [4Fe-4S] proteins[2-5]. Anamorsin was also found to work as electron donor in an another process, i.e. in the reduction of the [2Fe-2S] clusters bound to human mitoNEET[6], a protein capable of repairing the iron-sulfur cluster of the cytosolic iron regulatory protein 1, a key regulator of cellular iron homeostasis in mammalian cells[7-9].

Anamorsin is composed of a well folded N-terminal S-adenosyl methionine (SAM) methyl transferase-like domain, connected via a linker of 51 residues to a C-terminal cytokine-induced apoptosis inhibitor 1 (CIAPIN1) domain[10]. The latter domain contains two conserved cysteine-rich motifs, arranged as a CX_8CX_2CXC pattern (M1 motif, hereafter), followed by a $CX_2CX_7CX_2C$ pattern (M2 motif, hereafter), each binding a Fe-S cluster *in vitro*[10-12]. Conversely to the yeast homologue of anamorsin (Dre2), which binds a [2Fe-2S] cluster and a [4Fe-4S] cluster at the M1 and M2 motifs, respectively[13], the M2 cysteine-rich motif of human anamorsin has been found to bind a [4Fe-4S] or a [2Fe-2S] cluster, depending on the experimental conditions applied to isolate the holo form of anamorsin[10,11]. There is indeed an ongoing debate in the most recent literature regarding whether a [4Fe-4S] or a [2Fe-2S] cluster is bound to the M2 motif. In order to shed light on this matter, the Fe-S binding properties of holo anamorsin were here investigated by *in cellulo* Mössbauer and *in cellulo* EPR spectroscopies. Our study, showing that *in cellulo* anamorsin binds two $[2Fe\text{-}2S]^{2+}$ clusters at both M1 and M2 motifs, supports the hypothesis that this holo form of anamorsin is the physiologically relevant species.

3.1.2. Published Paper

Angewandte Chemie - International Edition, 2021, 25; 60(27):14841-14845.
doi:10.1002/anie.202102910.

In-cellulo Mössbauer and EPR studies bring new evidences to the long-standing debate on the iron-sulfur cluster binding in human anamorsin

Sara Matteucci,[+] Francesca Camponeschi,[+] Martin Clémancey, Simone Ciofi-Baffoni, Geneviève Blondin* and Lucia Banci*

[1]Magnetic Resonance Center CERM, University of Florence, Via Luigi Sacconi 6, 50019, Sesto Fiorentino, Florence, Italy

[2]Department of Chemistry, University of Florence, Via della Lastruccia 3, 50019 Sesto Fiorentino, Florence, Italy

[3]Univ. Grenoble Alpes, CNRS, CEA, IRIG, Laboratoire de Chimie et Biologie des Métaux, UMR 5249, 17 rue des Martyrs, 38000 Grenoble, France

[‡]These authors contributed equally

Abstract: Human anamorsin is an iron-sulfur (Fe-S) cluster binding protein acting as an electron donor in the early steps of cytosolic iron-sulfur protein biogenesis. Human anamorsin belongs to the eukaryotic CIAPIN1 protein family and contains two highly conserved cysteine-rich motifs each binding an Fe-S cluster. *In vitro* works by various groups has provided rather controversial results for the type of Fe-S clusters bound to the CIAPIN1 proteins. In order to solve this debate, we exploited an *in cellulo* approach combining Mössbauer and EPR spectroscopies to characterize the iron-sulfur cluster bound form of human anamorsin. We found that the protein binds two [2Fe-2S] clusters at both its cysteine-rich motifs.

Iron-sulfur (Fe-S) clusters are ancient, polynuclear inorganic cofactors, containing iron ions ($Fe^{2+/3+}$) and inorganic sulfide (S^{2-}), present in all kingdoms of life. Proteins that bind Fe-S clusters are involved in many essential life processes, ranging from metabolic reactions to electron transport, DNA maintenance and gene expression regulation[2,3]. Among the Fe-S binding proteins, the eukaryotic CIAPIN1 protein family is characterized by the presence of a N-terminal S-adenosyl methionine methyl transferase-like domain connected via a flexible linker to a C-terminal cytokine-induced apoptosis inhibitor 1 (CIAPIN1) domain[4-6]. The hallmark of this protein family is the presence, in the CIAPIN1 domain, of two highly

conserved cysteine-rich motifs (a CX_8CX_2CXC motif (M1 motif, hereafter) followed by a $CX_2CX_7CX_2C$ motif (M2 motif, hereafter)), each able to bind an Fe-S cluster[6-10]. This protein in human[11], yeast[12], plant[13-15] and in the protist *Trypanosoma brucei*[16] has been proposed to act in the early stages of the cytoplasmic Fe-S protein biogenesis by working as an electron donor in an electron transfer chain required for the assembly of $[4Fe\text{-}4S]^{2+}$ clusters.

There is an ongoing debate in the literature on the type of Fe-S clusters bound to the CIAPIN1 proteins, which have been found indeed to bind [4Fe-4S] or [2Fe-2S] clusters, depending on the experimental *in vitro* conditions used to isolate the holo species[6-10,12]. In order to shed light on this matter, the Fe-S binding properties of human anamorsin were here investigated by *in cellulo* Mössbauer and *in cellulo* EPR spectroscopies. Specifically, wild-type protein (WT-anamorsin, hereafter) and a mutant containing only the M2 cysteine-rich motif (M2-anamorsin, hereafter), obtained by mutating the four cysteines of the M1 motif of anamorsin into alanines, were used to characterize the nature of the Fe-S clusters bound to anamorsin directly in cell.

Mössbauer spectra of *E. coli* cells expressing WT- and M2-anamorsin in the presence of ^{57}Fe and of the related control cells (see Supplementary Information for details) were recorded at ca. 6 K in a 60 mT external magnetic field applied parallel to the γ-rays. The spectra recorded on the cells expressing M2- and WT-anamorsin (Figure 1A and 1C, respectively) clearly showed two lines at ≈ 0.0 and ≈ 0.5 mm s^{-1}. These lines were absent in the spectra recorded on the control cells samples (Figure 1B and 1D), that were similar to spectra previously reported for control cells[17-22]. Spectra of control cells exhibited signatures from high-spin ferrous species, that were clearly evidenced by the presence of the high velocity line at ≈ 3 mm s^{-1}, whose absorption profile suggested the presence of two different components. The spectra also showed a signal between ≈ 0 and ≈ 1 mm s^{-1} corresponding to the combination of nanoparticles (NP), and of low-spin ferrous heme and diamagnetic $[4Fe\text{-}4S]^{2+}$ clusters, the latter two species presenting similar nuclear parameters, and usually denoted as the Central Doublet (CD). Accordingly, four doublets were considered to reproduce the spectra of control cells. A fifth doublet was introduced to fit the spectra of induced cells. This additional doublet corresponds to the difference spectrum obtained by subtracting the control cells spectrum from that of the induced cells (see Supporting Information, **Figure S1**). The simulations (see Supporting Information for details) and the experimental spectra are shown in **Figure 1**, where the different contributions of the Fe sites are displayed above each spectrum. The parameters used for the simulations are listed in **Table 1**.

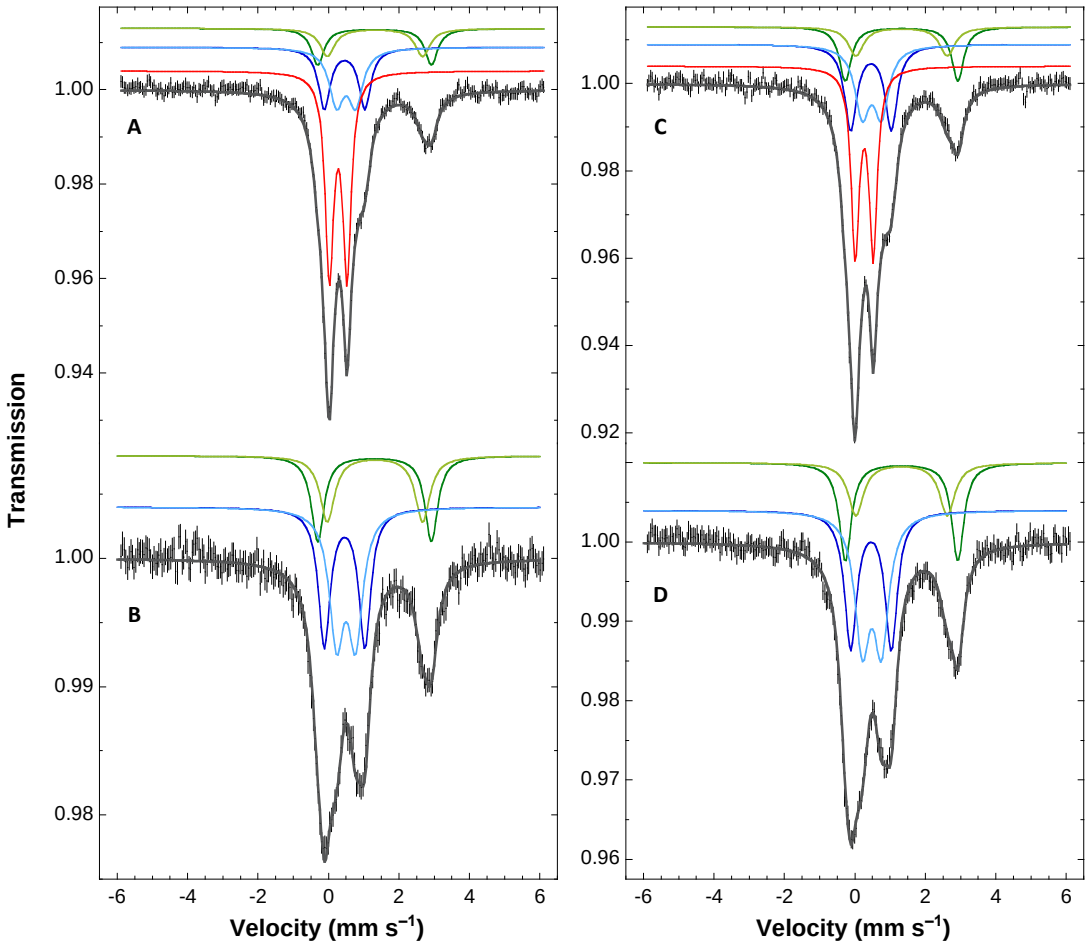

Figure 1. *M2- and WT-anamorsin expressed in E. coli cells bind [2Fe-2S]$^{2+}$ clusters by Mössbauer spectroscopy. Experimental Mössbauer spectra (hatched bars) recorded at ca. 6 K on cells samples with (A and C) or without (B and D) induction of the expression of M2- (left panel) and WT-anamorsin (right panel). A 60 mT external magnetic field was applied parallel to the γ-rays. The grey solid lines are simulations of the spectra with parameters listed in Table 1. Contributions are displayed as solid lines above the spectra using the following color code: HS Fe^{II} (1) in green, HS Fe^{II} (2) in light green, CD in blue, NP in light blue, [2Fe-2S] in red.*

Table 1. *Parameters used for the simulated spectra shown as solid grey lines in Figure 1. Uncertainties are ± 0.02, ± 0.05, ± 0.04, and ± 4 for the isomer shift (δ), the quadrupole splitting (ΔE_Q), the Lorentzian full-width at half-maximum (Γ), and the relative area, respectively.*

Proteins	**Fe sites[a]**	**δ (mm s^{-1})**	**ΔE$_Q$ (mm s^{-1})**	**Γ (mm s^{-1})[b]**	**% in control cells[c]**	**% in induced cells**
M2-anamorsin	HS Fe^{II} (1)	1.30	3.22	0.44	20	11
	HS Fe^{II} (2)	1.31	2.71	0.50	18	10
	CD[d]	0.45	1.15	0.40	30	18
	NP	0.49	0.54	0.49	33	19
	[2Fe-2S]	0.27	0.50	0.28	0	41
WT-anamorsin	HS Fe^{II} (1)	1.32	3.19	0.41	21	14
	HS Fe^{II} (2)	1.32	2.59	0.52	14	10
	CD[d]	0.45	1.15	0.42	30	22
	NP	0.47	0.54	0.50	34	21
	[2Fe-2S]	0.26	0.51	0.27	0	32

[a] The two HS Fe^{II} populations were assumed to be in the same ratio in the control and induced cells. [b] For each Fe site, a common linewidth was assumed in the control and induced cells spectra. [c] A zero contribution was fixed for the [2Fe-2S] clusters in control cells. [d] The Central Doublet (CD) reproduced the low-spin ferrous hemes and the diamagnetic $[4Fe\text{-}4S]^{2+}$ clusters. δ and ΔEQ were fixed to their usual values[19,23].

The nuclear parameters of the additional Fe site detected upon induction were typical of oxidized $[2Fe\text{-}2S]^{2+}$ clusters[17,18,24]. This Fe site accounted for 32% and 41% of the total iron content for WT- and M2-anamorsin induced cells, respectively. The higher percentage of [2Fe-2S] cluster in M2-anamorsin is in agreement with its higher expression level with respect to that of WT-anamorsin, as detected by Western blot gel analysis (**Figure S2**). It is worth noticing that the iron distribution determined in the control cells was not modified upon the induction of protein expression. More

specifically, the contribution of CD partly accounting for $[4Fe\text{-}4S]^{2+}$ clusters, did not vary significantly upon expression of WT- and M2-anamorsin (see Supporting Information **Table S1**). The observed 1-2% variations found in CD contribution are more than ten times below the amount of $[2Fe\text{-}2S]^{2+}$ clusters detected upon anamorsin expression. Consequently, the incorporation of a $[4Fe\text{-}4S]^{2+}$ cluster in the M1 or M2 motif of WT-anamorsin is essentially negligible, and it can be safely concluded that both WT- and M2-anamorsin accommodate $[2Fe\text{-}2S]^{2+}$ clusters.

In combination with *in cellulo* Mössbauer spectra, we acquired continuous wave (CW) *in cellulo* EPR spectra of *E. coli* cells expressing WT- and M2-anamorsin of the related control cells, all treated with 10 mM sodium dithionite underanaerobic conditions (**Figure S3**). Thein cellulo EPR difference spectra (obtained as reported in the Supporting Information) of reduced *E. coli* cells expressing M2-anamorsin exhibited a rhombic spectrum over a wide range of temperatures (**Figure 2A**), indicating that the signal arises from a single paramagnetic species. The EPR signal experienced the highest intensity at 10 K and was significantly broadened above 70 K (**Figure 2A**). The *in cellulo* EPR difference spectrum recorded at 10 K was readily simulated with a single set of principal g values of 2.016, 1.935, 1.890 (**Figure S4** and **Table S2**). When the microwave power was increased from 0.5 mW to 5 mW at 10 K, or the temperature was further lowered to 5 K the signal was easily saturated (**Figure 2A**).

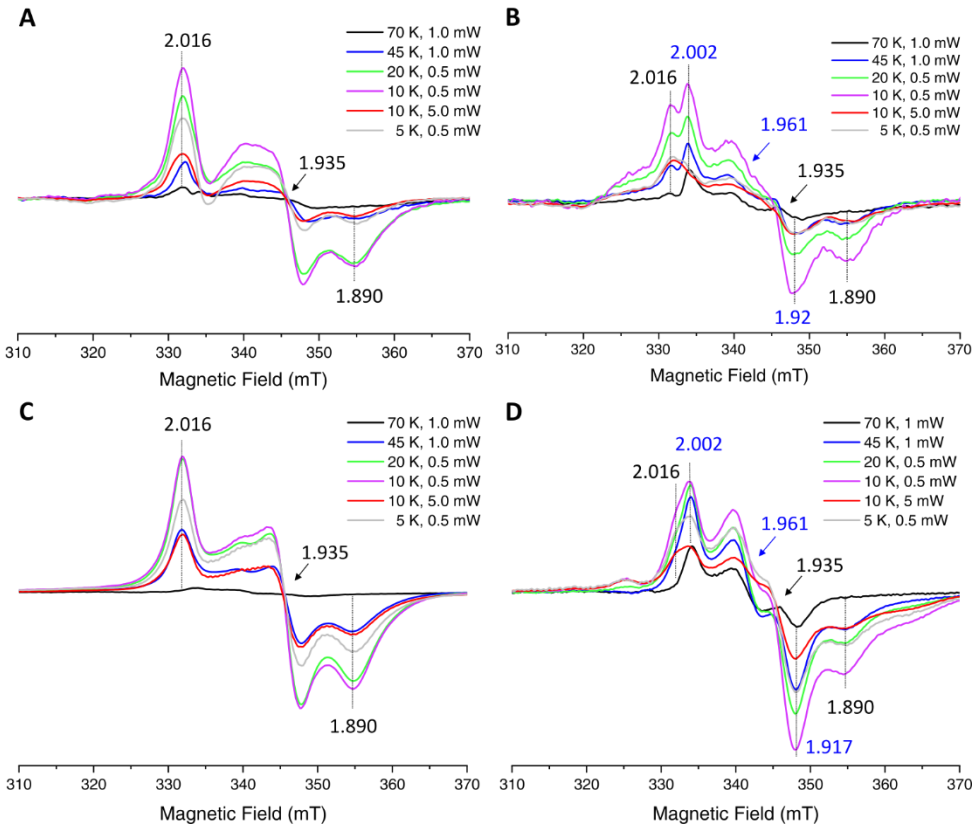

Figure 2. *The M1- and M2-motifs of anamorsin binds a [2Fe-2S] cluster by EPR spectroscopy. CW X-band EPR spectra of reduced E. coli cells expressing A) M2-anamorsin and B) WT-anamorsin, at different temperatures and microwave powers, after subtraction of the spectra of the corresponding reduced control cells. EPR spectra of C) anaerobically purified M2-anamorsin and D) anaerobically purified WT-anamorsin after reduction with 10 mM sodium dithionite, at different temperatures and microwave powers. EPR spectra were recorded under the following conditions: microwave frequency, 9.36 GHz; modulation amplitude, 10 G; modulation frequency, 100 kHz; acquisition time constant, 163.84 ms; number of points 1024.*

This behavior is consistent with the presence of a S=1/2 spin of the $[2Fe\text{-}2S]^{+}$ cluster that experiences a relatively slow relaxation rate at variance with the behavior of $[4Fe\text{-}4S]^{+}$ clusters. Indeed, the half-integer electronic spin in a $[4Fe\text{-}4S]^{+}$ cluster generally has much faster electron spin relaxation rates, and consequently their EPR signals are broadened beyond detection at temperatures around ~25 K, while they are well detectable and hardly power saturated at lower temperatures[25]. These features of the EPR spectra thus indicate that the M2 motif coordinates a [2Fe-2S] cluster, in agreement with the *in cellulo* Mössbauer data. The electron spin relaxation properties of the $[2Fe\text{-}2S]^{+}$ cluster bound to M2-anamorsin are, however, peculiar with respect to what is usually observed in ferredoxin-type [2Fe-2S] clusters, resembling in part those of fast relaxing $[4Fe\text{-}4S]^{+}$ clusters. Indeed, in ferredoxin-type [2Fe-2S] clusters the slow spin relaxation rates make the EPR signal hardly detectable below 10 K[25], contrarily to what observed for the $[2Fe\text{-}2S]^{+}$ cluster bound to M2-anamorsin, whose EPR signal

is still detectable at 5 K (**Figure 2A**). This peculiar relaxation properties of the [2Fe-2S]$^{+}$ cluster bound to the M2 motif can be explained considering that the reduced cluster bound to the M2 motif revealed a valence localization-to-delocalization transition as a function of temperature, as previously described by us[7]. It has been previously demonstrated that the electron delocalization within mixed-valence $Fe^{II}Fe^{III}$ pairs favors the parallel alignment of the local spins of both the high-spin Fe^{II} ($S_{Fe(II)}$=2) and high-spin Fe^{III} ($S_{Fe(III)}$=5/2) ions, leading to a S=9/2 total spin ground state[26]. The detection of the EPR signal of a S=1/2 spin suggests that the partial electron delocalization observed in the [2Fe-2S]$^{+}$ cluster bound to M2 motif is not strong enough to make the maximal total spin value as the ground state. However, it could allow the lowering in energy of the excited S >1/2 spin states, thus leading to a faster electron spin relaxation rate for the ground S=1/2 state compared with those typically observed in ferredoxin-type [2Fe-2S] clusters, thus more closely mimicking a value typical of fast relaxing [4Fe-4S]$^{+}$ clusters.

Reduced *E. coli* cells expressing WT-anamorsin showed more complex *in cellulo* EPR difference spectra (obtained as reported in the Supporting Information), arising from the presence of two rhombic EPR signals (**Figure 2B**). The *in cellulo* EPR difference spectrum recorded at 10 K was readily simulated with two subspectra having principal g values of 2.002, 1.961, 1.917 and of 2.016, 1.935, 1.890 (**Figure S4** and **Table S2**), that were previously assigned to the two [2Fe-2S]$^{+}$ clusters bound to the M1 and M2 motifs of WT-anamorsin, respectively[7]. At 70 K, the spectrum was dominated by the signal arising from the S=1/2 spin of the [2Fe-2S]$^{+}$ cluster bound to the M1 motif of WT-anamorsin[7]. By lowering the temperature to 10 K, the contribution of the signal originating from the M2-bound [2Fe-2S]$^{+}$ cluster increased, as showed by the increase in the intensity of the signal at g = 2.01 and g = 1.89 (Figure 2B). As the microwave power was increased from 0.5 mW to 5 mW at 10 K, or the temperature was further lowered from 10 K to 5 K, the EPR signals of both clusters bound to WT-anamorsin were easily saturated, although to a different extent, being the EPR signal of the M1-bound [2Fe-2S]$^{+}$ cluster more easily saturated than that of the M2-bound [2Fe-2S]$^{+}$ cluster, as showed by the larger decrease in the intensity of the signal at g = 2.00 compared to that at g = 2.01 in Figure 2B. This behavior reproduces that observed for reduced *E. coli* cells expressing M2-anamorsin (Figure 2A) and is consistent with the binding of a [2Fe-2S]$^{+}$ cluster to both M1 and M2 anamorsin motifs, with very similar, low dispersed g values, but significantly different electron spin relaxation properties and thus different saturation characteristics, as already described above. To investigate whether the Fe-S clusters of anamorsin are modified along the purification procedure, we recorded the EPR spectra of WT- and M2-anamorsin anaerobically purified from *E. coli* and then treated with 10 mM sodium dithionite under anaerobic conditions. These EPR spectra exhibited

rhombic signals with the same sets of g values, relaxation and power saturation characteristics of those observed for reduced *E. coli* cells expressing WT- and M2-anamorsin, respectively (Figure 2C and 2D). These results clearly indicate that the clusters bound to human anamorsin in the cytoplasmic environment are conserved upon anaerobic purification.

It is remarkable to note that *in cellulo* EPR spectroscopy, at variance with *in cellulo* Mössbauer spectroscopy, is able to spectroscopically discern the presence of two S=1/2 spins arising from [2Fe-2S]$^{+}$ clusters bound to the M1 and M2 motifs of WT-anamorsin. Thus, *in cellulo* EPR data clearly demonstrate that M1- and M2-sites of WT-anamorsin are both occupied by [2Fe-2S] clusters in the *E. coli* cells. The differences in the electronic properties allowing the distinction between the two reduced clusters are suppressed in the oxidized state, which features a diamagnetic ground state. Furthermore, the isomer shift for the ferric sites in [2Fe-2S]$^{2+}$ is only moderately sensitive to the ligand environment. To the best of our knowledge, only the presence of one or two histidines in place of cysteines in the coordination sphere leads to a significant increase of δ.([27] and references therein)

Here, we have shown by *in cellulo* Mössbauer and *in cellulo* EPR spectroscopies that, at variance with what reported for yeast Dre2 that was described to bind a [2Fe–2S] cluster at the M1 motif and a [4Fe–4S] cluster at the M2-motif, human anamorsin coordinates two [2Fe–2S] clusters, one in each M1 and M2 motif. In addition, EPR spectra acquired on both reduced *E. coli* cells expressing WT- and M2-anamorsin and on anaerobically purified, reduced WT- and M2-anamorsin showed that the [2Fe–2S] cluster bound to the M2 motif of anamorsin displays enhanced electron spin relaxation rates, likely originating from local protein conformational heterogeneity.[7] Our study, showing that *in cellulo* anamorsin binds two [2Fe–2S] clusters at both M1 and M2 motifs, is consistent with the hypothesis that this holo form of anamorsin is the physiologically relevant species. Our data also showed that the reducing environment of the bacterial cytoplasm, and presumably also that of the human cytoplasm, is not sufficient to reduce the [2Fe–2S]$^{2+}$ clusters of anamorsin, but that a reductase is required to activate anamorsin function as cellular reductant to assemble [4Fe–4S] clusters in the early steps of cytosolic Fe–S protein biogenesis. The NADPH-dependent diflavin oxidoreductase 1 (Ndor1), which is responsible, in eukaryotic cells, for the reduction of the [2Fe–2S] cluster bound to the M1-site of anamorsin[7, 11, 12], is, however, not present in bacterial organisms, and thus this explains why the M1-bound [2Fe–2S] cluster of anamorsin is exclusively present in an oxidized state, when expressed in *E. coli* cells.

Acknowledgements

The authors acknowledge funding from the support of Instruct-ERIC, an ESFRI Landmark Research Infrastructure and specifically the use of the resources of the CERM/CIRMMP Italian Instruct Center. This research has been supported by Timb3, grant no. 810856, funded by the Horizon 2020 research and innovation programme of the European Commission, and by the Italian Ministry for University and Research (FOE funding) to the Italian Center (CERM/CIRMMP, University of Florence) of Instruct-ERIC. This article is based upon work from COST Action CA15133, supported by COST (European Co-operation in Science and Technology). MC and GB thank the Labex ARCANE and CBH-EUR-GS (ANR-17-EURE-0003) for partial funding. *anamorsin, Fe-S proteins, in-cellulo Mössbauer spectroscopy*.

Keywords: anamorsin • *in cellulo* EPR spectroscopy • *in cellulo* Mössbauer spectroscopy • iron-sulfur cluster • metalloproteins.

[1] H. Beinert, R. H. Holm, E. Münck, Science 1997, 277, 653–659.

[2] R. Lill, R. Dutkiewicz, S. A. Freibert, T. Heidenreich, J. Mascarenhas, D. J. Netz, V. D. Paul, A. J. Pierik, N. Richter, M. Stümpfig, V. Srinivasan, O. Stehling, U. Mühlenhoff, Eur. J. Cell Biol. 2015, 94, 280–291.

[3] S. Ciofi-Baffoni, V. Nasta, L. Banci, Metallomics 2018, 10, 49–72.

[4] L. Banci, I. Bertini, S. Ciofi-Baffoni, F. Boscaro, A. Chatzi, M. Mikolajczyk, K. Tokatlidis, J. Winkelmann, Chem. Biol. 2011, 18, 794–804.

[5] G. Song, C. Cheng, Y. Li, N. Shaw, Z.-C. Xiao, Z.-J. Liu, Proteins 2014, 82, 1066–1071.

[6] N. Soler, C. T. Craescu, J. Gallay, Y.-M. Frapart, D. Mansuy, B. Raynal, G. Baldacci, A. Pastore, M.-E. Huang, L. Vernis, FEBS J. 2012, 279, 2108–2119.

[7] L. Banci, S. Ciofi-Baffoni, M. Mikolajczyk, J. Winkelmann, E. Bill, M.-E. Pandelia, J. Biol. Inorg. Chem. 2013, 18, 883–893.

[8] Y. Zhang, C. Yang, A. Dancis, E. Nakamaru-Ogiso, J. Biochem. 2017, 161, 67–78.

[9] Y. Zhang, E. R. Lyver, E. Nakamaru-Ogiso, H. Yoon, B. Amutha, D.-W. Lee, E. Bi, T. Ohnishi, F. Daldal, D. Pain, A. Dancis, Mol. Cell. Biol. 2008, 28, 5569–5582.

[10] D. J. A. Netz, H. M. Genau, B. D. Weiler, E. Bill, A. J. Pierik, R. Lill, Biochem. J. 2016, 473, 2073–2085.

[11] L. Banci, I. Bertini, V. Calderone, S. Ciofi-Baffoni, A. Giachetti, D. Jaiswal, M. Mikolajczyk, M. Piccioli, J. Winkelmann, Proc. Natl. Acad. Sci. U.S.A. 2013, 110, 7136–7141.

[12] D. J. A. Netz, M. Stümpfig, C. Doré, U. Mühlenhoff, A. J. Pierik, R. Lill, Nat. Chem. Biol. 2010, 6, 758–765.

[13] E. L. Bastow, K. Bych, J. C. Crack, N. E. Le Brun, J. Balk, Plant J. 2017, 89, 590–600.

[14] D. G. Bernard, D. J. A. Netz, T. J. Lagny, A. J. Pierik, J. Balk, Philos Trans R Soc Lond B Biol Sci 2013, 368, 20120259.

[15] J. Couturier, B. Touraine, J.-F. Briat, F. Gaymard, N. Rouhier, Front Plant Sci 2013, 4, 259.

[16] S. Basu, D. J. Netz, A. C. Haindrich, N. Herlerth, T. J. Lagny, A. J. Pierik, R. Lill, J. Lukeš, Molecular Microbiology 2014, 93, 897–910.

[17] R. Benda, B. Tse Sum Bui, V. Schünemann, D. Florentin, A. Marquet, A. X. Trautwein, Biochemistry 2002, 41, 15000–15006.

[18] M. M. Cosper, G. N. L. Jameson, M. K. Eidsness, B. H. Huynh, M. K. Johnson, FEBS Letters 2002, 529, 332–336.

[19] M. M. Cosper, G. N. L. Jameson, H. L. Hernández, C. Krebs, B. H. Huynh, M. K. Johnson, Biochemistry 2004, 43, 2007–2021.

[20] M. Seemann, K. Janthawornpong, J. Schweizer, L. H. Böttger, A. Janoschka, A. Ahrens-Botzong, E. N. Tambou, O. Rotthaus, A. X. Trautwein, M. Rohmer, V. Schünemann, Journal of the American Chemical Society 2009, 131, 13184–13185.

[21] A. S. Fleischhacker, A. Stubna, K.-L. Hsueh, Y. Guo, S. J. Teter, J. C. Rose, T. C. Brunold, J. L. Markley, E. Münck, P. J. Kiley, Biochemistry 2012, 51, 4453–4462.

[22] J. Yang, S. G. Naik, D. O. Ortillo, R. García-Serres, M. Li, W. E. Broderick, B. H. Huynh, J. B. Broderick, Biochemistry 2009, 48, 9234–9241.

[23] G. P. Holmes-Hampton, R. Miao, J. Garber Morales, Y. Guo, E. Münck, P. A. Lindahl, Biochemistry 2010, 49, 4227–4234.

[24] L. Kristina Beilschmidt, S. Choudens, M. Fournier, Y. Sanakis, M.-A. Hograindleur, M. Clémancey, G. Blondin, S. Schmucker, A. Eisenmann, A. Weiss, P. Koebel, N. Messaddeq, H. Puccio, A. Martelli, Nature Communications 2017, 8, 15124.

[25] W. R. Hagen, J. Biol. Inorg. Chem. 2018, 23, 623–634.

[26] G. Blondin, J. J. Girerd, Chem. Rev. 1990, 90, 1359–1376.

[27] K. Stegmaier, C. M. Blinn, D. F. Bechtel, C. Greth, H. Auerbach, C. S. Müller, V. Jakob, E. J. Reijerse, D. J. A. Netz, V. Schünemann, A. J. Pierik, J Am Chem Soc 2019, 141, 5753–5765.

3.1.3. Supporting Information

In-cellulo Mössbauer and EPR studies bring new evidences to the long-standing debate on the iron-sulfur cluster binding in human anamorsin

Sara Matteucci[1‡], Francesca Camponeschi[1‡], Martin Clémancey[3], Simone Ciofi-Baffoni[1,2], Geneviève Blondin[3,*], and Lucia Banci[1,2,*]

[1]Magnetic Resonance Center CERM, University of Florence, Via Luigi Sacconi 6, 50019, Sesto Fiorentino, Florence, Italy

[2]Department of Chemistry, University of Florence, Via della Lastruccia 3, 50019 Sesto Fiorentino, Florence, Italy

[3]Univ. Grenoble Alpes, CNRS, CEA, IRIG, Laboratoire de Chimie et Biologie des Métaux, UMR 5249, 17 rue des Martyrs, 38000 Grenoble, France

[‡]These authors contributed equally

Table of Contents

1. Experimental Section

1.1 Cloning and overexpression of WT- and M2-anamorsin.

The plasmids for recombinant expression of wild-type (WT) human anamorsin (UniProtKB/Swiss-Prot: Q6FI81) and of a mutant containing only the second cluster binding motif (M2-anamorsin, hereafter) were obtained through the Gateway® cloning Technology (Invitrogen). The pENTR-TEV-d-Topo vectors containing the sequence coding for the two proteins were obtained as reported previously[1]. The two protein genes were cloned into the pTH34 expression vector. According to the vector construction, the proteins were expressed with an N-terminal GB1-His_6 fusion tag.

BL21(DE3) GOLD competent *Escherichia coli* cells were transformed with pTH34-WT and pTH34-M2 plasmids. Cells were grown in MOPS minimal medium[2,3], containing 1 mM ampicillin at 37 °C under vigorous shaking (180 rpm) up to OD_{600} ~ 0.6. Protein expression was induced by adding 0.2 mM isopropyl β- d-1-thiogalactopyranoside (IPTG) and 70 μM $^{57}FeCl_3$ for WT-anamorsin and 20 μM $^{57}FeCl_3$ for M2-anamorsin. Cells were grown at 25 °C for 4 hours. Control cultures for *in cellulo* Mössbauer and EPR and studies were obtained without IPTG induction. Cells were harvested by centrifugation (4000*g*, 20 min, 4 °C), washed twice in an anaerobic chamber (O2 < 1 ppm) with degassed MOPS buffer containing 50 mM NaCl and 22 mM glucose, pH 7.4 and centrifuged again for 10 min at 5000*g*, 4 °C[3].

1.2 Western blot gel analysis

The relative expression levels of M2- and WT-anamorsin in *E. coli* cells were estimated by densitometric analysis of western blot band intensities. *E. coli* cells were harvested and then resuspended in different volumes of final sample buffer for electrophoresis in order to have the same optical density at 600 nm for cells expressing M2- and WT-anamorsin. Lysates from cell samples were analyzed on the gel at increasing dilutions. The proteins were detected using a monoclonal mouse anti-His antibody conjugated to horseradish peroxidase (Miltenyi Biotec) diluted 1:5000. The molecular weight of M2- and WT-anamorsin expressed with the N-terminal GB1-His_6 fusion tag was ~ 44 kDa.

The densitometric analysis of the western blot bands was done using ImageJ software, by comparing the intensity of the bands corresponding to M2- and WT-anamorsin proteins.

1.3 *In cellulo* Mössbauer studies

E. coli cells containing overexpressed proteins and control cells harvested and washed as described above were immediately packed in Delrin cups (0.6-0.7 g of cells per cup) and frozen in liquid nitrogen before analysis. The Mössbauer spectra were recorded at ca. 5 K on a strong-field Mössbauer spectrometer equipped with an Oxford Instruments Spectromag 4000 cryostat containing an 8 T split-pair superconducting magnet. Both spectrometers were operated in a constant acceleration mode in transmission geometry. The isomer shifts were referenced against that of a room-temperature metallic iron foil. Analysis of the data was performed with a home-made program[4-6].

1.4 *In cellulo* and *in vitro* EPR studies

For the *in cellulo* EPR studies, *E. coli* cells containing the overexpressed proteins and the corresponding control cells were harvested and washed as described above. The cells were resuspended in 50 mM Tris buffer pH 8.0, 150 mM NaCl, and treated with 10 mM sodium dithionite. Cells were frozen in liquid nitrogen before analysis.

Protein purification for *in vitro* EPR studies was performed as follows. Total cell lysis was performed in CelLytic Express (Sigma-Aldrich) in an anaerobic chamber (O_2 < 1 ppm). WT- and M2-anamorsin were purified by Ni^{2+}-affinity chromatography on HisTrap FF column (GE Healthcare). The proteins were eluted with 50 mM Tris buffer pH 8, 500 mM NaCl, 500 mM imidazole and 5% glycerol, concentrated with Amicon Ultra-15 Centrifugal Filter Units with a MWCO of 10 kDa (Millipore), and the buffer exchanged by PD-10 desalting column (GE Healthcare) in degassed 50 mM Tris buffer pH 8.0, 150 mM NaCl, 10% glycerol. Protein concentration was ~ 0.3 mM.

CW EPR spectra of *E. coli* cells containing overexpressed anamorsin and of control cells (reported in Figure S3), and those of anaerobically purified WT- and M2-anamorsin were recorded after the addition of up to 10 mM sodium dithionite. EPR spectra were acquired in the 5-70 K temperature range, using a Bruker Elexsys 580 spectrometer working at a microwave frequency of ~ 9.36 GHz, equipped with a SHQ cavity and a continuous flow He cryostat (ESR900, Oxford instruments) for temperature control. Acquisition parameters were as following: microwave frequency, 9.36 GHz; microwave power range, 0.5-5 mW; modulation frequency, 100 kHz; modulation amplitude, 10 G; acquisition time constant, 163.84 ms; number of points 1024; number of scans 3; field range 2000-4000 G. For *in cellulo* EPR studies, the spectra of reduced control cells were subtracted from those of reduced *E. coli* cells expressing WT- and M2-anamorsin.

1.5 Procedure for the simulation of the Mössbauer spectra

An identical procedure was used for the WT- and M2-anamorsin samples. Details are given below for the WT-protein. Because the absorption at ≈ 3 mm s^{-1} presents the same profile for both the control and induced cells, the ratio between the two high-spin ferrous contributions was considered identical in both spectra. Thus, in a first step, the spectrum of the control cells was scaled to get the superimposition of the absorption line at ≈ 3 mm s^{-1} with that of the spectrum of the induced cells (see **Figure S1C**). The calculated difference spectrum clearly evidenced one doublet (see **Figure S1D**). The associated parameters (δ, ΔE_Q, Γ, and the area) were thus determined. In a second step, spectra shown in **Figure S1C** were simultaneously simulated with four and five doublets, respectively, with the following constraints. (i) Contributions in both samples were determined versus the total iron content of the induced cells (black spectrum in **Figure S1C**); (ii) For each of the four different iron sites further labeled HS Fe^{II} (1), HS Fe^{II} (2), CD, and NP, a unique linewidth was considered for the two spectra; (iii) Because the absorption at ≈ 3 mm s^{-1} is similar in the two spectra, the contributions of the two HS Fe^{II} were assumed to be identical in both samples; (iv) Parameters for the fifth iron species were fixed to the values determined from the difference spectrum. A zero contribution for this site in the control cells sample was set.

Resulting parameters are listed in **Table S1**. It is worth noticing that the variations determined for the CD and NP contributions between control and induced cells samples are within the uncertainties. Contributions of the four iron sites reported in **Table 1** for the control cells sample were obtained from those listed in **Table S1** and the area of the spectrum recorded on control cells.

1.6 Procedure for the simulation of the EPR spectra

The simulations of both M2- and WT-anamorsin were carried out on the spectra recorded at 10 K and 0.5 mW (see above for detailed experimental settings). The EPR spectra of the control cells were subtracted from that of the *E. coli* cells expressing the proteins using the Bruker WinEPR software. A polynomial baseline correction was applied to both spectra before subtraction. The obtained differential traces were simulated with the EasySpin software package[7], using the 'pepper' function. An anisotropic residual line width (H-strain) has been used in combination with a Lorentzian function, to account for the orientation-dependent phenomenological line broadening visible in the spectra. For M2-anamorsin, the fitting parameters were: Lorentzian peak-to-peak line width (lwpp) of 1.9 mT and 20 MHz, 40 MHz and 80 MHz in the x-, y- and z-direction, respectively, for H-strain. The simulation of the EPR spectra of WT-anamorsin required two subspectra (I and II), fitted with the following

parameters: Lorentzian lwpp of 2.35 mT and 0 MHz, 49 MHz and 100 MHz in the x-, y- and z-direction, respectively, for H-strain for subspectrum I; Lorentzian lwpp of 1.3 mT and 0 MHz, 100 MHz and 45 MHz in the x-, y- and z-direction, respectively, for H-strain for subspectrum II. The best fits (reported in Figure S4) were obtained with the parameters reported in Table S2.

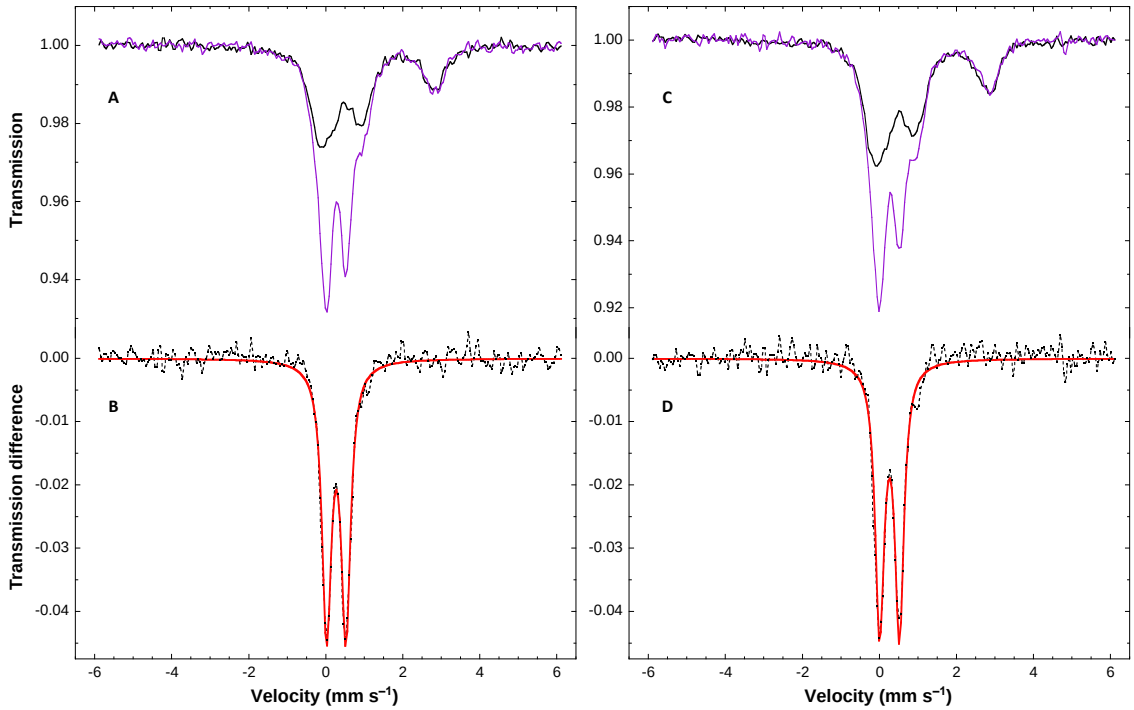

Figure S1. *Top: Comparison of the experimental Mössbauer spectra recorded at ca. 6 K on cells samples with (solid mauve lines) or without (solid black lines) induction of the overexpression of M2- (panel A) and WT-anamorsin (panel C). A 60 mT external magnetic field was applied parallel to the γ-rays. Spectra of the control cells sample were scaled to get the superimposition of the absorption at ≈ 3 mm s^{-1}. Bottom: Induced minus control cells difference spectra (dashed black lines) calculated from spectra shown in panels A and C. The red solid lines correspond to the contribution of the [2Fe-2S] cluster as shown in Figure 1A and 1C. For both the M2- (panel B) and WT-anamorsin (panel D), this doublet is almost superimposable to the difference spectrum*

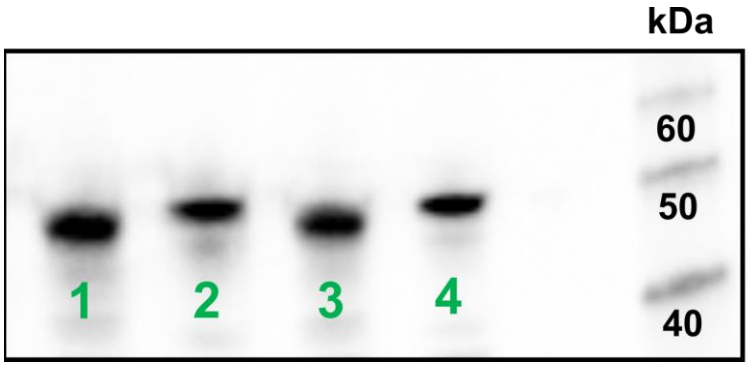

Figure S2. *Western blot gel on lysates obtained from E. coli cells expressing M2- and WT anamorsin. Lane 1) and 2) 1:5 dilutions of resuspended cells expressing M2- and WT-anamorsin, respectively. Lane 3) and 4) are 1:10 dilutions of resuspended cells expressing M2- and WT anamorsin, respectively. The densitometric analysis of the western blot band intensities indicate that M2-anamorsin is 1.3 times more expressed than WT-anamorsin.*

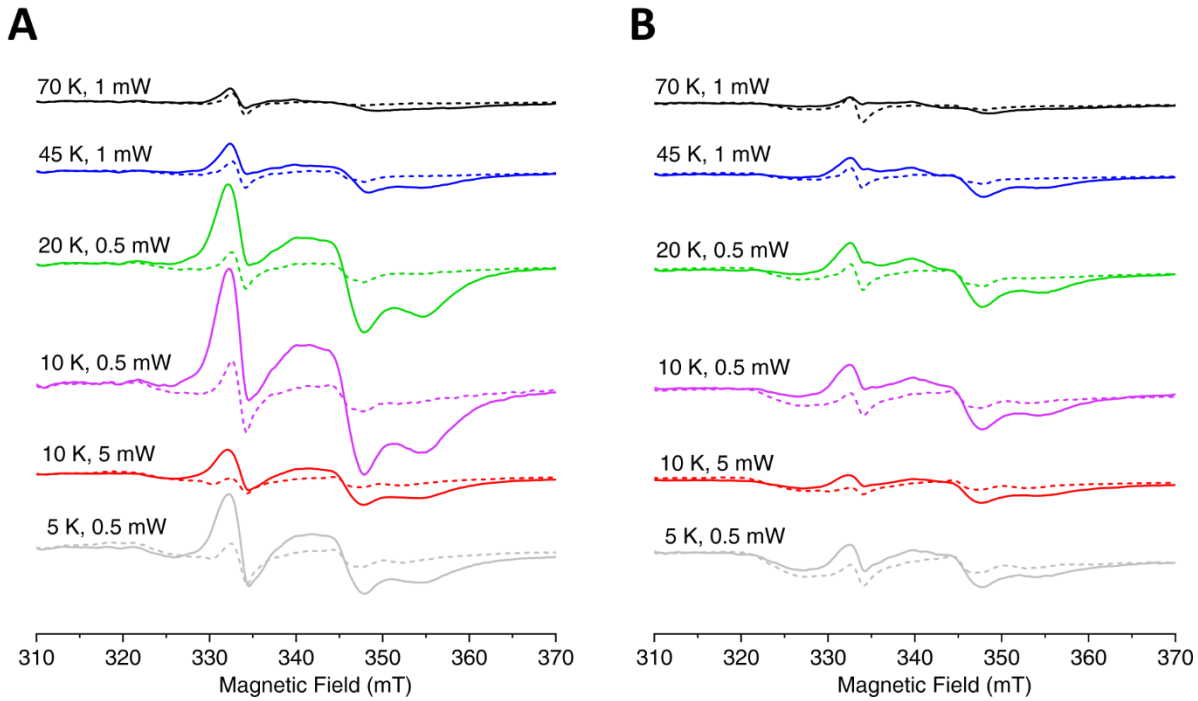

Figure S3. *CW EPR spectra of reduced control cells (dotted lines) and reduced E. coli cells expressing M2- (A) and WT- anamorsin (B) (solid lines).*

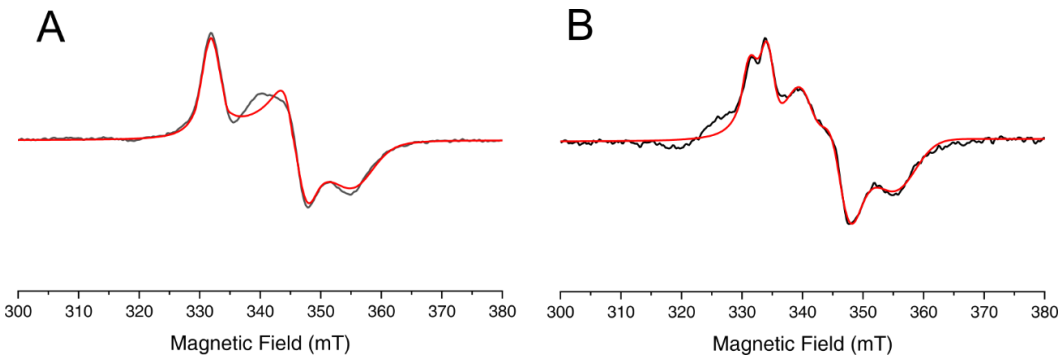

Figure S4. *Simulations (red lines) of the EPR difference spectra (black lines) obtained for reduced E. coli cells expressing M2- (A) and WT-anamorsin (B) at 10 K. The best fit were obtained with Easyspin software*[7] *with the parameters reported in Table S2. The primary EPR spectra of the cells were recorded under the following conditions: temperature, 10 K; microwave power, 0.5 mW; microwave frequency, 9.36 GHz; modulation amplitude, 10 G; modulation frequency, 100 kHz; acquisition time constant, 163.84 ms; number of points 1024.*

Table S1. *Parameters issued from the simulations of the Mössbauer spectra. The contributions for the different Fe sites are calculated versus the total iron content in induced cells. Uncertainties are ±0.02, ±0.05, ±0.04, and ±4 for the isomer shift (δ), the quadrupole splitting (ΔE_Q), the Lorentzian full-width at half-maximum (Γ), and the relative area, respectively.*

Protein	**Fe sites**	**δ (mm s^{-1})**	**ΔE_Q (mm s^{-1})**	**Γ (mm s^{-1})**	**% in control cells[a]**	**% in induced cells**
M2-anamorsin	HS Fe^{II} (1)	1.30	3.22	0.44	11	11
	HS Fe^{II} (2)	1.31	2.71	0.50	10	10
	CD	0.45	1.15	0.40	17	18
	NP	0.49	0.54	0.49	19	19
	[2Fe-2S]	0.27	0.50	0.28	0	41
WT-anamorsin	HS Fe^{II} (1)	1.32	3.19	0.41	14	14
	HS Fe^{II} (2)	1.32	2.59	0.52	10	10
	CD	0.45	1.15	0.42	20	22
	NP	0.47	0.54	0.50	23	21
	[2Fe-2S]	0.26	0.51	0.27	0	32

[a] The control cells spectra were scaled to get the superimposition of the absorption observed at ≈ 3 mm s^{-1} in induced cells spectra (black spectra in **Figure S1A** and **S1C**).

Table S2. *Parameters issued from the simulation of the in cellulo EPR difference spectra of M2- and WT-anamorsin at 10 K. The line shapes were modelled with a combination of Lorentzian function and H-strain (see the text for details).*

Protein	**Spin System**	$\mathbf{g_{max}}$	$\mathbf{g_{mid}}$	$\mathbf{g_{min}}$
M2-anamorsin	S_1=1/2	2.016	1.935	1.890
WT-anamorsin	S_1=1/2	2.016	1.935	1.890
	S_2=1/2	2.002	1.961	1.917

References

(1) Banci, L.; Bertini, I.; Ciofi-Baffoni, S.; Boscaro, F.; Chatzi, A.; Mikolajczyk, M.; Tokatlidis, K.; Winkelmann, J. Anamorsin Is a [2Fe-2S] Cluster-Containing Substrate of the Mia40-Dependent Mitochondrial Protein Trapping Machinery. Chem. Biol. 2011, 18 (6), 794–804. https://doi.org/10.1016/j.chembiol.2011.03.015.

(2) Garboczi, D. N.; Hullihen, J. H.; Pedersen, P. L. Mitochondrial ATP Synthase. Overexpression in Escherichia Coli of a Rat Liver Beta Subunit Peptide and Its Interaction with Adenine Nucleotides. J. Biol. Chem. 1988, 263 (30), 15694–15698.

(3) Beilschmidt, L. K.; Ollagnier de Choudens, S.; Fournier, M.; Sanakis, I.; Hograindleur, M.-A.; Clémancey, M.; Blondin, G.; Schmucker, S.; Eisenmann, A.; Weiss, A.; Koebel, P.; Messaddeq, N.; Puccio, H.; Martelli, A. ISCA1 Is Essential for Mitochondrial Fe4S4 Biogenesis in Vivo. Nat Commun 2017, 8, 15124. https://doi.org/10.1038/ncomms15124.

(4) Carboni, M.; Clémancey, M.; Molton, F.; Pécaut, J.; Lebrun, C.; Dubois, L.; Blondin, G.; Latour, J. M. Biologically Relevant Heterodinuclear Iron–Manganese Complexes. Inorganic Chemistry 2012, 51 (19), 10447–10460. https://doi.org/10.1021/ic301725z.

(5) Carboni, M.; Clémancey, M.; Molton, F.; Pécaut, J.; Lebrun, C.; Dubois, L.; Blondin, G.; Latour, J. M. Correction to Biologically Relevant Heterodinuclear Iron–Manganese Complexes. Inorganic Chemistry 2012, 51 (21), 12053–12053. https://doi.org/10.1021/ic302144r.

(6) Charavay, C.; Segard, S.; Edon, F.; Clémancey, M.; Blondin, G. SimuMoss Software; Univ. Grenoble Alpes, CEA, CNRS, 2012.

(7) Stoll, S.; Schweiger, A. EasySpin, a Comprehensive Software Package for Spectral Simulation and Analysis in EPR. J Magn Reson 2006, 178 (1), 42–55. https://doi.org/10.1016/j.jmr.2005.08.013.

RESULTS

Unraveling the mechanism of cluster and electron transfer from GLRX3 and anamorsin to assemble [4Fe-4S] clusters on the scaffold protein NUBP1

3.2. Unraveling the mechanism of cluster and electron transfer from GLRX3 and anamorsin to assemble [4Fe-4S] clusters on the scaffold protein NUBP1

In preparation

Francesca Camponeschi[1], Sara Matteucci[1], Simone Ciofi-Baffoni[1,2], Lucia Banci[1,2,*]

[1] Magnetic Resonance Center CERM, University of Florence, Via della Lastruccia 3, 50019 Sesto Fiorentino, Florence, Italy

[2] Department of Chemistry, University of Florence, Via della Lastruccia 3, 50019 Sesto Fiorentino, Florence, Italy

[*] E-mail: banci@cerm.unifi.it

Abstract

Human cytosolic monothiol glutaredoxin GLRX3, is an essential component of the cytosolic iron-sulfur cluster assembly machinery, acting as a [2Fe-2S] cluster chaperone. We previously showed that GLRX3 is able to transfer *in vitro* its two $[2Fe\text{-}2S]^{2+}$ clusters to NUBP1. The two clusters are reductively coupled to form a [4Fe-4S] cluster in the presence of generic reductants such as GSH or DTT. Here we show that the two electrons required for the reductive coupling of the two [2Fe-2S]-GLRX3 donated clusters on NUBP1 are provided by human anamorsin, a protein forming in the cell an electron transfer chain with NDOR1. We found through various spectroscopic and biochemical techniques that [2Fe-2S]-anamorsin and $[2Fe\text{-}2S]_2$-$GLRX3_2$-GS_4 form a stable protein-protein complex, which provides [2Fe-2S] clusters and electrons for the assembly of $[4Fe\text{-}4S]^{2+}$ clusters on NUBP1. Moreover, we found that only the $[2Fe\text{-}2S]^{+}$ cluster bound to the M1 motif of [2Fe-2S]-anamorsin, and not that bound to the M2 motif, is able to act as electron donor for the reductive coupling of the two $[2Fe\text{-}2S]^{2+}$ clusters donated by $[2Fe\text{-}2S]_2$-$GLRX3_2$-GS_4.

3.2.1. Introduction

The maturation of iron-sulfur (Fe-S) proteins is a highly conserved, multistep process, involving sophisticated machineries[1,2]. In humans, this process is carried out by a mitochondrial and a cytosolic iron-sulfur assembly (CIA) machinery[3] and the latter was proposed to begin with the assembly of a [4Fe-4S] cluster on a scaffold complex formed by two homologous P-loop nucleoside triphosphatases (NTPases), named NUBP1 and NUBP2[4,5], with the assistance of an electron transfer chain composed by the proteins NDOR1 and anamorsin[6]. Human NUBP1 and NUBP2 form homo- and hetero-complexes *in vitro* and *in vivo*[4,7]. Both proteins have a conserved C-terminal CPXC cluster binding

motif that binds a labile [4Fe-4S] cluster, bridging two protein molecules in the homo- and hetero-complexes[7-9]. In addition, NUBP1 has a conserved N-terminal $CX_{13}CX_2CX_5C$ motif, that tightly binds a second [4Fe-4S] cluster[4,7,9]. The mechanism of the assembly of [4Fe-4S] cluster on these scaffold proteins is still elusive, and the source of iron, sulfide and electrons necessary for the biosynthesis of these [4Fe-4S] clusters is still a matter of debate[2,10].

We recently demonstrated that human cytosolic monothiol glutaredoxin GLRX3, which acts as a [2Fe-2S] cluster chaperone in the early stages of the CIA machinery[11-13], and which is essential *in vivo* for the maturation of cytosolic [4Fe-4S] proteins[14], is able to transfer its two $[2Fe\text{-}2S]^{2+}$ clusters to NUBP1 *in vitro*. The two clusters are then converted into a [4Fe-4S] cluster on NUBP1 thanks to the electrons donated by generic reductants, such as GSH and DTT[7]. *In vivo*, the two electrons required for the reductive coupling of the two [2Fe-2S] clusters on NUBP1 might be provided by an electron transfer chain formed by the CIA components NDOR1 and anamorsin[15,16], since it has been shown that the yeast homologues of NDOR1/anamorsin (i.e. Tah18/Dre2) are strictly required for the maturation of the [4Fe–4S] cluster at the N-terminal motif of the yeast homologue of NUBP1, i.e. Nbp35, as well as that they can be functionally replaced by human NDOR1 and anamorsin proteins.[6] However, no data are to date available showing how the NDOR1/anamorsin-dependent electron transfer chain operates in the [4Fe-4S] cluster assembly on the NTPases.

Anamorsin is a Fe-S binding protein, containing two conserved cysteine-rich motifs, each binding *in vitro* and *in cell* a [2Fe-2S] cluster[15,17,18]: a CX_8CX_2CXC motif (M1 hereafter), followed by a $CX_2CX_7CX_2C$ motif (M2 hereafter). Only the [2Fe-2S] cluster bound to the M1 motif of anamorsin receives electrons from NDOR1, in the electron transfer chain formed by NADPH/NDOR1/anamorsin[16,19], while the [2Fe-2S] cluster bound to the M2 motif does not, and its function is still unknown.

In this work, we investigated, through various spectroscopic and biochemical techniques, the role of anamorsin in the GLRX3-dependent maturation of [4Fe-4S]-NUBP1. We found that [2Fe-2S]-anamorsin and $[2Fe\text{-}2S]_2$-$GLRX3_2$-GS_4 form a stable protein-protein complex, which provides [2Fe-2S] clusters and electrons for the assembly of $[4Fe\text{-}4S]^{2+}$ clusters on NUBP1. Moreover, we found that only the $[2Fe\text{-}2S]^{+}$ cluster bound to the M1 motif of [2Fe-2S]-anamorsin, and not that bound to the M2 motif, is able to act as electron donor for the reductive coupling of the two $[2Fe\text{-}2S]^{2+}$ clusters donated by $[2Fe\text{-}2S]_2$-$GLRX3_2$-GS_4.

3.2.2. Results

Anamorsin provides electrons for the reductive coupling of $[2Fe\text{-}2S]^{2+}$ clusters on NUBP1

Monomeric apo His_6-tagged NUBP1 was mixed with 1.5 equivalents of chemically reconstituted, untagged $[2Fe\text{-}2S]_2$-$GLRX3_2$-GS_4 and 3.0 equivalents of reduced, untagged $[2Fe\text{-}2S]^+$-anamorsin under anaerobic conditions (see Experimental section for details). After ~1 hour, His_6-tagged NUBP1 was isolated from the reaction mixture by Ni^{2+}-affinity chromatography. The isolated NUBP1 protein was then characterized by UV–visible (UV-vis) and NMR spectroscopy, size exclusion chromatography (SEC) and by performing acid-labile sulfide and iron quantification. The UV-vis spectrum was characteristic of a $[4Fe\text{-}4S]^{2+}$-bound protein, with the presence of a broad absorbance band at ~ 410 nm (**Figure 1A**). The paramagnetic 1D ^1H NMR spectrum showed four intense hyperfine shifted signals in the 18-11 ppm spectral region (**Figure 1B**), whose chemical shift values and temperature dependence (**figure S1**) are typical of βCH_2 of cysteines bound to a $[4Fe\text{-}4S]^{2+}$ cluster[20,21], and that are well superimposable with those that we previously observed for the oxidized $[4Fe\text{-}4S]^{2+}$ cluster-bound form of NUBP1.

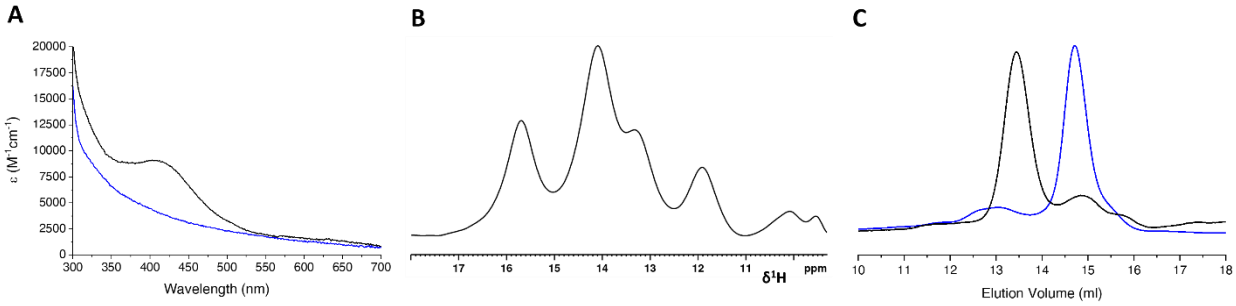

Figure 1. *A) UV-vis spectra of NUBP1 before (blue line) and after (black line) the incubation and isolation from $[2Fe\text{-}2S]_2$-$GLRX3_2$-GS_4 and $[2Fe\text{-}2S]^+$ anamorsin; B) paramagnetic ^1H 1D NMR spectrum of NUBP1 after incubation and isolation from $[2Fe\text{-}2S]_2$-$GLRX3_2$-GS_4 and $[2Fe\text{-}2S]^+$ anamorsin; C) analytical size exclusion chromatography of NUBP1 before (blue line) and after (black line) the incubation and isolation from $[2Fe\text{-}2S]_2$-$GLRX3_2$-GS_4 and $[2Fe\text{-}2S]^+$ anamorsin.*

Acid-labile sulfide and iron analysis on NUBP1 showed the presence of ~0.6 [4Fe-4S] clusters per dimer, which is comparable with the assembly efficiency observed when the cluster transfer reaction was performed in the presence of GSH[7]. Analytical SEC showed that cluster transfer from $[2Fe\text{-}2S]_2$-$GLRX3_2$-GS_4 to NUBP1 in the presence of $[2Fe\text{-}2S]^+$-anamorsin induces protein dimerization (**Figure 1C**). Indeed, the apparent molecular mass of NUBP1 changes from 55.1 kDa, detected for monomeric apo NUBP1 before the mixing, to 102.0 kDa, detected for NUBP1 after incubation and isolation from the reaction mixture, that is very close to the apparent molecular mass expected for dimeric NUBP1, i.e. 111.0 kDa. Overall, these data suggest that anamorsin is able to promote [4Fe-

4S] assembly on NUBP1 providing the electrons required to reductively couple two [2Fe-2S] clusters donated by GLRX3. Moreover, since the C-terminal motif of NUBP1 was exclusively found to promote NUBP1 dimerization by bridging a Fe-S cluster between the two subunits of NUBP1[7], these data indicate that [4Fe-4S] cluster assembly occurs at both the N- and C-terminal motifs of NUBP1.

Table 2. Iron and acid-labile sulfide quantification of NUBP1 after cluster transfer/assembly reaction.

Sample	***Fe[a]***	***S[a]***	***[2Fe-2S]***	***[4Fe-4S]***
NUBP1* after mixing with $[2Fe\text{-}2S]_2$-$GLRX3_2$-GS_4 and WT-anamorsin	2.3± 0.1	2.3± 0.1	-	0.6 ± 0.1
NUBP1* after mixing with $[2Fe\text{-}2S]_2$-$GLRX3_2$-GS_4 and M1-anamorsin	2.6± 0.1	2.9± 0.1	-	0.7 ± 0.1
NUBP1* after mixing with $[2Fe\text{-}2S]_2$-$GLRX3_2$-GS_4 and M2-anamorsin	1.1± 0.1	1.2± 0.1	0.6 ± 0.1	-

a Fe and acid-labile S measurements are reported as mol Fe or S per mol of dimeric protein. Data are the average of three independent samples.

The M1-bound cluster of [2Fe-2S]-anamorsin, but not the M2-bound cluster, provides electrons for the assembly of [4Fe-4S] clusters on NUBP1

As following step, we have characterized which is the [2Fe-2S] cluster of anamorsin between M1- and M2-bound clusters providing the electrons required for the formation of [4Fe-4S] clusters on NUBP1. To do that, the same experiment describe above for wild-type anamorsin (WT-anamorsin, hereafter) was repeated in the presence of i) a construct of anamorsin lacking the last 49 C-terminal residues, and therefore containing only the M1-motif (M1-anamorsin, hereafter), and of ii) a mutant containing only the M2 cluster binding site, obtained by mutating the four cysteines of the M1 motif into alanines (M2-anamorsin, hereafter). His_6-taged monomeric apo NUBP1 was mixed with 1.5 eq of chemically reconstituted, untagged $[2Fe\text{-}2S]_2$-$GLRX3_2$-GS_4 and 3 equivalents of reduced, untagged $[2Fe\text{-}2S]^+$ M1-anamorsin and then isolated from the mixture. It showed a broad absorbance band at ~ 410 nm in the UV-vis spectra characteristic of the oxidized $[4Fe\text{-}4S]^{2+}$ cluster-bound form of NUBP1 (**Figure 2A**), and the four intense hyperfine shifted signals in the paramagnetic 1D ^1H NMR spectrum, characteristic of the oxidized $[4Fe\text{-}4S]^{2+}$ cluster-bound form of NUBP1 (**Figure 2B**). Acid-labile sulfide and iron analysis performed on isolated NUBP1 showed the presence of ~ 0.7 [4Fe-4S] clusters per dimer, which is comparable with what observed when the reaction was performed in the presence of WT-anamorsin. On the contrary, when His_6-tagged apo monomeric

NUBP1 was mixed, and then isolated, with 1.5 equivalents of chemically reconstituted, untagged $[2Fe\text{-}2S]_2$-$GLRX3_2$-GS_4 and 3 equivalents of reduced, untagged $[2Fe\text{-}2S]^+$ M2-anamorsin, the UV-vis spectrum did not match that of NUBP1 isolated from the reaction with $[2Fe\text{-}2S]^+$ WT- or M1-anamorsin. Indeed, broad bands at 320, 460 and 580 nm were observed, which are typical of the binding of a $[2Fe\text{-}2S]^{2+}$ cluster, instead of a $[4Fe\text{-}4S]^{2+}$ cluster (**Figure 2A**). The 1D ^1H NMR spectrum of isolated NUBP1 from the latter mixture showed a broad, unresolved signal in the 30-20 ppm region (**Figure 2B**), that is typical of βCH_2 of cysteines bound to a $[2Fe\text{-}2S]^{2+}$ cluster[20,22]. NUBP1 dimerized upon incubation with $[2Fe\text{-}2S]_2$-$GLRX3_2$-GS_4 and either M1-or M2-anamorsin constructs, as showed by analytical SEC on the NUBP1 after it is isolated from the mixture (**Figure 2C**), indicating that a Fe-S cluster is bridged between two NUBP1 subunits.

Overall, these results indicate that a [2Fe-2S] cluster transfer from $[2Fe\text{-}2S]_2$-$GLRX3_2$-GS_4 occurs to both the N- and C-terminal binding sites of NUBP1, but only the $[2Fe\text{-}2S]^+$ cluster bound to the M1 motif of anamorsin is able to transfer electrons to reductively couple the GLRX3-donated [2Fe-2S] clusters and to assemble a [4Fe-4S] cluster. It is worth noting that the amount of $[4Fe\text{-}4S]^{2+}$ cluster bound to dimeric NUBP1 after incubation and isolation from $[2Fe\text{-}2S]_2$-$GLRX3_2$-GS_4 /$[2Fe\text{-}2S]^+$ M1-anamorsin mixture is almost identical to that observed after incubation and isolation from $[2Fe\text{-}2S]_2$-$GLRX3_2$-GS_4 /$[2Fe\text{-}2S]^+$ WT-anamorsin mixture. This suggests that the M1-bound cluster of anamorsin acts as an electron donor for the assembly of [4Fe-4S] clusters on NUBP1 independently of the M2-bound cluster, with the lack of any cooperativity between the two clusters in the electron transfer event. The M2-bound cluster is thus not playing a role in the electron transfer event and further studies will be required to establish its functional role. This is in agreement with previous finding showing that NDOR1 (or Tah18) is able to reduce exclusively the M1-bound [2Fe-2S] cluster of anamorsin (or Dre2)[6,15].

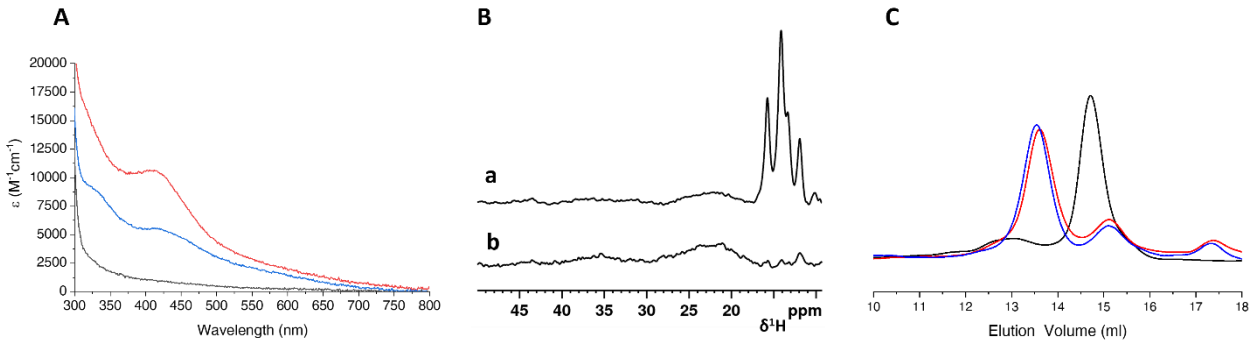

Figure 2. *A) UV-vis spectra of NUBP1 before (black line) and after the incubation and isolation from $[2Fe\text{-}2S]_2$-$GLRX3_2$-GS_4 and M1- (red line) and M2-anamorsin (red line); B) paramagnetic ^1H 1D NMR spectra of NUBP1 after incubation and isolation from $[2Fe\text{-}2S]_2$-$GLRX3_2$-GS_4 and a) M1- and b) M2-anamorsin; C) analytical size exclusion chromatography of NUBP1 before (black line) and after the incubation and isolation from $[2Fe\text{-}2S]_2$-$GLRX3_2$-GS_4 and M1- (red line) and M2-anamorsin (red line).*

A complex between $[2Fe\text{-}2S]_2$-$GLRX3_2$-GS_4 and [2Fe-2S]-anamorsin is the key intermediate driving the assembly of [4Fe-4S] clusters on NUBP1

In order to clarify the mechanism of the GLRX3/anamorsin-dependent $[4Fe\text{-}4S]^{2+}$ $NUBP1_2$ maturation, we investigated the interaction between $[2Fe\text{-}2S]_2$-$GLRX3_2$-GS_4 and $[2Fe\text{-}2S]^{2+}$ WT-anamorsin. $[2Fe\text{-}2S]_2$-$GLRX3_2$-GS_4 and $[2Fe\text{-}2S]^{2+}$-anamorsin were mixed at different protein:protein ratio and these mixtures were then analyzed by analytical SEC. $[2Fe\text{-}2S]_2$-$GLRX3_2$-GS_4 elutes with two peaks, corresponding to homodimeric $[2Fe\text{-}2S]_2$-$GLRX3_2$-GS_4 (12.95 ml) and apo monomeric GLRX3 (14.60 ml), with apparent molecular mass of 132.5 and 62.4 kDa, respectively. $[2Fe\text{-}2S]^{2+}$ WT-anamorsin elutes with a main peak at 14.09 ml, corresponding to an apparent molecular mass of 78.7 kDa. When sub-stoichiometric amounts of $[2Fe\text{-}2S]^{2+}$ WT-anamorsin were added to $[2Fe\text{-}2S]_2$-$GLRX3_2$-GS_4 (i.e. up to 0.5 equivalents), the peak corresponding to $[2Fe\text{-}2S]_2$-$GLRX3_2$-GS_4 species, progressively decreased in intensity (**figure 3A**), and, at the same time, a new peak eluting at 12.10 ml, was observed (**figure 3A**), suggesting the formation of a GLRX3-anamorsin heterocomplex. The apparent molecular mass of this new species was 197.7 kDa, that is very close to the sum of the apparent molecular mass of one molecule of $[2Fe\text{-}2S]_2$-$GLRX3_2$-GS_4 and one molecule of [2Fe-2S] WT-anamorsin, i.e. 211.2 kDa. The elution volume of this complex was significantly different from that observed for a 1:1 mixture of apo GLRX3 and $[2Fe\text{-}2S]^{2+}$ WT-anamorsin, eluting as a single peak at 12.75 ml (**figure 3A**) and having the corresponding species an apparent molecular mass of 142.7 kDa. This species corresponds to a heterodimeric complex between apo GLRX3 and [2Fe-2S]-anamorsin having indeed an apparent molecular mass very close to the sum of the apparent molecular masses of one molecule of apo GLRX3 and one molecule of $[2Fe\text{-}2S]^{2+}$ WT-anamorsin, i.e. 141.1 kDa. By further increasing the amount of $[2Fe\text{-}2S]^{2+}$ WT-anamorsin up to 2 eq., the peak corresponding to $[2Fe\text{-}2S]_2$-$GLRX3_2$-GS_4/$[2Fe\text{-}2S]^{2+}$ WT-anamorsin complex decreased in intensity and a new peak at 11.23 ml is formed. This suggests an increase in the size of the complex formed by the two proteins. The apparent molecular mass of the new species at 11.23 ml is 288.4 kDa, that is very close to the apparent molecular mass expected for the formation of a complex between one $[2Fe\text{-}2S]_2$-$GLRX3_2$-GS_4 molecule and two $[2Fe\text{-}2S]^{2+}$ WT-anamorsin molecules (i.e. 289.8 kDa). The complete formation of this larger MW complex was reached at 2 eq. of anamorsin, in agreement with a 1:2 stoichiometry of the complex, i.e. one homodimer of GLRX3 per two monomers of anamorsin.

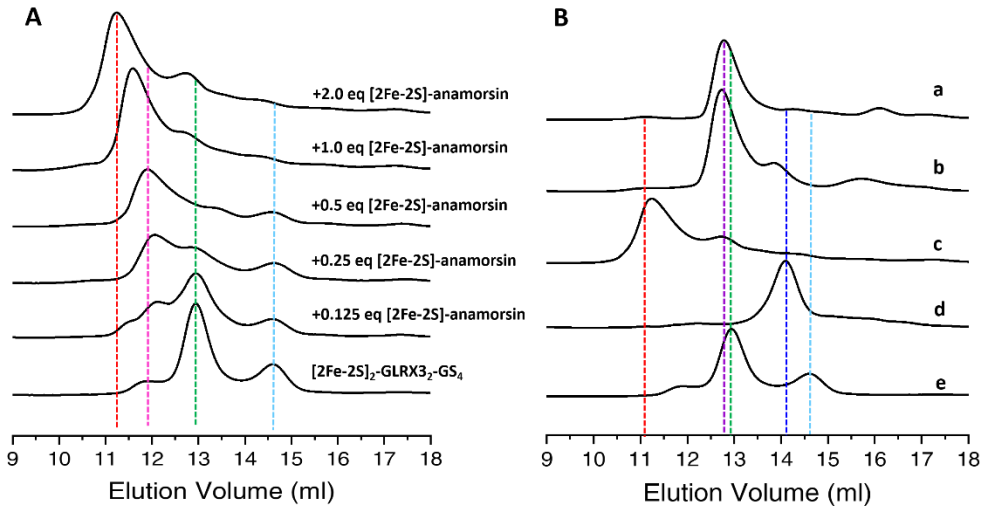

Figure 3. *[2Fe-2S]$_2$-GLRX3$_2$-GS$_4$ and [2Fe-2S]-anamorsin form a stable heterotrimeric complex that drives the assembly of [4Fe-4S] clusters on NUBP1. A) Analytical size exclusion chromatography of [2Fe-2S]$_2$-GLRX3$_2$-GS$_4$ /[2Fe-2S]$^{2+}$-anamorsin mixtures.. B) The quaternary structure of GLRX3-anamorsin complex changes upon cluster transfer to NUBP1. Analytical size exclusion chromatography of a) a 1:1 mixture of apo GLRX3 and [2Fe-2S]$^{2+}$-anamorsin; b) [2Fe-2S]$_2$-GLRX3$_2$-GS$_4$/[2Fe-2S]$^{2+}$-anamorsin 1:2 mixture after incubation and isolation from NUBP1; [2Fe-2S]$_2$-GLRX3$_2$-GS$_4$/[2Fe-2S]$^{2+}$-anamorsin 1:2 mixture before incubation with NUBP1; d) [2Fe-2S]$^{2+}$-anamorsin; e) [2Fe-2S]$_2$-GLRX3$_2$-GS$_4$. Vertical, dotted lines in A and B panels indicate the main peaks with their elution volumes: cyan = apo GLRX3; green = [2Fe-2S]$_2$-GLRX3$_2$-GS$_4$; blue = [2Fe-2S]$^{2+}$-anamorsin; purple = apo GLRX3:[2Fe-2S]$^{2+}$-anamorsin 1:1 complex; magenta = [2Fe-2S]$_2$-GLRX3$_2$-GS$_4$:[2Fe-2S]$^{2+}$-anamorsin 1:1 complex; red = [2Fe-2S]$_2$-GLRX3$_2$-GS$_4$:[2Fe-2S]$^{2+}$-anamorsin 1:2 complex*

Analytical SEC was also applied to investigate changes in the quaternary structure of [2Fe-2S]$_2$-GLRX3$_2$-GS$_4$/[2Fe-2S]$^+$ WT-anamorsin$_2$ complex upon the interaction with His$_6$-tagged apo NUBP1. The [2Fe-2S]$_2$-GLRX3$_2$-GS$_4$/[2Fe-2S]$^+$ WT-anamorsin$_2$ complex was incubated with His$_6$-tagged apo NUBP1 and then separated from NUBP1 by Ni^{2+}-affinity chromatography. The unbound fraction containing [2Fe-2S]$_2$-GLRX3$_2$-GS$_4$ and [2Fe-2S] WT-anamorsin was then analyzed by analytical SEC. The two proteins co-elutes with a main single peak, which has a different elution volume and therefore a different apparent molecular mass from that observed for the starting [2Fe-2S]$_2$-GLRX3$_2$-GS$_4$/[2Fe-2S]$^+$ WT-anamorsin$_2$ complex (**figure 3B**), indicating the occurrence of significant changes in the quaternary structure of the GLRX3/anamorsin complex. The new peak, eluting at 12.73 ml, corresponds to a major species with an apparent molecular mass of 146.0 kDa, that is very close to the sum of the apparent molecular masses of one molecule of apo GLRX3 and one molecule of [2Fe-2S] WT-anamorsin, i.e. 146.9 kDa, indicating the formation of a 1:1 GLRX3-anamorsin heterodimer. This can be reasonably interpreted as the result of the transfer of two clusters from GLRX3 to NUBP1 to assemble [4Fe-4S] clusters. Indeed, the two [2Fe-2S] clusters bridging the two subunits of dimeric [2Fe-2S]$_2$-GLRX3$_2$-GS$_4$ are required for the stability of the quaternary structure of [2Fe-2S]$_2$-GLRX3$_2$-GS$_4$:[2Fe-2S] WT-anamorsin$_2$ complex.

3.2.3. Discussion

NUBP1, which is essential for cytosolic Fe-S protein assembly[4], has been proposed to act in the early stages of the CIA machinery as a scaffold protein[4,5], where the [4Fe-4S] clusters are formed and then distributed in the cytosol. However, the mechanism of the *de novo* assembly of [4Fe-4S] clusters on NUBP1 is still elusive. Recently, we proposed that the cytosolic [2Fe-2S] cluster chaperone GLRX3 is the source of Fe and S necessary for the assembly of [4Fe-4S] clusters on NUBP1 in cell[7]. Indeed, we showed that $[2Fe\text{-}2S]_2$-$GLRX3_2$-GS_4 transfers $[2Fe\text{-}2S]^{2+}$ clusters to both N-terminal and C-terminal motifs of monomeric apo NUBP1 *in vitro*, inducing protein dimerization. Two $[2Fe\text{-}2S]^{2+}$ clusters donated by $[2Fe\text{-}2S]_2$-$GLRX3_2$-GS_4 were then reductively coupled to form a $[4Fe\text{-}4S]^{2+}$ cluster at the N-terminal motif of NUBP1, but not at the C-terminal cluster binding motif, where only a $[2Fe\text{-}2S]^{2+}$ cluster was observed. Functional data available on yeast Nbp35 supported the proposed GLRX3 chaperone function, as depletion of Nbp35 resulted in an accumulation of iron on GLRX3 yeast homologs, Grx3/4,[23] likely in the form of a [2Fe-2S] cluster, that cannot be transferred anymore to Nbp35. The two electrons required to generate *in vitro* the $[4Fe\text{-}4S]^{2+}$ cluster on NUBP1 were provided in our previous *in vitro* experiments by GSH. However, anamorsin and the NADPH-dependent diflavin oxidoreductase 1 (NDOR1), that form a stable complex,[6,16] as well as the yeast homolog Dre2/Tah18 complex, are thought to provide reducing equivalents for the assembly of [4Fe-4S] clusters. In the current working model, NADPH/NDOR1/anamorsin electron transfer chain provides electrons for the maturation of the [4Fe-4S] cluster at the N-terminal motif of the P-loop NTPases protein NUBP1. Moreover, a specific interaction between anamorsin and NUBP1 homologues has been reported in plants,[25,26] supporting the model where the NDOR1/anamorsin electron transfer chain assembles a $[4Fe–4S]^{2+}$ cluster on the N-terminal motif of NUBP1.

In this work, we showed that anamorsin acts as an electron donor in the GLRX3-dependent [4Fe-4S]-NUBP1 maturation process and we have elucidated the mechanism of this process. Our work thus provides the first evidence of the role of this human protein as an early constituent of the CIA machinery.

We showed that the two electrons required for the conversion of two $[2Fe\text{-}2S]^{2+}$ clusters donated by GLRX3 into a $[4Fe\text{-}4S]^{2+}$ cluster on the N-terminal site of NUBP1 are supplied *in vitro* by $[2Fe\text{-}2S]^{+}$-anamorsin.

We also found that the $[2Fe\text{-}2S]^{+}$ cluster bound to the M1 motif of reduced anamorsin was able to donate electrons for the reductive coupling process, independently of the presence of the $[2Fe\text{-}2S]^{+}$ cluster bound to the M2 motif. On the contrary, the M2-bound cluster was not able to transfer

electrons to NUBP1 once the M1-bound cluster was absent. No significant differences where observed in the efficiency of the cluster transfer/assembly process when only the M1-bound cluster or both M1- and M2-bound clusters were present. This indicates that only the $[2Fe\text{-}2S]^{+}$ cluster bound to the M1 motif of anamorsin transfers electrons for the [4Fe-4S] cluster assembly process, allowing to exclude any cooperativity effect between the [2Fe-2S] clusters bound to the M1- and M2-motif of anamorsin in the formation of a [4Fe-4S] cluster on NUBP1. These results nicely fit with what reported about the function of the two clusters of anamorsin. Indeed, during the electron transfer chain, the FMN moiety of NDOR1 receives electrons from NADPH[19] and then exclusively transfers them to the oxidized $[2Fe\text{-}2S]^{2+}$ cluster bound to the M1 motif of anamorsin.[6,16,17] On the contrary, the $[2Fe\text{-}2S]^{2+}$ cluster bound to the M2 motif of anamorsin seems not to take part in the electron transfer process *in vitro*, and its function is currently unknown. Our findings support that the M1 cluster of anamorsin has a redox function in cell.

We showed that the cluster transfer/assembly mechanism on NUBP1 involves the formation of a protein-protein complex between dimeric $[2Fe\text{-}2S]_2$-$GLRX3_2$-GS_4 and [2Fe-2S]-anamorsin. The two holo proteins form a stable 1:2 hetero-complex, able to provide two GLRX3-bound $[2Fe\text{-}2S]^{2+}$ clusters and two electrons, one from each M1-bound cluster on each anamorsin molecule in the complex, to stoichiometrically assemble a [4Fe-4S] cluster on NUBP1. We might speculate that the protein-protein interaction, that involves the N-terminal domains of GLRX3 and anamorsin,[27] bring closer together the two [2Fe-2S] clusters of $[2Fe\text{-}2S]_2$-$GLRX3_2$-GS_4 and the two electrons on the reduced cluster bound to the M1 motif of anamorsin, allowing the [2Fe-2S] clusters- and electron-transfer events to take place through a concerted mechanism (**scheme 1**).

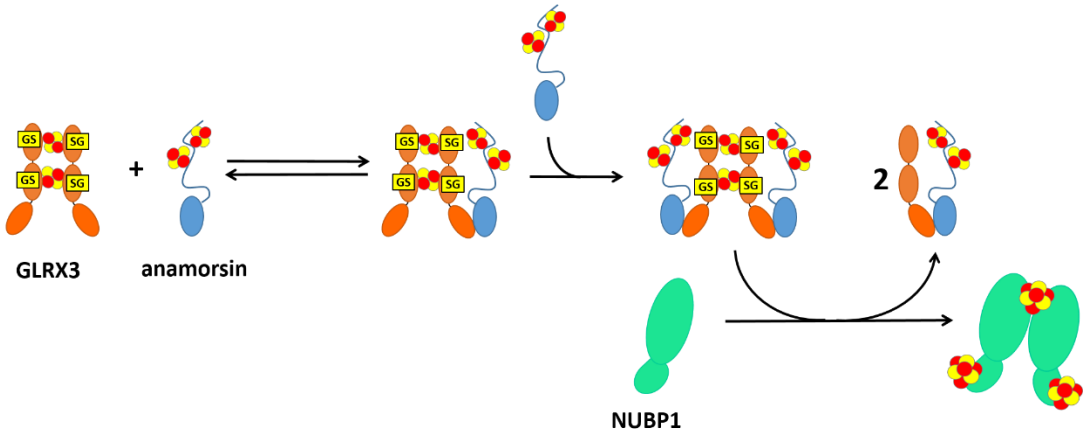

Scheme 1. *Mechanism of the [4Fe-4S] cluster assembly on NUBP1.When $[2Fe\text{-}2S]_2$-$GLRX3_2$-GS_4 is mixed with $[2Fe\text{-}2S]_2^{+}$-anamorsin, the N-terminal domain of the two proteins interact and a 1:2 $[2Fe\text{-}2S]_2$-$GLRX3_2$-GS_4:$[2Fe\text{-}2S]_2^{+}$-anamorsin complex is formed. This complex transfers two [2Fe-2S] clusters from $[2Fe\text{-}2S]_2$-$GLRX3_2$-GS_4 and two electrons for the assembly of [4Fe-4S] clusters on NUBP1. The latter process induces changes in the quaternary structure of the $[2Fe\text{-}2S]_2$-$GLRX3_2$-GS_4/$[2Fe\text{-}2S]_2$-anamorsin complex, with the production of a 1:1 apo GLRX3:$[2Fe\text{-}2S]_2$-anamorsin complex.*

Conclusions

Our study contributes to the understanding of the mechanism of Fe-S protein biogenesis in the cytosol, providing evidences for role of anamorsin as an electron donor in the cytosolic [4Fe-4S] clusters assembly process. We propose that one molecule of $[2Fe\text{-}2S]_2$-$GLRX3_2$-GS_4 and two molecules of [2Fe-2S] anamorsin form a stable complex, that acts as a component of the CIA machinery at its early stage, by transferring two GLRX3-bound [2Fe-2S] clusters to NUBP1 and providing two electrons, one from each reduced cluster bound to the M1 motif of anamorsin, to stoichiometrically assemble a [4Fe-4S] cluster on NUBP1.

3.2.4. Experimental Section

Protein production

Human monomeric apo NUBP1, human $[2Fe\text{-}2S]_2$-$GLRX3_2$-GS_4 and human $[2Fe\text{-}2S]^{2+}$ WT- M1- and M2-anamorsin were expressed and purified following previously reported procedures[7,18,27].

Reduced $[2Fe\text{-}2S]^{+}$ WT- M1- and M2-anamorsin were obtained by adding sodium dithionite in stoichiometric amount. The buffer was then exchanged by PD10 desalting column (GE Healthcare) to remove any excess of sodium dithionite.

Protein, iron and acid-labile sulfide quantification.

Protein quantification was carried out with the Bradford protein assay, using BSA as a standard. Non-heme iron and acid-labile sulfide content was determined as described previously[28].

Biochemical and spectroscopic UV-vis and NMR methods.

For all the measurements, the protein samples were in degassed 50 mM Tris buffer pH 8.0, 150 mM NaCl, if not differently specified.

The quaternary structure of the proteins was analyzed through analytical SEC on a Superdex 200 10/300 Increase column (GE Healthcare). Column was calibrated with gel filtration marker calibration kit, 12.4-2000 kDa (Sigma-Aldrich), to obtain the apparent molecular masses of the detected species. Samples were loaded on the pre-equilibrated column. Elution profiles were recorded at 280 nm with a flow rate of 0.7 mL/min.

UV-visible (UV-vis) spectra were anaerobically acquired on a Cary 50 Eclipse spectrophotometer.

Paramagnetic 1D ^{1}H NMR experiment were performed on a Bruker Avance spectrometer operating at 400 MHz ^{1}H Larmor frequency an equipped with a ^{1}H optimized 5 mm probe. Water signal was suppressed via fast repetition experiments and water selective irradiation[29]. Experiments were typically performed using an acquisition time of 50 ms, and an overall recycle delay of 80 ms. Sample concentration was in the range 0.2-0.4 mM, in degassed 50 mM Tris buffer pH 8.0, 150 mM NaCl, 100 % D_2O. Squared cosine and exponential multiplications were applied prior to Fourier Transformation. Manual baseline correction was performed using polynomial functions.

Cluster transfer from $[2Fe\text{-}2S]_2$-$GLRX3_2$-GS_4 to His_6-tagged apo wtNUBP1

His_6-tagged monomeric apo NUBP1 was incubated under anaerobic conditions with 1.5 equivalents of $[2Fe\text{-}2S]_2$-$GLRX3_2$-GS_4, and 3.0 equivalents of reduced, $[2Fe\text{-}2S]^{+}$ WT-anamorsin or 1.5 equivalents reduced, $[2Fe\text{-}2S]^{+}$ M1-anamorsin or $[2Fe\text{-}2S]^{+}$ M2-anamorsin for 1 hour at room temperature in 40 mM sodium phosphate buffer pH 8.0, 400 mM NaCl and 5 mM imidazole. The final NUBP1: $[2Fe\text{-}2S]_2$-$GLRX3_2$-GS_4: $[2Fe\text{-}2S]^{+}$-anamorsin ratio correspond to the stoichiometric amounts of [2Fe-2S] clusters from $[2Fe\text{-}2S]_2$-$GLRX3_2$-GS_4 and electrons from $[2Fe\text{-}2S]^{+}$-anamorsin, required to fully saturate the cluster binding motifs present in NUBP1 with a [4Fe-4S] cluster, i.e. three per dimeric wtNUBP1.[7] Separation of His_6-tagged NUBP1 from untagged GLRX3 and untagged anamorsin after the reaction was performed in anaerobic conditions, by loading the reaction mixtures on a His GraviTrap column pre-equilibrated with 40 mM sodium phosphate buffer pH 8.0, 400 mM NaCl and 5 mM imidazole. The His_6-tagged NUBP1 species was eluted with 40 mM sodium phosphate buffer pH 8.0, 400 mM NaCl and 400 mM imidazole. After concentration the buffer was exchanged by PD-10 desalting column in the appropriate degassed buffer required to perform analytical gel filtration, iron and acid-labile sulfide quantification and to acquire UV-vis and paramagnetic 1D ^{1}H NMR spectra.

References

1. Lill, R. Function and biogenesis of iron-sulphur proteins. Nature 460, 831–838 (2009).

2. Ciofi-Baffoni, S., Nasta, V. & Banci, L. Protein networks in the maturation of human iron–sulfur proteins. Metallomics 10, 49–72 (2018).

3. Netz, D. J. A., Mascarenhas, J., Stehling, O., Pierik, A. J. & Lill, R. Maturation of cytosolic and nuclear iron-sulfur proteins. Trends Cell Biol. 24, 303–312 (2014).

4. Stehling, O. et al. Human Nbp35 is essential for both cytosolic iron-sulfur protein assembly and iron homeostasis. Mol. Cell. Biol. 28, 5517–5528 (2008).

5. Stehling, O. et al. Function and crystal structure of the dimeric P-loop ATPase CFD1 coordinating an exposed [4Fe-4S] cluster for transfer to apoproteins. Proc. Natl. Acad. Sci. U.S.A. 115, E9085–E9094 (2018).

6. Netz, D. J. A. et al. Tah18 transfers electrons to Dre2 in cytosolic iron-sulfur protein biogenesis. Nat. Chem. Biol. 6, 758–765 (2010).

7. Camponeschi, F., Prusty, N. R., Heider, S. A. E., Ciofi-Baffoni, S. & Banci, L. GLRX3 Acts as a [2Fe–2S] Cluster Chaperone in the Cytosolic Iron–Sulfur Assembly Machinery Transferring [2Fe–2S] Clusters to NUBP1. J. Am. Chem. Soc. 142, 10794–10805 (2020).

8. Netz, D. J. A., Pierik, A. J., Stümpfig, M., Mühlenhoff, U. & Lill, R. The Cfd1-Nbp35 complex acts as a scaffold for iron-sulfur protein assembly in the yeast cytosol. Nat. Chem. Biol. 3, 278–286 (2007).

9. Netz, D. J. A. et al. A bridging [4Fe-4S] cluster and nucleotide binding are essential for function of the Cfd1-Nbp35 complex as a scaffold in iron-sulfur protein maturation. J. Biol. Chem. 287, 12365–12378 (2012).

10. Paul, V. D. & Lill, R. Biogenesis of cytosolic and nuclear iron-sulfur proteins and their role in genome stability. Biochim. Biophys. Acta 1853, 1528–1539 (2015).

11. Banci, L. et al. N-terminal domains mediate [2Fe-2S] cluster transfer from glutaredoxin-3 to anamorsin. Nat. Chem. Biol. 11, 772–778 (2015).

12. Banci, L., Camponeschi, F., Ciofi-Baffoni, S. & Muzzioli, R. Elucidating the Molecular Function of Human BOLA2 in GRX3-Dependent Anamorsin Maturation Pathway. J. Am. Chem. Soc. 137, 16133–16143 (2015).

13. Frey, A. G., Palenchar, D. J., Wildemann, J. D. & Philpott, C. C. A Glutaredoxin·BolA Complex Serves as an Iron-Sulfur Cluster Chaperone for the Cytosolic Cluster Assembly Machinery. J. Biol. Chem. 291, 22344–22356 (2016).

14. Haunhorst, P. et al. Crucial function of vertebrate glutaredoxin 3 (PICOT) in iron homeostasis and hemoglobin maturation. Mol. Biol. Cell 24, 1895–1903 (2013).

15. Banci, L. et al. Human anamorsin binds [2Fe-2S] clusters with unique electronic properties. J. Biol. Inorg. Chem. 18, 883–893 (2013).

16. Banci, L. et al. Molecular view of an electron transfer process essential for iron-sulfur protein biogenesis. Proc. Natl. Acad. Sci. U.S.A. 110, 7136–7141 (2013).

17. Banci, L. et al. Anamorsin is a [2Fe-2S] cluster-containing substrate of the Mia40-dependent mitochondrial protein trapping machinery. Chem. Biol. 18, 794–804 (2011).

18. Matteucci, S. et al. In Cellulo Mössbauer and EPR Studies Bring New Evidence to the Long-Standing Debate on Iron–Sulfur Cluster Binding in Human Anamorsin. Angewandte Chemie International Edition 60, 14841–14845 (2021).

19. Murataliev, M. B., Feyereisen, R. & Walker, F. A. Electron transfer by diflavin reductases. Biochim. Biophys. Acta 1698, 1–26 (2004).

20. Banci, L., Camponeschi, F., Ciofi-Baffoni, S. & Piccioli, M. The NMR contribution to protein-protein networking in Fe-S protein maturation. J. Biol. Inorg. Chem. 23, 665–685 (2018).

21. Bertini, I., Capozzi, F., Luchinat, C., Piccioli, M. & Vila, A. J. The Fe4S4 Centers in Ferredoxins Studied through Proton and Carbon Hyperfine Coupling. Sequence-Specific Assignments of Cysteines in Ferredoxins from Clostridium acidi urici and Clostridium pasteurianum. J. Am. Chem. Soc. 116, 651–660 (1994).

22. Banci, L., Bertini, I. & Luchinat, C. The 1H NMR parameters of magnetically coupled dimers—The Fe2S2 proteins as an example. in Bioinorganic Chemistry 113–136 (Springer Berlin Heidelberg, 1990).

23. Mühlenhoff, U. et al. Cytosolic monothiol glutaredoxins function in intracellular iron sensing and trafficking via their bound iron-sulfur cluster. Cell Metab. 12, 373–385 (2010).

24. Zhang, Y. et al. Dre2, a conserved eukaryotic Fe/S cluster protein, functions in cytosolic Fe/S protein biogenesis. Mol. Cell. Biol. 28, 5569–5582 (2008).

25. Bych, K. et al. The essential cytosolic iron-sulfur protein Nbp35 acts without Cfd1 partner in the green lineage. J. Biol. Chem. 283, 35797–35804 (2008).

26. Bastow, E. L., Bych, K., Crack, J. C., Le Brun, N. E. & Balk, J. NBP35 interacts with DRE2 in the maturation of cytosolic iron-sulphur proteins in Arabidopsis thaliana. Plant J. 89, 590–600 (2017).

27. Banci, L. et al. N-terminal domains mediate [2Fe-2S] cluster transfer from glutaredoxin-3 to anamorsin. Nat. Chem. Biol. 11, 772–778 (2015).

28. Banci, L. et al. Anamorsin is a [2Fe-2S] cluster-containing substrate of the Mia40-dependent mitochondrial protein trapping machinery. Chem. Biol. 18, 794–804 (2011).

29. Patt, S. L. & Sykes, B. D. Water Eliminated Fourier Transform NMR Spectroscopy. J. Chem. Phys. 56, 3182–3184 (1972).

RESULTS

Study of the [4Fe-4S] clusters assembly process on the cytosolic NUBP1-NUBP2 scaffold complex

3.3. Study of the [4Fe-4S] clusters assembly process on the cytosolic NUBP1-NUBP2 scaffold complex

3.3.1. Introduction

The cytosolic Fe-S protein assembly machinery is structured in main two steps, the early one, necessary for Fe-S cluster assembly, and the last one, responsible for cluster transfer and insertion into target cytosolic and nuclear proteins. The process has been mostly characterized in yeast, where the first component to be identified was the essential and highly conserved nucleotide triphosphatases (NTPases) CFD1 and NBP35 proteins[2728]. These two proteins form a CFD1-NBP35 heterocomplex, that performs a scaffold function in the early step of the CIA machinery by *de novo* assembling [4Fe-4S] clusters[29,30]. This process is assisted by an electron transfer chain composed by Tah18 and Dre2 proteins[31].

The human homologues of NBP35 and CFD1 are NUBP1 and NUBP2, respectively. NUBP1 and NUBP2 share a high degree of sequence identity with NBP35 and CFD1, respectively, and it has been proposed that the two human proteins cooperate in the same molecular process of the yeast homologues[29,30], being responsible for the assembly of nascent Fe-S clusters that are ultimately inserted into the active sites of apo Fe-S enzymes localized to the cytosol and nucleus. Accordingly, it has been shown that NUBP1 and NUBP2 interact *in vivo*. NUBP1 has a highly conserved N-terminal $CX_{13}CX_2CX_5C$ motif[29,46,47], that is absent in the NUBP2 family, and a conserved C-terminal CPXC motif, that is also present in NUBP2. The latter motif coordinates a labile [4Fe–4S] cluster bridging two protein molecules in homodimeric NUBP1, NBP35, CFD1, and in the CFD1–NBP35 heterocomplex[30] and it was found to be essential for the function of the yeast CFD1 and NBP35 in the assembly of cytosolic [4Fe–4S] proteins[48]. Moreover, NUBP1 binds a second [4Fe-4S] cluster to the N-terminal motif[48], which is essential for the protein function [30,49]. The characterization of the Fe–S cluster binding properties and quaternary structure of NUBP1-NUBP2 complex is an essential prerequisite to investigate in detail the Fe–S cluster assembly pathway in the cytosol. However, while the quaternary structure and cluster binding properties of NUBP1 have been recently elucidated[33], those of NUBP2 and of NUBP1-NUBP2 heterocomplex are still poorly investigated. My work was therefore focused on the production and characterization of the NUBP1-NUBP2 heterocomplex, and on the study of the *de novo* assembly of [4Fe-4S] clusters in cytosol.

The protocol for the production of NUBP1 protein was previously developed by Prof. Banci's group, while any attempt to purify NUBP2 by the same group failed. Indeed, the protein was expressed in high yield, but it showed high instability. Two strategies were therefore adopted in my PhD work to

overcome the problems related to NUBP2 production: i) the use of a stable homologue of NUBP2, to reconstitute *in vitro* a model for the NUBP1-NUBP2 heterocomplex and ii) the coexpression and copurification of the human NUBP1-NUBP2 heterocomplex.

3.3.2. ctCFD1 as a model for NUBP2 protein

Recently, the crystal structure of the *Chaetomium thermophilum* homologue of NUBP2, i.e. ctCFD1, was determined at 2.6 Å-resolution[50]. ctCFD1 was reported to have higher stability than the yeast CFD1 and the human NUBP2[11] ; the X-ray crystallographic study showed that the protein forms a dimer, where the two ctCFD1 monomers coordinate a bridging [4Fe-4S] cluster via two conserved cysteine residues[11], as suggested for the yeast CFD1 and the human NUBP2.

Bioinformatics analysis was therefore performed to establish if ctCFD1 protein could be an adequate model for NUBP2 protein

3.3.3. Bioinformatics analysis

The crystal structure of ctCFD1 at 2.57 Å of resolution (PDB: 6G2G) showed a homodimer that forms a new structural subclass which binds a bridging [4Fe-4S] cluster at surface-exposed CPXC motifves(Fig. 1). The cluster is coordinated by cysteine residues C199 and C202 of the conserved CPXC motif of each subunit. The corresponding residues of *S. cerevisiae* CFD1 and NBP35 have been found to be essential for both cell viability and Fe-S cluster binding, and hence a bridging Fe-S cluster coordination had been demonstrated.

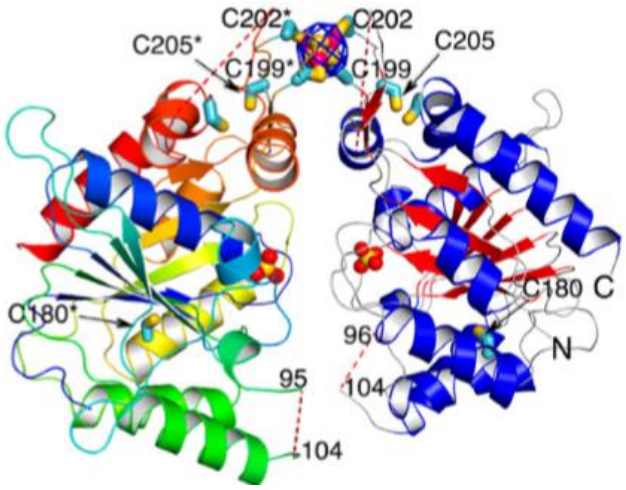

Fig. 1 – Crystal structure of dimeric ctCfd1. The [4Fe-4S] cluster at the dimer interface is shown. Conserved cysteine residues are highlighted as sticks with carbon in cyan and sulfur in gold. Stars indicate residues belonging to the symmetry mate. Dashed lines indicate regions with weak electron density

Sequence alignment of the fungus and human proteins performed by ClustalW Omega Alignment program showed that ctCFD1 has 62% of sequence homology with the human protein NUBP2 (Fig. 2) in which are conserved the CPXC motifs.

```
Chaetomium      -------MSLSQVKHIILVLSGKGGVGKSSVTTQLALSLSQAGYSVGVLDVDLTGPSIPR 53
Human           MEAAAEPGNLAGVRHIILVLSGKGGVGKSTISTELALALRHAGKKVGILDVDLCGPSIPR 60
.*: *:*****************:::*:***:* :** .**:***** ******

Chaetomium      MFAVEDAKVKQGSGGWLPVVVHEANPSTGIGSLRVMSLGFLLPRRGDAVIWRGPKKTAMV 113
Human           MLGAQGRAVHQCDRGWAPVFLDRE------QSISLMSVGFLLEKPDEAVVWRGPKKNALI 114
*:..:.  *:* . ** **.:..        *: :**:**** : .:**:******.*::

Chaetomium      RQFMSDVLWDELDFLLVDTPPGTSDEHISLAETLLQEARPGQLSGAIVVTTPQAVATADV 173
Human           KQFVSDVAWGELDYLVVDTPPGTSDEHMATIEA----LRPYQPLGALVVTTPQAVSVGDV 170
:**:*** *.***:*:***********::  *:     ** *  **:********:..**

Chaetomium      RKELNFCKKTGIRVLGVVENMSGFVCPNCSECTNIFSSGGGEIMANDFNVRFLGRVPIDP 233
Human           RRELTFCRKTGLRVMGIVENMSGFTCPHCTECTSVFSRGGGEELAQLAGVPFLGSVPLDP 230
*:**.**:***:**:*:*******.**:*:***.:** **** :*:  .* *** **:**

Chaetomium      QFLVLIETGKRPR--YPEGTKVNSQDLSFQHLEQVDNADNPETPNSSLLVDKYRDCSLAP 291
Human           ALMRTLEEGHDFIQEFPGSPAF-------AALTSIAQ----------KILDATPACLP-- 271
::  :* *:     :* .  .         * .: :           ::*    *

Chaetomium      IFRAITADVVVAVEQASGS    310
Human           -------------------    271
```

Fig. 2 – Sequence alignment of ctCFD1 and NUBP2 proteins

ctCFD1 was then used as a template to obtain a structural model of NUBP2, using the Modeller 3.11 software (Fig. 3). The global RMSD between the two structures is 1.86 Å, while the local RMSD around the cysteines region is 0.4 Å, indicating that the fungus protein is a good candidate model for NUBP2 protein.

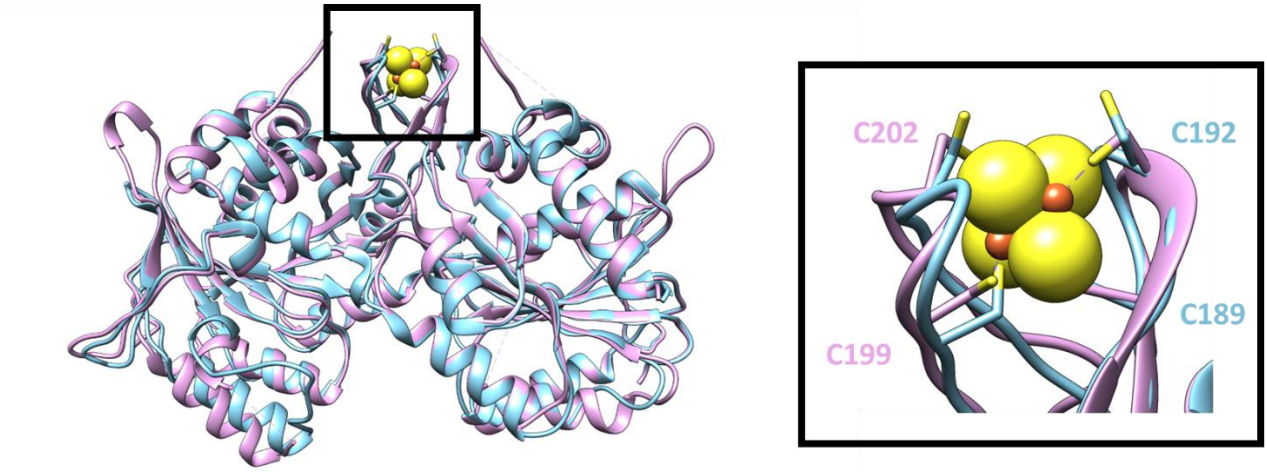

Fig. 3 – Experimental model of NUBP2 (blue) overlapped of ctCFD1 (violet). The conserved cysteines are shown in yellow

3.3.4. Recombinant production and spectroscopic characterization of ctCFD1

The cDNA coding for the fungus protein ctCFD1 was inserted into the pET28 plasmid for expression in E.coli, using NdeI and XhoI as restriction enzymes. The final construct contained at the N-termini of the protein two different tags, i.e. a His_6tag and a StrepII-tag, each followed by the relative cleavage site, for the following step of isolation and purification of ctCFD1 and NUBP1 complex (Fig. 4).

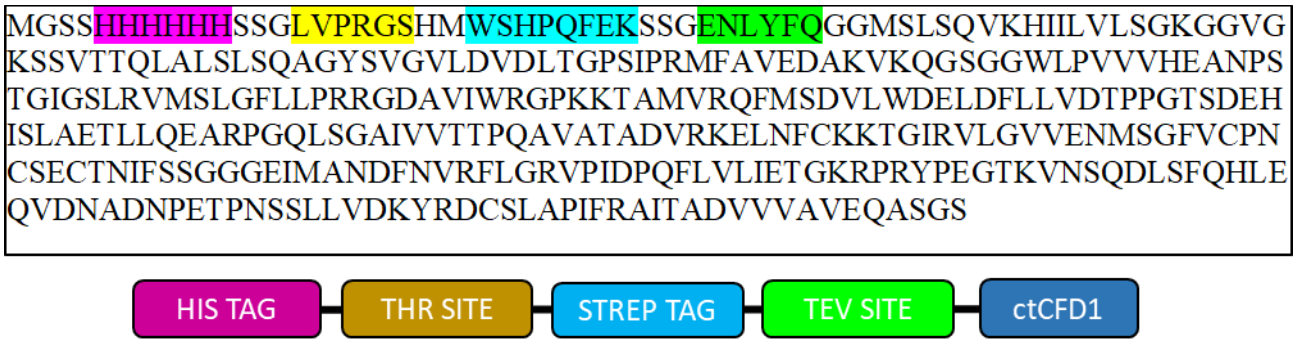

Fig. 4 - Sequence ctCFD1 inserted into the pET28 plasmid

E. coli BL21 (DE3) and RIPL Codon Plus cells were transformed with pET28a plasmid and tested for expression of ctCFD1 protein. Cells were allowed to grow to OD_{600nm} 0.6-0.8 at 37 °C. $FeCl_3$ (250 μM) was added before induction. Induction was performed at 37 °C and 20 °C by addition of 0.5 and 1 mM IPTG, for 4 h and overnight. (Fig. 5) Cells were lysed by sonication and the protein was purified by immobilized metal ion affinity chromatography, under anaerobic conditions because the ctCFD1 protein is unstable in presence of oxygen.

The final protocol for the expression and purification of ctCFD1 in pET28 plasmid is reported in Table 1. The final yield was 40 mg/L in M9 medium.

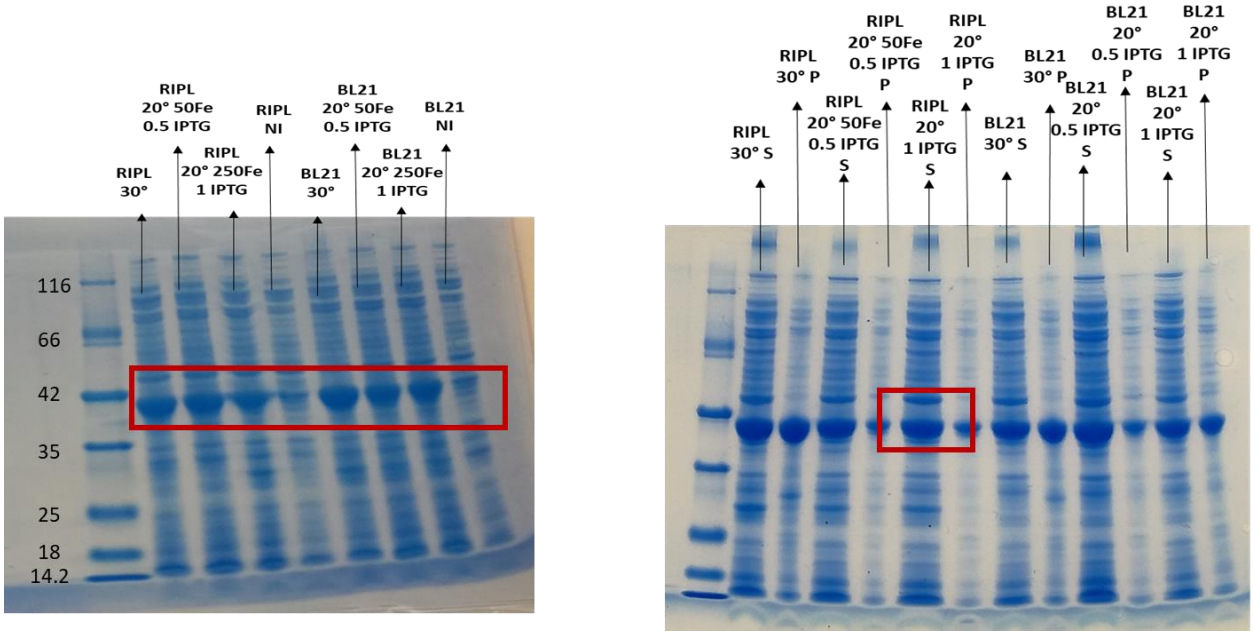

Fig. 5 – Expression tests of ctCFD1 protein

Table 1 – Expression and anaerobic purification of ctCFD1 protocols

Cells	Plasmid	Medium	OD of induction	IPTG	Temperature	Time of induction	Additional
RIPL CODON PLUS	pET28	M9	0.6 – 0.8	1 mM	20°C	ON	250µM $FeCl_3$

Column	Sonication	Lysis Buffer (LB)	Binding Buffer (BB)	Elution Buffer (EB)	Thrombin cut
His Trap FF 2x5mL	30'' ON 3' OFF	BB DNAse 0.01mg/mL $MgSO_4$ 40mM DTT 5mM	Tris 50mM NaCl 500mM Imidazole 30mM Glycerol 10% pH 8.0	Tris 50mM NaCl 500mM Imidazole 500mM Glycerol 10% pH 8.0	1 µL/mg

The ctCFD1 protein purified from *E.coli* cells was colorless, as verified by UV-vis spectroscopy (data not shown). A chemical reconstitution protocol was developed to obtain the holo protein . The protein was incubated overnight in degassed 50 mM Tris buffer pH 8.0, 100 mM NaCl, 5 mM DTT with up to a 6-fold excess of $FeCl_3$ and Na_2S, inside an anaerobic chamber (Table 2). The buffer was then exchanged by PD10 desalting column in order to remove any excess of Fe and S. The holo protein was recovered with a brown colour. The UV-visible spectrum showed an absorbance band at 420 nm, which is characteristic of [4Fe-4S] binding proteins. This result is therefore consistent with the binding of a [4Fe-4S] cluster to ctCFD1 (Fig. 6A). The visible CD spectrum was also consistent with the binding of a [4Fe-4S] cluster that generally do not show any positive Cotton effect in the 300-700 spectral region (Fig. 6B).

Table 2 – Reconstitution protocol of ctCFD1

Buffer	cfCFD1 concentration	$FeCl_3$ 6x	Na_2S 6x	DTT
Tris 50mM NaCl 100mM pH 8.0	60µM	Divided into 4 additions (waiting 2' for each one)	Divided into 9 additions (waiting 10' for each one)	5mM

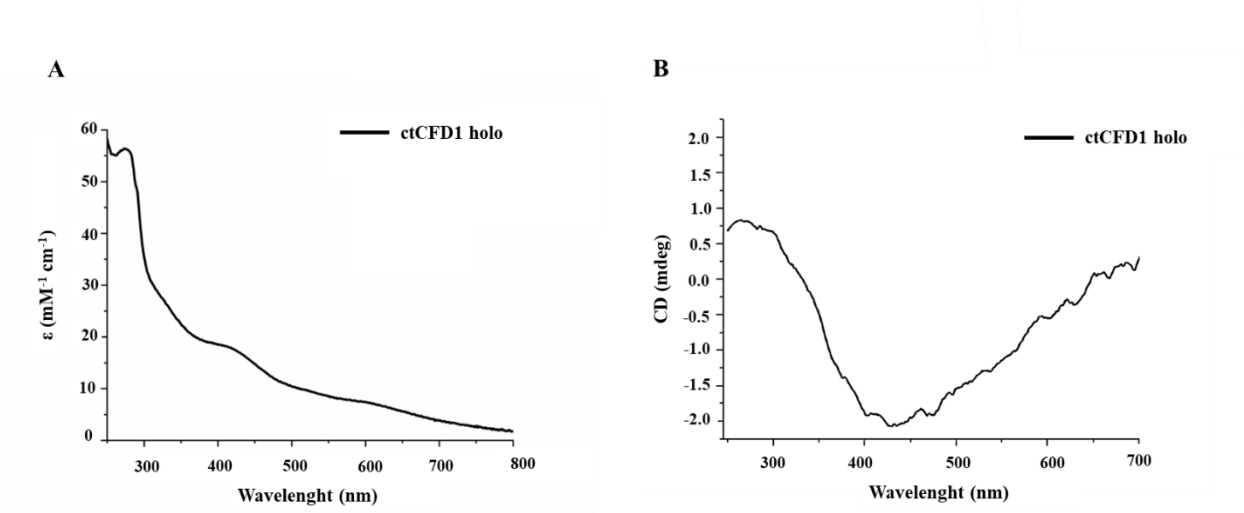

Fig. 6 – A) UV-vis and B) CD spectra of holo ctCFD1 protein

The 1D ^1H paramagnetic NMR spectrum of the chemically reconstituted ctCFD1 showed four intense hyperfine shifted signals in the 17-10 ppm spectral region, whose chemical shift values and linewidths are typical of βCH_2 of cysteines bound to a $[4Fe\text{-}4S]^{2+}$ cluster. The anti-Curie temperature dependence of these signals further confirmed the presence of an oxidized $[4Fe\text{-}4S]^{2+}$ cluster bound to ctCFD1 (Fig. 7).

and the spectra were acquired in different buffer conditions

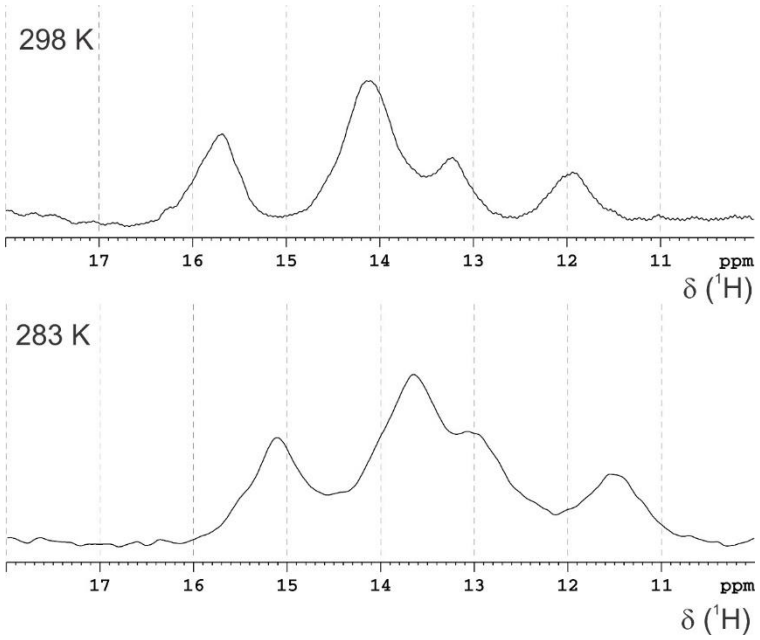

Fig. 7 – 1D ^{1}H NMR paramagnetic of holo ctCFD1

Overall, these results confirmed the presence of [4Fe-4S] cluster bound to ctCFD1.

3.3.5. ctCFD1 and NUBP1 form a weak heterocomplex

In order to understand whether ctCFD1 and NUBP1 can form a heterocomplex *in vitro*, His_6-tagged NUBP1 and Strep-tagged ctCFD1 were incubated for 1 h, under anaerobic conditions. The mixture was then purified through sequential steps of purification, using a HisTrap column, to separate unbound StrepII-tagged ctCFD1 from His_6-tagged NUBP1, as a homodimer and in a complex with StrepII-tagged ctCFD1. The second step of purification was followed by a StrepTrap column, to separate homodimeric His_6-tagged NUBP1 from ctCFD1-NUBP1 heterocomplex, thanks to the StrepII-tag present on ctCFD1. The purification protocol and strategy are reported below (Table 3 and Fig. 8)

Table 3 – Buffers table for the isolation of complex

First Column	Binding Buffer HisTrap column	Elution Buffer HisTrap column	Second Column	Binding Buffer StrepTrap column	Elution Buffer StrepTrap column
His Trap FF 5mL	NaPi 20mM, NaCl 280mM, KCl 6mM, Imidazole 5mM pH 7.4	NaPi 20mM, NaCl 280mM, KCl 6mM, Imidazole 400mM pH 7.4	Strep Trap 5mL	NaPi 20mM, NaCl 280mM, KCl 6mM, pH 7.4	NaPi 20mM, NaCl 280mM, KCl 6mM, DThB 2.5mM, pH 7.4

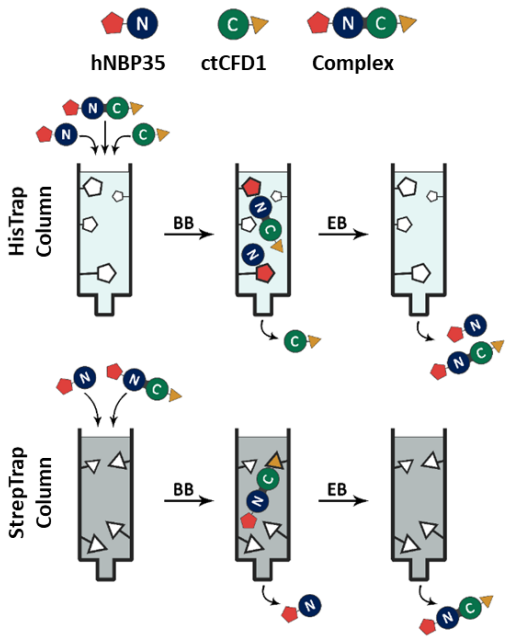

Fig. 8 – Scheme of purification of the ctCFD1-hNBP35 complex

In order to increase the yield of complex formation, several conditions were tested. The two proteins were mixed at different ratios, in their apo and holo states, and in the absence and in the presence of cofactors such as ATP and GTP, which specifically bind to CFD1 and NBP35, respectively[50]. In all the tested conditions, two bands were observed in the SDS PAGE after the isolation of the complex, indicating the formation of a ctCFD1-NUBP1 heterocomplex (Fig. 9). However, for all the tested conditions, the maximum obtained concentration was about 4 µM, as determined by UV-vis measurements, and did not allow for any spectroscopic characterization of the heterocomplex.

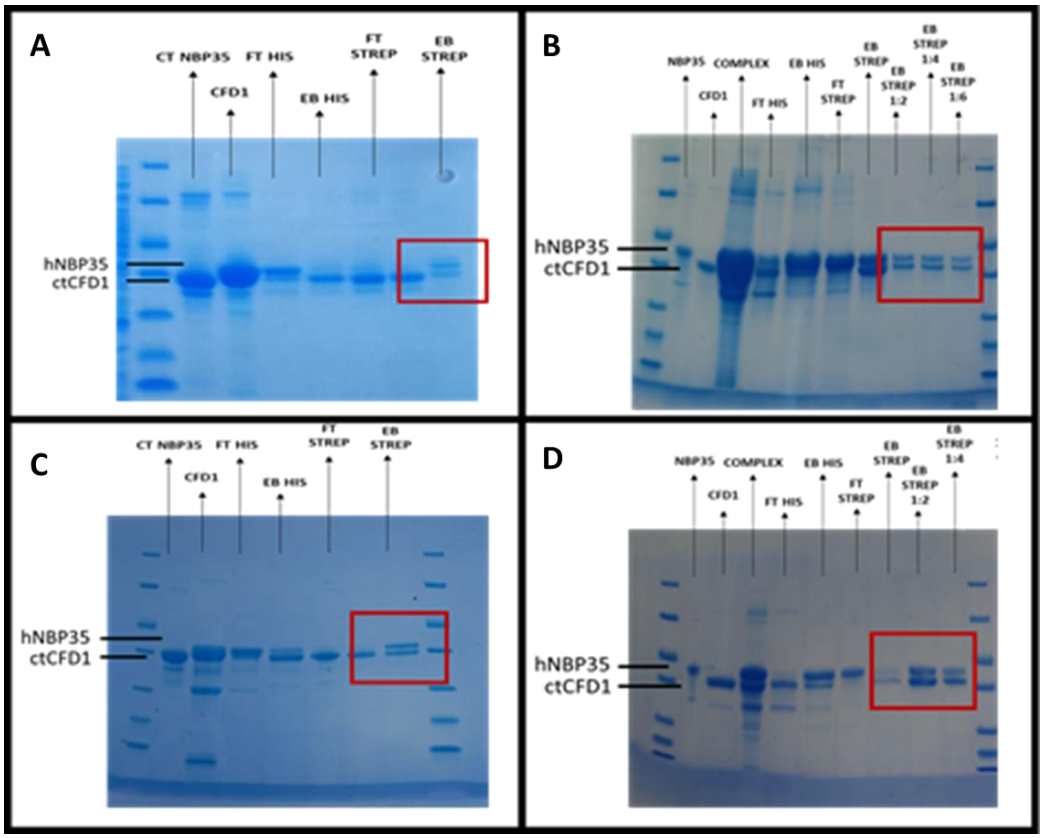

Fig. 9 – SDS page after the isolation of reconstituted complex. The reactions were performed using in A) ctCFD1 and hNBP35 1:2 B) ctCFD1 holo and hNBP35 apo C) ctCFD1 apo and hNBP35 holo D) apo protein in presence of ATP and GTP

3.3.6. Coexpression of NUBP1-NUBP2 complex

Coexpression of the NUBP1-NUBP2 heterocomplex was used as an approach to overcome the instability of isolated NUBP2. The NUBP1 and NUBP2 genes were inserted into two distinct multiple cloning sites of a pDUET plasmid, with a His_6-tag and a StrepII-tag at the N-termini of NUBP1 and NUBP2, respectively (Fig. 10)

MGSS**HHHHHH**SSGENLYFQGGMEEVPHDCPGADSAQAGRGASCQGCPNQRLCASGA
GATPDTAIEEIKEKMKTVKHKILVLSGKGGVGKSTFSAHLAHGLAEDENTQIALLDIDIC
GPSIPKIMGLEGEQVHQSGSGWSPVYVEDNLGVMSVGFLLSSPDDAVIWRGPKKNGMIK
QFLRDVDWGEVDYLIVDTPPGTSDEHLSVVRYLATAHIDGAVIITTPQEVSLQDVRKEIN
FCRKVKLPIIGVVENMSGFICPKCKKESQIFPPTTGGAELMCQDLEVPLLGRVPLDPLIGK
NCDKGQSFFIDAPDSPA

GDIHWSHPQFEKAAVLENLYFQGGMEAAAEPGNLAGVRHIILVLSGKGGVGKSTISTEL
ALALRHAGKKVGILDVDLCGPSIPRMLGAQGRAVHQCDRGWAPVFLDREQSISLMSVG
FLLEKPDEAVVWRGPKKNALIKQFVSDVAWGELDYLVVDTPPGTSDEHMATIEALRPYQ
PLGALVVTTPQAVSVGDVRRELTFCRKTGLRVMGIVENMSGFTCPHCTECTSVFSRGGG
EELAQLAG

Fig. 10 - Sequence of NUBP1 and NUBP2 inserted into pDUET plasmid

The proteins were purified through immobilized metal ion affinity chromatography, under anaerobic conditions, because NUBP2 is unstable in presence of oxygen. The expression and solubility tests were performed with *E. coli* BL21 (DE3) and RIPL Codon Plus cells transformed with pDUET plasmid and allowed to grow to OD_{600nm} 0.6-0.8 at 37 °C. $FeCl_3$ (500 µM) was added before induction. Induction was performed at 37 °C and 20 °C by addition of 1 mM IPTG for overnight. I obtained the protocol for the expression and purification (Fig. 11 and Table 4).

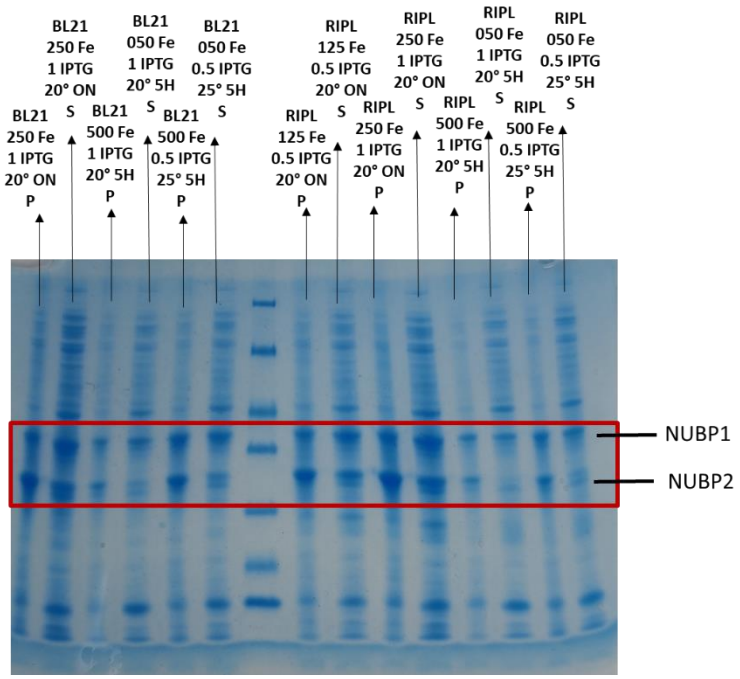

Fig. 11 – SDS page of expression and solubility tests on NUBP1-NUBP2 complex

Table 4 – Expression and anaerobic purification of NUBP1-NUBP2 protocols

Cells	Plasmid	Medium	OD of induction	IPTG	Temperature	Time of induction	Additional (Final conc.)
RIPL CODON PLUS	pDUET	M9	0.6 – 0.8	1 mM	20°C	O/N	500µM $FeCl_3$

First Column	Binding Buffer	Elution Buffer	Second Column	Binding Buffer	Elution Buffer
His Trap FF	NaPi 40mM NaCl 280mM KCl 6mM Imidazole 5mM pH 7.4	NaPi 40mM NaCl 280mM KCl 6mM Imidazole 400mM pH 7.4	Strep Trap FF	NaPi 20mM NaCl 280mM KCl 6mM pH 7.4	NaPi 20mM NaCl 280mM KCl 6mM DThB 2.5mM pH 7.4

The purification was performed using two different affinity columns that recognized two different tags, in order to remove from the solution the possible homodimer of NUBP1 and NUBP2 (Scheme of purification in Fig. 12). In spite of the anaerobic conditions, the complex was purified devoid of any cluster (data not shown). The total protein concentration, as determined by UV-vis spectroscopy, was approximately 8 mg/L.

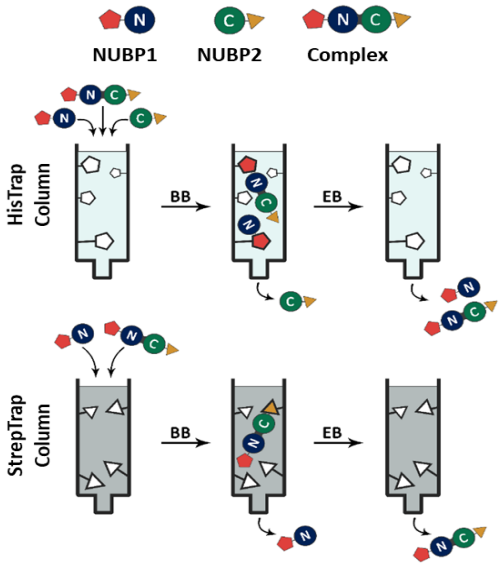

Fig. 12 – Scheme of purification of the complex

3.3.7. Spectroscopic characterization of chemically reconstituted NUBP1-NUBP2 heterocomplex

The NUBP1-NUBP2 holo complex was obtained by chemical reconstitution with a 10-fold excess of inorganic iron and sulphur, and the cluster assembly event was monitored by UV−vis and paramagnetic 1D ^{1}H NMR spectra (Fig. 13).

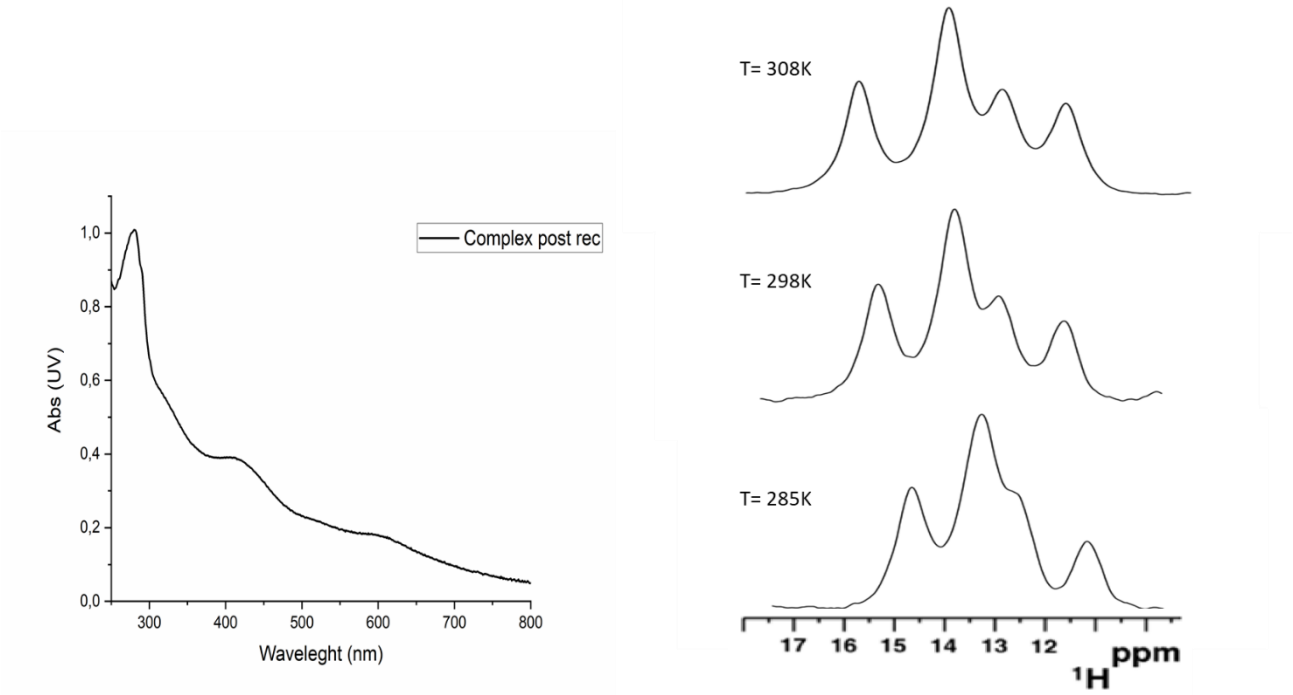

Fig. 13 – UV-vis spectroscopy and 1D ^{1}H NMR paramagnetic of holo NUBP1-NUBP2 complex

The UV-vis spectrum showed a band at 420nm that is typical of [4Fe-4S] clusters.

The paramagnetic spectra showed four intense hyperfine shifted signals in the 17-10 ppm spectral region, whose chemical shift values and linewidths are typical of βCH_2 of cysteines bound to a [4Fe-4S]$^{2+}$ cluster. These paramagnetic features were observed also for the cluster bound to the N-terminal site of holo NUBP1 homodimer[33] and for the cluster bridging in the two C-terminal CPXC motifs in holo ctCFD1 homodimer (Fig. 14). Since both cluster binding motifs are present in NUBP1-NUBP2 heterocomplex[33,50], it was not possible to establish if the signals observed in the NMR spectrum arise from the cluster bound to the N-terminal or C-terminal binding site.

To clarify this aspect, in addition to the wild type heterocomplex, I produced a mutant where the four cysteines of the N-terminal domain of NUBP1 were mutated into alanines, in order to eliminate the second cluster binding site and to obtain information about the bridging cluster.

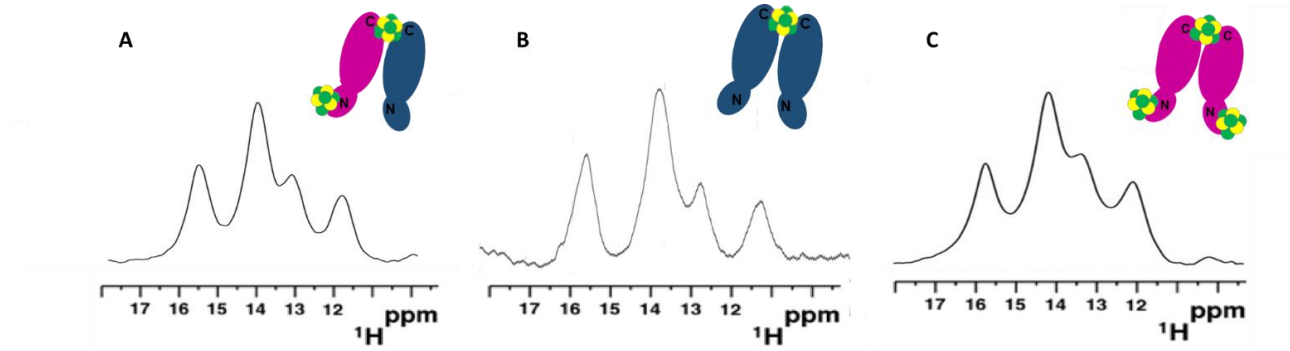

Fig. 14 – 1D ^{1}H NMR paramagnetic of A) NUBP1-NUBP2 heterodimer B) ctCFD1 homodimer and C) NUBP1 homodimer

3.3.8. NUBP1 mutant and NUBP2 complex

The mutant NUBP1 gene was inserted into pDUET plasmid, using the restriction enzyme cloning approach. The EcoRI and HindIII enzymes were used to cleave the plasmid into two distinct sites respect to NUBP2 gene, in order to obtain the pDUET that contains mutant NUBP1 and NUBP2 genes (Fig. 15).

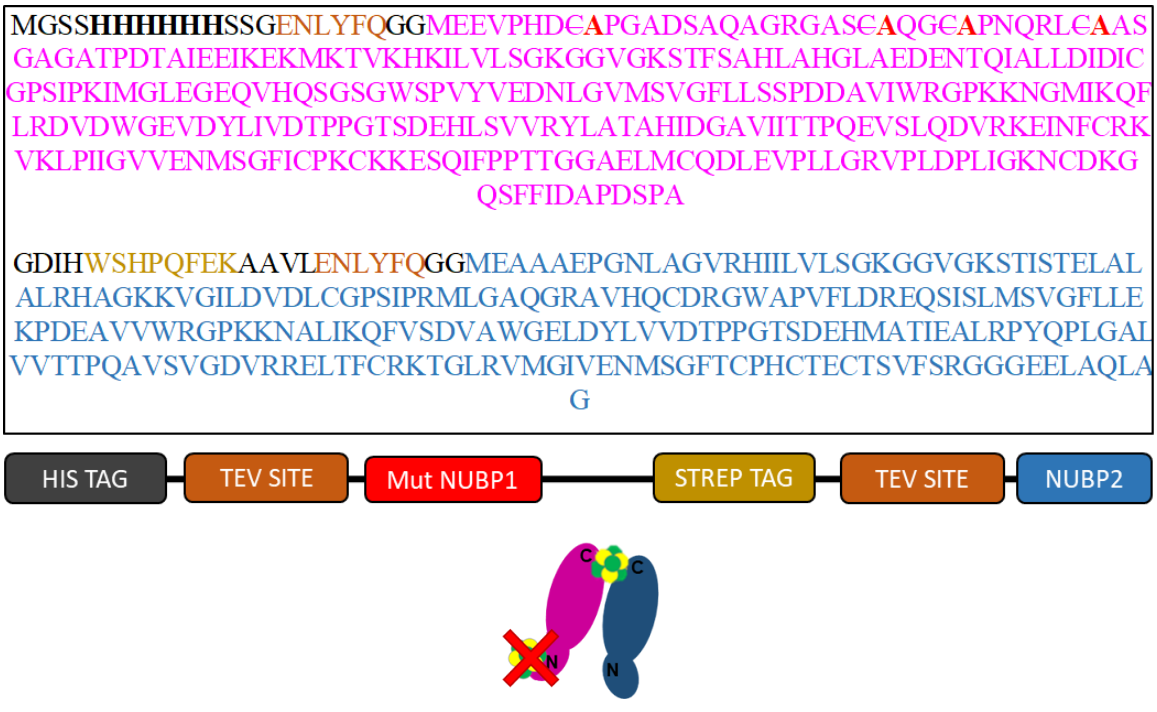

Fig. 15 – Sequence of mutant NUBP1 and NUBP2 inserted into the plasmid and model of structure of mutant NUBP1-NUBP2 complex

Several expression conditions were tested, but in none of them the NUBP1 mutant was overexpressed (data not shown). In order to overcome this problem, a different strategy was used. E.coli cells were co-transformed with the two different plasmids, containing the sequences for the expression of Strep-tagged NUBP2 and His_6-tagged mutant NUBP1, respectively (Fig. 16). The complex was expressed and purified in its apo state using the same protocol used for the wild-type (WT) complex, obtaining a yield of 10mg/L from M9 medium (Fig. 17). The chemical reconstitution protocol was performed on the apo complex in order to obtain the holo state of the protein, in the presence of up to 10 equivalents of $FeCl_3$ and Na_2S. The UV-vis spectra, acquired complex reconstitution, did not show any absorbance bands tin the spectra region typical of any type of cluster (data not shown).

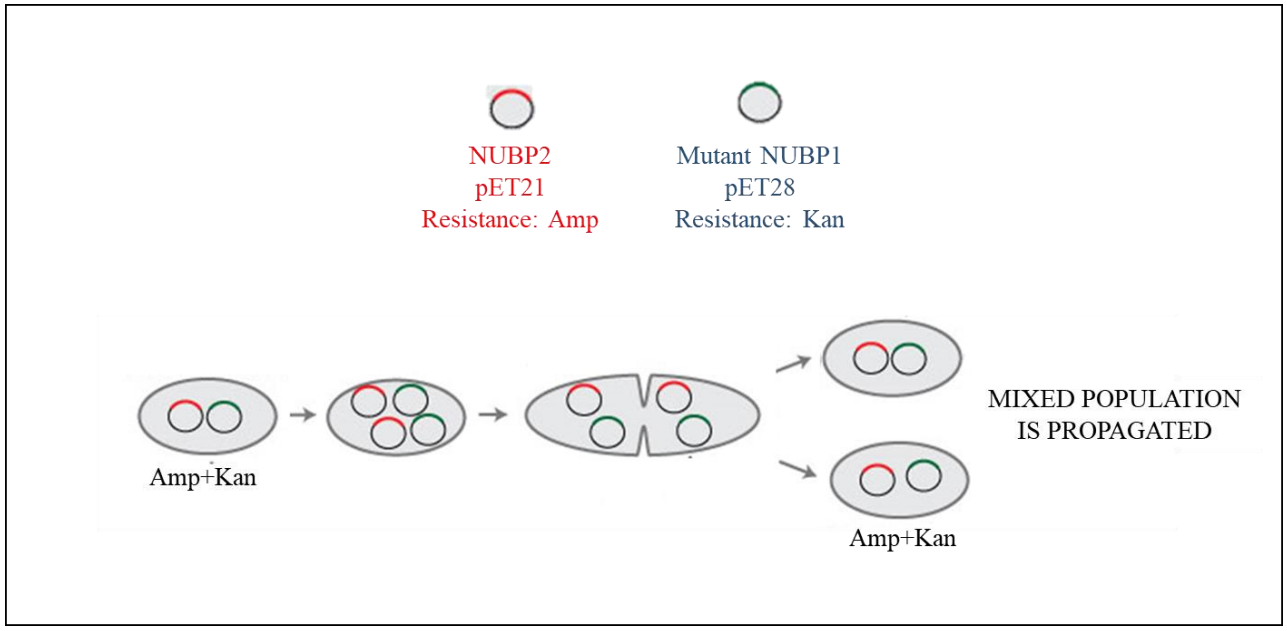

Fig. 16 – Co-transformation scheme

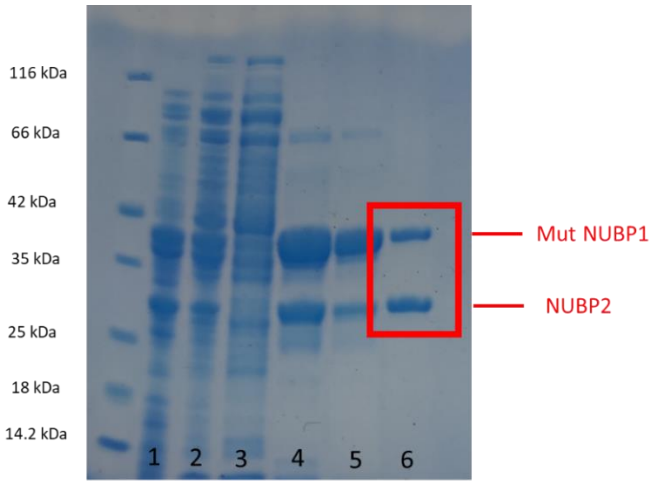

Fig. 17 – SDS page after the complex purification. The bands define 1) insoluble part 2) soluble part 3) the proteins unbound to the column 4) the fraction bound to the first column 5) the homodimer of mut NUBP1 eliminated from the solution 6) the isolated bands after the purification, NUBP1 and NUBP2 respectively.

3.3.9. NUBP1 mutant protein

In order to assess whether the absence of clusters bound to the mutant NUBP1-NUBP2 heterocomplex was due to an intrinsic lability of its binding to the C-terminal motif or to a decreased stability of the heterocomplex between mutant NUBP1 and NUBP2, with respect to that of the WT heterocomplex, I investigated the cluster binding properties of mutant NUBP1. The protein was produced and purified with the protocols reported in Table 5.

Table 5 – Expression and purification protocols for NUBP1 mutant

Cells	Plasmid	Medium	OD of induction	IPTG	Temperature	Time of induction	Additional
RIPL CODON PLUS	pET28	LB	0.6 – 0.8	0.5 mM	21°C	O/N	250µM $FeCl_3$

Column	Sonication	Lysis Buffer	Binding Buffer	Elution Buffer	TEV cut
His Trap FF 2x5mL	30'' ON 3' OFF	BB DNAse 0.01mg/mL $MgSO_4$ 40mM DTT 5mM	NaPi 40mM NaCl 280mM Imidazole 5mM pH 7.4	NaPi 40mM NaCl 280mM Imidazole 500mM pH 7.4	5 µL/mg

The anaerobically purified mutant NUBP1 was colorless and UV-vis spectroscopy confirmed the absence of any cluster bound to the protein (Fig. 18A). Several chemical reconstitution conditions were applied to the monomeric apo mutant NUBP1. UV-vis spectroscopy showed the presence of very broad bands at ca 420 nm that can be attributed to [4Fe-4S] clusters (Fig. 18A). However, the binding of [4Fe-4S] clusters could not be detected by paramagnetic NMR, suggesting a lability of the [4Fe–4S] cluster binding at the C-terminal motif of mutant NUBP1, as reported for wild type NUBP1[33]. The quaternary structure of the NUBP1 mutant changed upon chemical reconstitution, as showed by analytical gel filtration (Fig. 18B). Indeed, the fraction of dimeric protein increased upon chemical reconstitution. Previously, it was demonstrated that the binding of Fe-S cluster to the C-terminal motif of NUBP1 promotes protein dimerization[33]. Overall, these results are consistent with the labile binding of a Fe-S cluster at the C-terminal motif of mutant NUBP1.

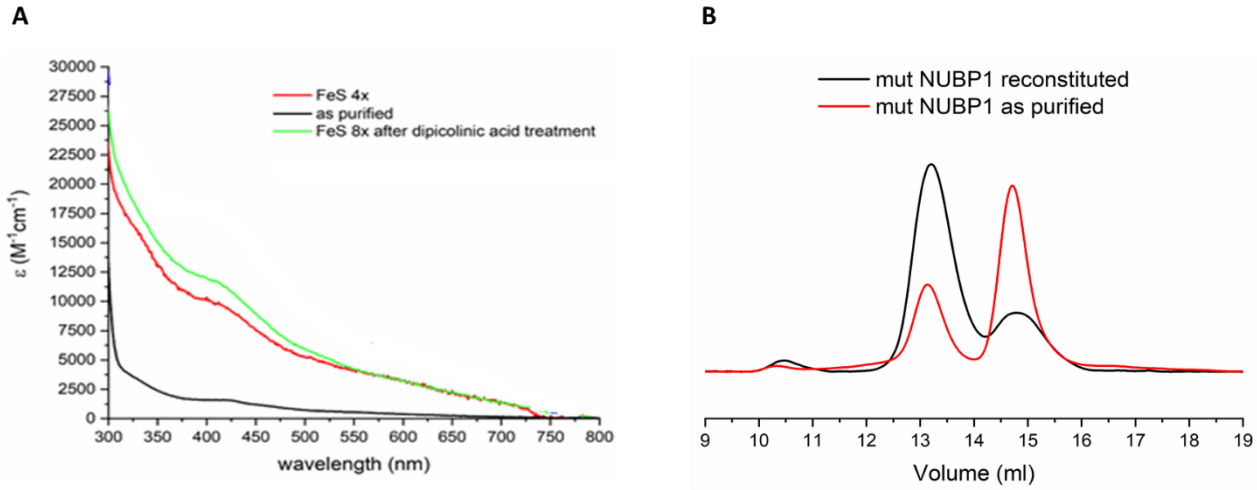

*Fig. 18 – A) UV-vis spectra of mutant NUBP1 pre and post reconstitution protocol and B) analytical gelfiltration graph of mutant NUBP1 after chemical reconstitution (**black** line) and as purified (red line)*

3.3.10. Discussion

The characterization of the NUBP1-NUBP2 complex showed the binding of a [4Fe-4S] cluster to the heterocomplex, with the same paramagnetic features of the N-terminal cluster bound to homodimeric NUBP1[33] and of the cluster bridging the two C-terminal CPXC motifs in homodimeric ctCFD1. Spectroscopic and analytical gel filtration studies performed on a mutant of NUBP1 lacking the N-terminal binding motif, suggested that the C-terminal motif of NUBP1 might bind a labile cluster, that thus could not be characterized. The lability of the binding of such cluster could be related to its function. Indeed, it has been proposed that the NUBP1-NUBP2 complex participates in the CIA

machinery donating the cluster bound to the C-terminal CPXC motifs to other components of the CIA machinery.

3.4. GLRX3 as [2Fe-2S] chaperone for the de novo formation of clusters on heterocomplex

In vivo, the assembly of Fe-S clusters relies on the action of several proteins that specifically interact each other to de novo synthesize and to insert the [2Fe−2S] and [4Fe−4S] clusters into apo recipient proteins. The mechanism for the maturation of the [4Fe−4S] clusters at both N- and C-terminal motifs of the two human NTPases NUBP1 and NUBP2 is still elusive[18]. The human glutaredoxin-3 protein (GLRX3) is a possible player of the CIA machinery responsible for the maturation of the [4Fe−4S] clusters on NUBP1-NUBP2. GLRX3 protein consists of three domains: one N-terminal thioredoxin domain and two monothiol glutaredoxin domains, each able to bind a glutathione-coordinated $[2Fe–2S]^{2+}$ cluster, via protein dimerization. It has been demonstrated that GLRX3 *de facto* acts as a [2Fe–2S] cluster chaperone in the cytosol, transferring its two [2Fe–2S] clusters to apo anamorsin *in vitro*[25,34] and *in vivo*[35]. Recently, it was showed that GLRX3 transfers its two [2Fe–2S] clusters also to NUBP1, and, in the presence of GSH, the two [2Fe–2S] clusters are converted into a [4Fe−4S] cluster.

I investigated therefore the ability of GLRX3 to assemble [4Fe−4S] cluster(s) on NUBP1-NUBP2 heterocomplex.

An excess of $[2Fe–2S]_2$-$GLRX3_2$-GS_4 was incubated with apo His_6-tagged NUBP1-NUBP2 heterocomplex in anaerobic conditions, in the presence of GSH as a reductant. After one hour, the heterocomplex was separated from untagged GLRX3 by affinity chromatography and characterized by UV-vis and NMR spectroscopy (Fig. 19).

The UV-visible spectrum of the NUBP1-NUBP2 heterocomplex after incubation and isolation from GLRX3 showed an absorbance band at 420 nm, which is characteristic of [4Fe-4S] binding proteins (Fig. 8). The paramagnetic NMR spectra showed four signals in the 10-17 ppm spectral region, with anti-Curie temperature dependence, that are typical of βCH_2 of cysteines bound to a $[4Fe-4S]^{2+}$ cluster, and that are very similar to those observed for the chemically reconstituted NUBP1-NUBP2 heterocomplex (Fig. 13). These results indicate that two [2Fe-2S] clusters are transferred from $[2Fe–2S]_2$-$GLRX3_2$-GS_4 to NUBP1-NUBP2 heterocomplex, and the two clusters are reductively coupled to form a [4Fe-4S] cluster on the heterocomplex.

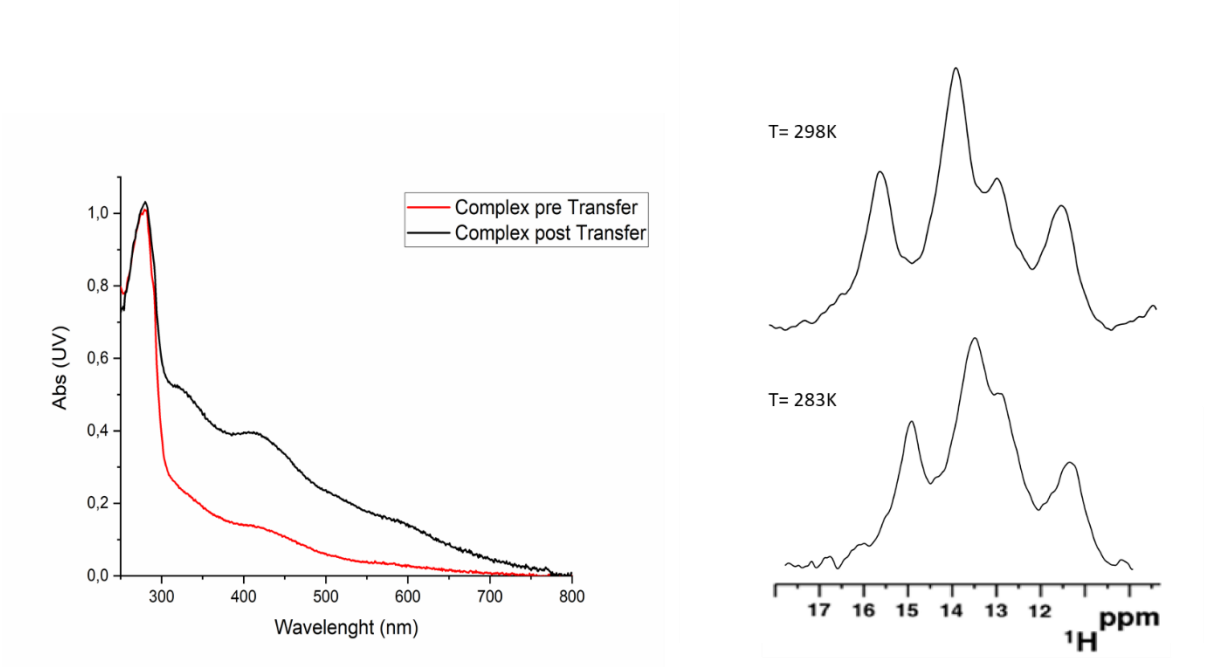

Fig. 19 – UV-vis and 1D ^{1}H NMR paramagnetic spectra of transferred NUBP1-NUBP2 complex

Since NUBP1-NUBP2 heterocomplex has an N-terminal and a C-terminal cluster binding site, in order to establish whether GLRX3 can transfer its clusters to both sites, the same cluster transfer experiment was repeated by incubating an excess of $[2Fe–2S]_2$-$GLRX3_2$-GS_4 with mutant NUBP1 containing only the C-terminal cluster binding motif, and with the heterocomplex formed by mutant NUBP1 and NUBP2 (mutNUBP1-NUBP2), obtained as described above. After the reaction, the proteins were separated using the same protocol as that applied to the wild type heterocomplex. After incubation, the UV–vis spectrum of isolated mutant NUBP1 and mutNUBP1-NUBP2, did not match that of the reconstituted protein, and did not show any absorbance band typical of [2Fe–2S] or [4Fe–4S] clusters (data not shown). Overall, these results indicate that the cluster transfer from GLRX3 to NUBP1-NUBP2 heterocomplex does not promote the formation of a [4Fe–4S] cluster on the C-terminal site of the complex.

3.4.1. Discussion

The GLRX3 protein acts as [2Fe-2S] clusters chaperone for NUBP1-NUBP2 complex, with the formation of a [4Fe-4S] cluster thanks to the electrons donated by GSH. Spectroscopic characterization of the wild type heterocomplex and of a mutant hereocomplex containing only the C-terminal cluster binding site, did not allow to observe the cluster bound to the C-terminal motif and bridging the two subunits of the dimer. Whether GLRX3 can transfer its clusters to the C-terminal motif of NUBP1-NUBP2 complex, and more in general, whether the C-terminal motif of NUBP1-NUBP2 heterocomplex can bind a [4Fe-4S] cluster, remain an open question and requires further investigation. As previously discussed, the binding of the cluster at the C-terminal motif of NUBP1-NUBP2 heterocomplex might be characterized by an intrinsic kinetic lability, related to its cellular function. Indeed, it has been proposed that the complex participates in the iron-sulfur assembly machinery assembling and donating a [4Fe-4S] cluster which bridges the two C-terminal motifs of NUBP1 and NUBP2, to the other components of the CIA machinery, and the kinetic lability of the binding of such cluster could be required to facilitate the cluster transfer event.

A possible strategy to assess whether a C-terminal [4Fe-4S] cluster is bound or not to the heterocomplex after the interaction with GLRX3, could be the investigation of the maturation of the late CIA components by the NUBP1-NUBP2 heterocomplex. Indeed, it was reported that, in yeast, depletion of all four early-acting CIA factors (CDF1, NBP35, Tah18, Dre2) impairs Fe-S cluster incorporation into Nar1 *in vivo*. [35-36-37] Assuming that all the *in vivo* findings on yeast hold in human cells, the most reliable model is that the NUBP1-NUBP2 complex could be responsible for the maturation process of NARFL, by transferring the [4Fe-4S] newly assembled on the C-terminal cluster binding site of the heterocomplex to NARFL protein. This model needs further experimental confirmations, but the study of the cluster trafficking from GLRX3 to NARFL, mediated by the assembly of the [4Fe-4S] cluster on NUBP1-NUBP2 scaffold complex, could answer the question about the presence of the [4Fe-4S] bridging cluster in NUBP1-NUBP2 upon interaction with GLRX3.

RESULTS

An alternative model for the biogenesis of Fe-S clusters in cytosol

3.5. An alternative model for the biogenesis of Fe-S clusters in cytosol

3.5.1. Introduction

The biogenesis of Fe-S clusters in cytosol is performed by the CIA machinery, whose composition and mechanism of action have been only partially elucidated. Specifically, the source of iron and sulfur for the assembly of Fe-S cluster in cytosol is still unknown. Two different models have been proposed for the iron and sulfur pooling in the cytosol. In the first proposed model, a still unknown [2Fe-2S]-binding compound is assembled in mitochondria and exported in the cytosol via the ISC export machinery. The latter machinery is composed by the ABCB7 membrane transporter[20] and by GSH. It was recently reported that GSH can form *in vitro* a stable tetra-GSH-coordinated $(GS)_4$-[2Fe-2S] complex [51], that might represent a viable substrate candidate for the mitochondrial ABCB7 export protein[22]. However, this model needs *in vivo* experimental confirmations.

Recently, a second model has been proposed by Philpott and coworkers, where a [2Fe-2S] cluster is *de novo* assembled in cytosol. In this alternative model, an inorganic sulfur species is generated in mitochondria by cysteine desulfurase and is exported in the cytosol via the ABCB7 transporter[23] while Fe(II) ions are distributed in cytosol by the poly(C)-binding proteins (PCBPs) family[24,52]. Specifically, Philpott's group reported that the αCP1 member of the PCBPs family (also known as PCBP1) coordinates iron(II) in complex with BOLA2[35], a protein involved in the cytosolic Fe-S biogenesis[25,26]. *In vivo* and *in vitro* experiments indicated that PCBP1–Fe(II)–GSH–BOLA2 serves as an intermediate complex that is required for the assembly of [2Fe–2S] clusters on the cytosolic [2Fe-2S] chaperone BOLA2–GLRX3[25], thereby linking the ferrous iron and Fe–S cluster distribution systems in cells. In collaboration with Philpott's group, I have recently started an atomic level investigation of the interaction between PCBP1, Fe(II), GSH and BOLA2 in order to define the mechanism of action of the proposed alternative CIA pathway.

3.5.2. PCBP1 protein

PCBP1 protein is a member of the PCBPs proteins family that includes aCP1, aCP2, aCP3, aCP4. These proteins contain a triplet K homology (KH) RNA-binding motif[53], with the two N-terminal domains closely spaced, whereas the C-terminal KH domain is separated by a linking segment of variable length. Philpott and coworkers recently demonstrated that the latter KH domain of aCP1 (KH3) binds Fe(II) and forms a complex with BOLA2, in the presence of GSH[7], and *in vivo* studies demonstrated that the KH3 domain of PCBP1 was functionally sufficient to promote the formation of the complex with Fe(II), GSH and BOLA2 in cells lacking endogenous PCBP1. Mutagenesis experiments indicated that residues C293 and E350 are involved in iron binding, and residues N301,

E304 and R346 are responsible for the interaction of KH3 with GSH, suggesting that KH3 can directly coordinate both GSH and iron at adjacent sites on the domain, as showed by the X-ray crystallographic structure of the KH3 domain of PCBP1[53] (Fig. 1). Co-precipitation studies indicated that both ligands are required for the interaction of KH3 with BOLA2[7], and that C293 of KH3 is a key residue for the interaction of the protein with Fe(II), GSH and BOLA2. Indeed, when similar experiments were performed using a KH3 mutant in which the C293 was replaced by serine, the KH3-Fe(II)-GSH-BOLA2 complex was not detected. In my project KH3 domain was therefore used as a substitute for the full-length PCBP1 to study the interaction with BOLA2 and Fe(II).

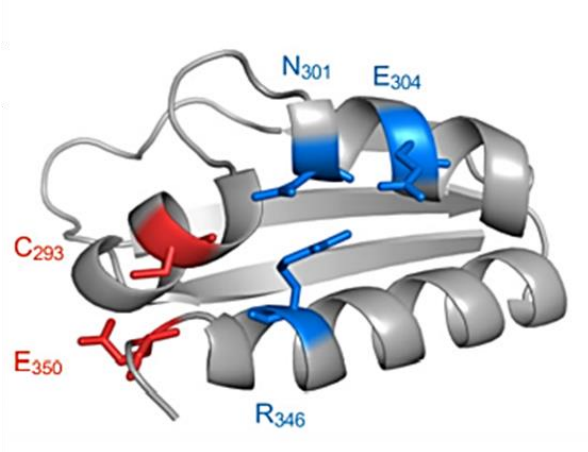

Fig. 1 - Ribbon representation of the X-ray crystallographic structure of KH3 domain, solved at 2.1 Å resolution (PDB: 1WVN). Ligands for GSH binding are showed as blue sticks and ligand for iron binding as red sticks.

3.5.3. Cloning, expression and purification of the KH3 domain of PCBP1

The PCBP1 KH3 domain (residue 279-356, KH3 hereafter) was amplified from PCBP1 gene by Polymerase Chain Reaction (PCR) and inserted into pET28a plasmid. The PCR is commonly used to amplify a gene or DNA fragment of interest, from any source of DNA, using specific primers. Indeed, I designed two primers, reverse and forward (reported in Table 1), for the amplification of KH3 (Fig. 2). The PCR amplified gene was run on agarose gel (Fig. 3B), and the corresponding DNA band was cut from the gel and purified using PureLink Quick Gel Extraction Kit (purchased from ThermoFisher) and then it was subcloned into the pET28a destination vector. For cohesive ligation, the empty destination vector was double digested with 3 units each of restriction enzymes XhoI and NdeI (Invitrogen), analyzed by agarose gel electrophoresis, purified using phenol-chloroform extraction and ethanol precipitation (Fig. 3A). The ligation step was performed using 6 units of T4 DNA ligase enzyme in 300mM Tris-HCl (pH 7.8), 100mM $MgCl_2$, 100mM DTT and 10mM ATP buffer (purchased from ThermoFisher); the vector to KH3 insert ratio was about 1:6 and the reaction was carried out at 25°C for 3h in a bench. The ligation mixtures were used for transformation of

chemically competent TOP10 *E.coli* cells (Invitrogen). The transformed colonies were diluted in 20 µL of milli-Q water and 2X master mix buffer (dye, TAC polymerase) and the mixture was screened by PCR using T7-reverse and T7-forward plasmid specific primes (purchased from ThermoFisher). The amplification products were analyzed by agarose gel electrophoresis in order to identify the cells transformed with KH3-pET28a plasmid. The KH3-pET28a plasmid was extracted from the chosen colonies, purified and amplified using Plasmid DNA Midiprep Kits (ThermoFisher) and used for the expression of KH3 protein.

Table 1 – Primers for KH3 gene amplification

KH3 / FW primer	5' - ATATCATATGCAAACGACGCACGAGTTAACGATCCC- 3'
KH3 / RV primer	5' - TACTCGAGTCATTAACTACATCCCATCCCCTTCTCC - 3'

MGSS**HHHHHH**SSGLVPRGSHMENLYFQGHMASLDASTQTTHELTIPNNLI
GCIIGRQGANINEIRQMSGAQIKIANPVEGSSGRQVTITGSAASISLAQYLIN
ARLSSEKGMGCS

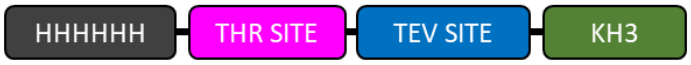

Fig. 2 – Sequence of KH3 protein inserted into pET28a plasmid

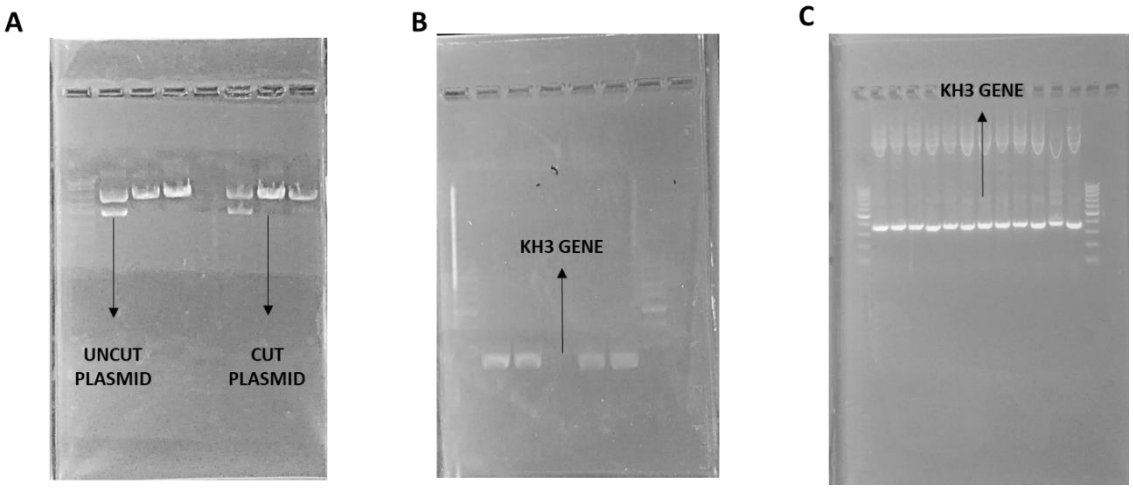

Fig. 3 – Analysis of pET28a destination vector and KH3 gene fragment by agarose gel electrophoresis. A) Digestion with XhOI and NdeI restrictions enzymes, B) PCR amplification of KH3 gene from PCBP1 using the two primers reported in table 1 and C) PCR screening after the ligation step into pET28a plasmid.

E. coli BL21 (DE3) and RIPL codon plus cells were transformed with pET28a plasmid containing KH3 gene (KH3-pET28a) and tested for expression of KH3 protein. Cells were allowed to grow to OD_{600nm} 0.6-0.8 at 37 °C. $FeCl_3$ (125 µM) was added before induction. Induction was performed at 37 °C, 25 °C and 17 °C by addition of 0.5 and 1 mM IPTG, for overnight. (Fig. 4). Cells were lysed by sonication and the protein was purified by immobilized metal ion affinity chromatography.

The final protocol for the expression and purification of KH3 in pET28 plasmid is reported in Table 2. The final yield was about 50 mg/L in M9 medium.

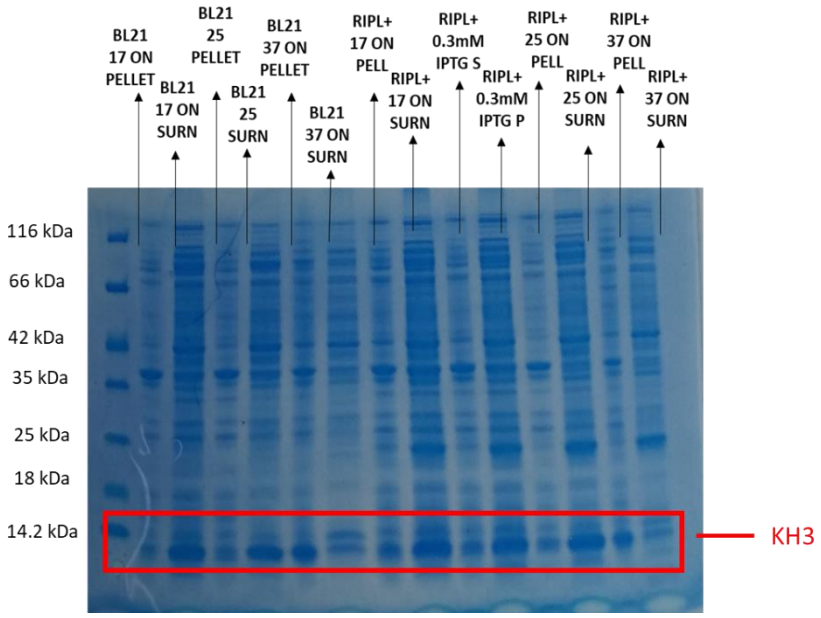

Fig. 4 – Expression and solubility tests of KH3 protein

Table 2 – Expression and purification protocols for KH3

Cells	Plasmid	OD of induction	IPTG	Temperature	Time of induction	Additional (Final conc.)
BL21 (DE3)	pET28a	0.6 – 0.8	0.5 mM	25°C	O/N	125µM $FeCl_3$

Column	Sonication	Lysis Buffer	Binding Buffer	Elution Buffer	Thrombin cut
His Trap FF 2x5mL	30'' ON 3' OFF	BB DNAse 0.01mg/mL $MgSO_4$ 40mM DTT 5mM	Tris 50mM NaCl 300mM Imidazole 5mM pH 8.0	Tris 50mM NaCl 300mM Imidazole 300mM pH 8.0	1 µL/mg

The UV-vis spectrum of purified KH3 showed an absorption band at 260 nm, indicating that a KH3-RNA complex was extracted from *E.coli* cells. Indeed, it was reported that C293 residue, that is critical for iron binding on KH3, also modulates the RNA binding activity of PCBP1[53]. Therefore, the protein was separated by RNA by precipitation with 0.5 M of ammonium sulfate. After resuspension in 100 mM Tris, 40 mM KCl, 1 mM TCEP, 1 mM GSH buffer, the protein was further purified through SEC using HiLoad 16/600 Superdex 75 prep grade. The KH3 protein was eluted with two peaks (Fig. 5), with the first one (eluting at 80 ml) corresponding to the KH3 protein, as indicted by SDS-page.

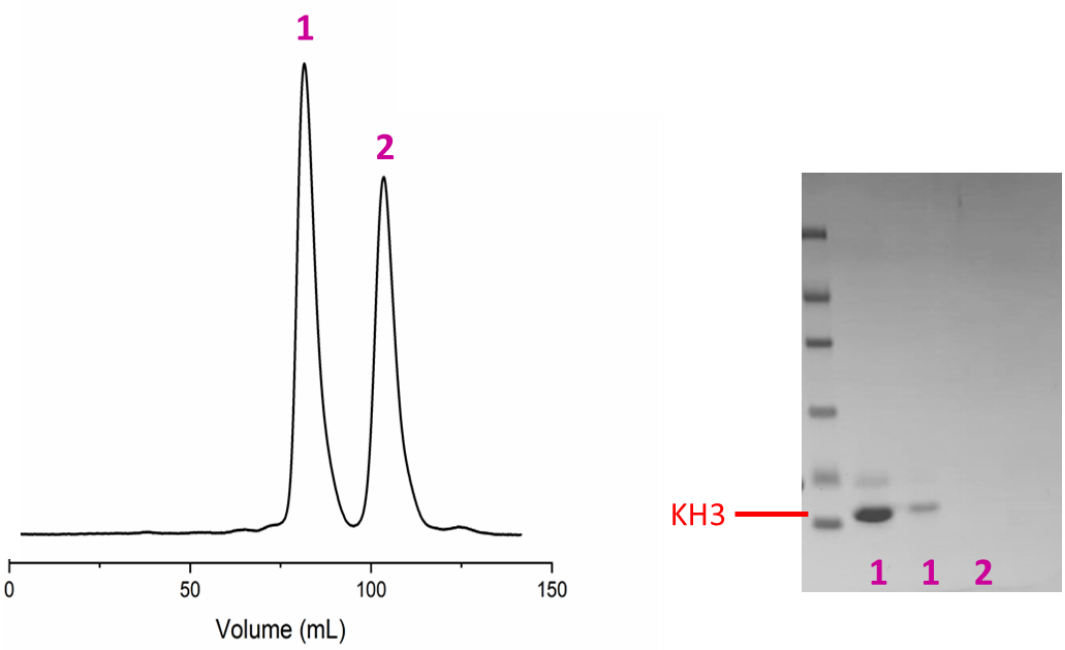

Fig. 5 - Gelfiltration and SDS page of KH3 after the treatment with ammonium sulfate

3.5.4. Analysis of the putative interaction between KH3 and BOLA2 proteins

Co-precipitation studies performed by Philpott's group showed that KH3 protein interacts with iron(II), GSH and BOLA2 protein, forming a complex. A K_d of 80 ± 10 μM was estimated by microscale thermophoresis of fluorescently labeled KH3. The stoichiometry of the KH3–BOLA2 complex was determined using size exclusion chromatography, and the result indicates the formation of a 1:1 BOLA2–KH3 heterodimer. Co-precipitation studies coupled to mutagenesis studies also suggested that BOLA2 is involved in KH3-Fe(II) binding using its H68 and C31 residues.

In order to obtain structural confirmations of the *in vitro* findings, ^{15}N BOLA2 was produced using a protocol previously developed by Prof. Banci's group[8], and NMR chemical shift perturbation experiments were performed by titrating ^{15}N-labelled BOLA2 with unlabelled KH3.

3.5.5. Analysis of the interaction between ^{15}N-labeled BOLA2 and Fe(II) ion

In the previous study no evidence were obtained about the interaction of BOLA2 with Fe(II) in the absence of KH3 protein. In order to clarify this aspect, we recorded NMR spectra in the absence of KH3. Samples were prepared, that is. A ^{15}N-BOLA2-Fe(II) mixture was prepared aerobically, using the same experimental conditions reported in Philpott's paper[35] for the *in vitro* reconstitution of the BOLA2- Fe(II)-KH3- complex. 50 µM ^{15}N-labeled BOLA2 and 100 µM $(NH_4)_2Fe(SO_4)_2$ were mixed in 100mM Tris buffer, 40mM KCl, 1mM TCEP, 1mM GSH, pH 7.5. The mixture was incubated on ice for 20 minutes. ^{1}H-^{15}N HSQC spectra of ^{15}N-labeled BOLA2 and of the ^{15}N-labeled BOLA2-$(NH_4)_2Fe(SO_4)_2$ mixture. A superimposition of the two spectra is reported in Figure 5. If a protein binds paramagnetic Fe(II) ion, line broadening effects on the NMR signals of the residues that are close in space to the bound metal center are expected. Since no significant changes were observed in the HSQC spectrum of ^{15}N-BOLA2 upon mixing with Fe(II), our data indicate that ^{15}N-BOLA2 does not bind the metal ion in the absence of KH3 and they confirm the Philpott's data (Fig. 6).

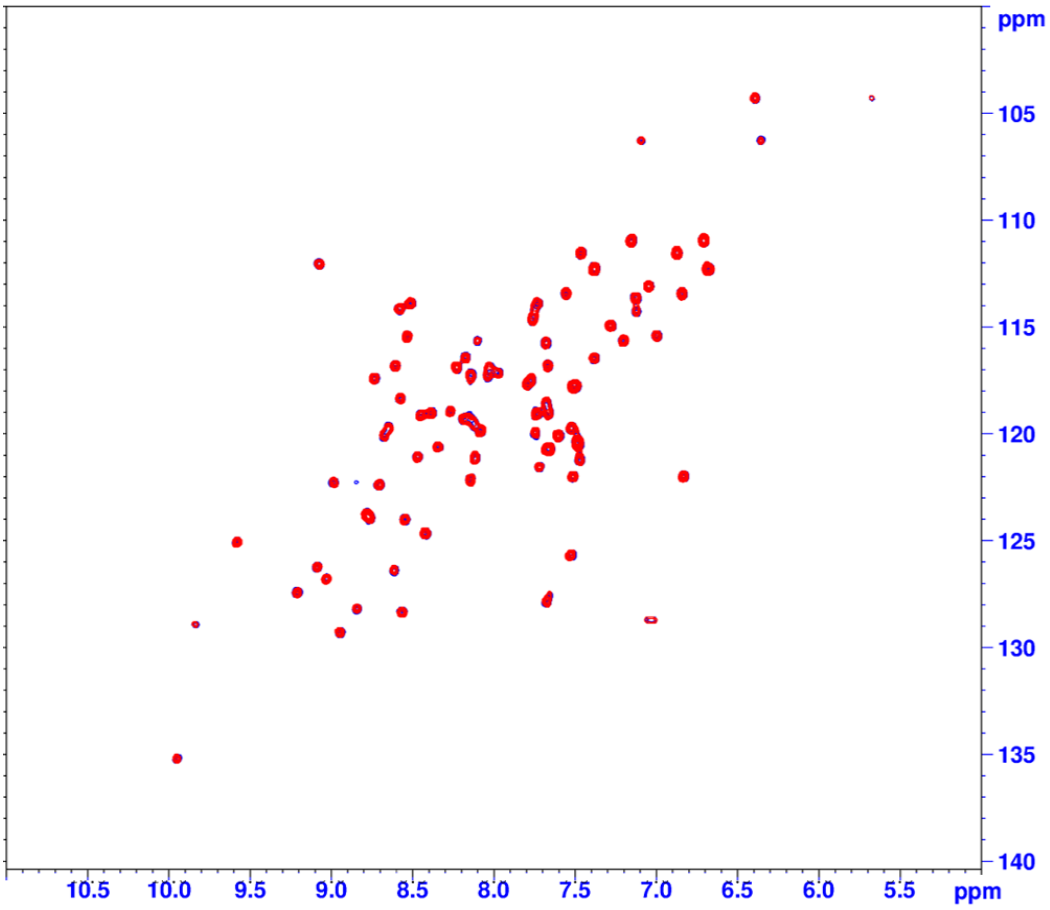

Fig. 6 - Superimposition of the ^{1}H-^{15}N HSQC spectra of 50 µM ^{15}N-labelled BOLA2 acquired in the absence (blue contours) and in the presence of 100 µM $(NH_4)_2Fe(SO_4)_2$ (red contours). Spectra were acquired at 900 MHz, at 298 K.

3.5.6. Analysis of the putative interaction between ^{15}N-labeled BOLA2, unlabeled KH3 and Fe(II) ion

The interaction between KH3 and BOLA2, in the presence of Fe(II) and GSH were initially monitored by size exclusion chromatography and SDS-PAGE. 50 µM ^{15}N-BOLA2 was incubated with 50 µM KH3 and 100 µM $(NH_4)_2Fe(SO_4)_2$ in 100mM Tris, 40mM KCl, 1mM TCEP, 1mM GSH, pH 7.5 buffer, for 20 minutes in ice in order to promote the formation of the complex, as reported previously[7]. The mixture was eluted with four peaks (Fig. 7), that where collected and analyzed by SDS-PAGE. Only the peak eluting at ~ 17.8 ml (light blue in the graph) showed the presence of both BOLA2 and KH3 proteins (Fig. 7B), indicating that the reaction for the formation of the complex was not complete. The fraction containing both KH3 and BOLA2 proteins was then analyzed by NMR spectroscopy. Line broadening effects were observed for residues V21 and C33 (Fig. 8). These data do not correspond to what previously reported by Philpott's group, i.e. that the amino acids involved in the interaction of BOLA2 with KH3 were H68 and C31.

.

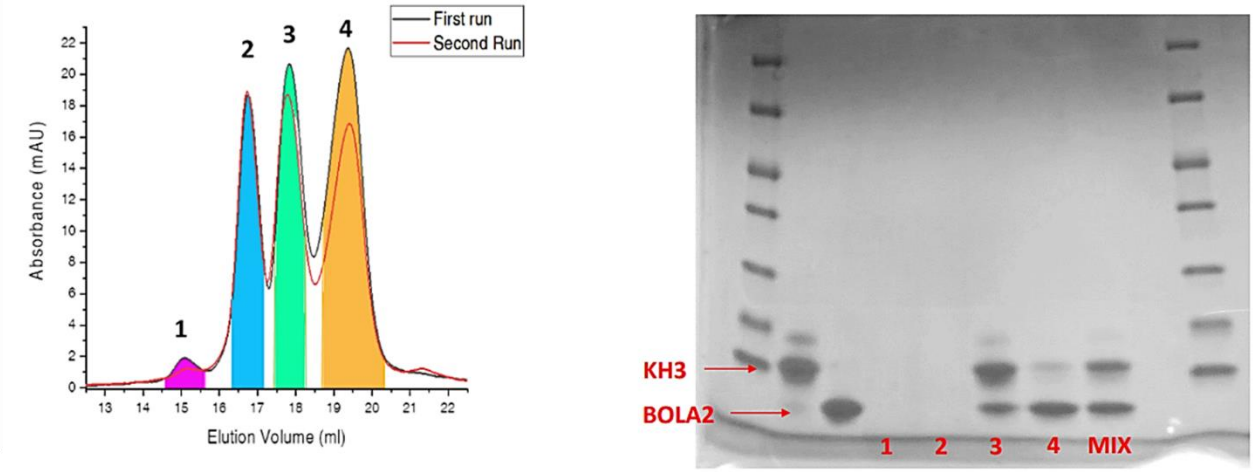

Fig. 7 – Left: Gelfiltration graph of the mixture between ^{15}N-BOLA2, KH3, iron (II) and GSH; right: SDS page of the fractions recovered from the SEC.

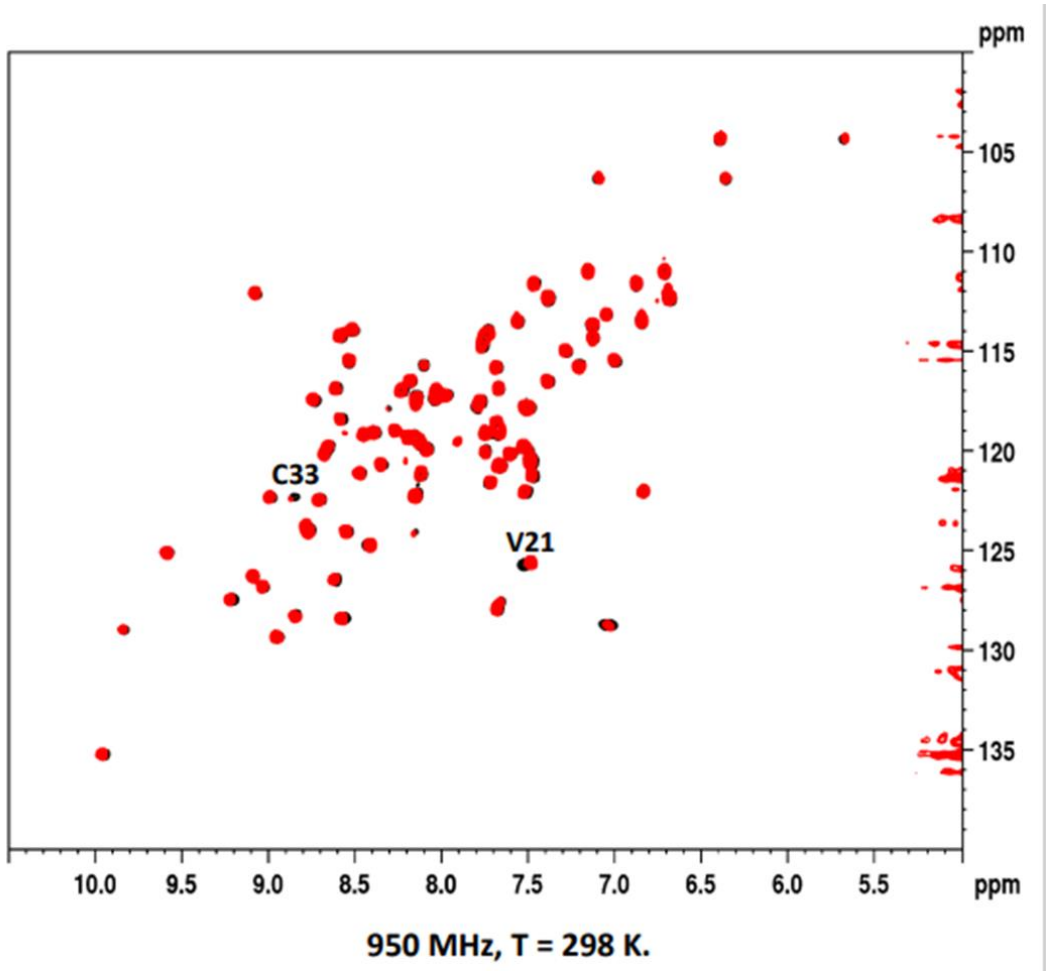

Fig. 8 - Superimposition of the ^{15}N HSQC spectra of 50 µM ^{15}N-labelled BOLA2 (black contours) and of fraction 3, isolated through SEC performed on the ^{15}N-BOLA2/KH3/Fe(II)/GSH mixture (red contours)

In order to understand if the proteins formed the complex, 50 µM ^{15}N-labeled BOLA2 was mixed with 50 µM unlabeled KH3 and 100 µM $(NH_4)_2Fe(SO_4)_2$ using the experimental conditions reported in Philpott's paper, and the mixture was analyzed by NMR. The ^{1}H-^{15}N HSQC spectrum of the mixture was acquired and compared with those obtained for ^{15}N-labeled BOLA2 in the absence and in the presence of $(NH_4)_2Fe(SO_4)_2$ (Fig. 9). Line broadening effects were observed for residues V21, R30, C33, K43, K47 and K73 (Fig. 10). Further addition of $(NH_4)_2Fe(SO_4)_2$, up to a 200 µM concentration, did not affect the HSQC spectrum of the mixture (Figure 11). These results confirmed the previous NMR data for C33 and V21 residues, and added other residues involved in the binding, which however do not correspond to the literature data.

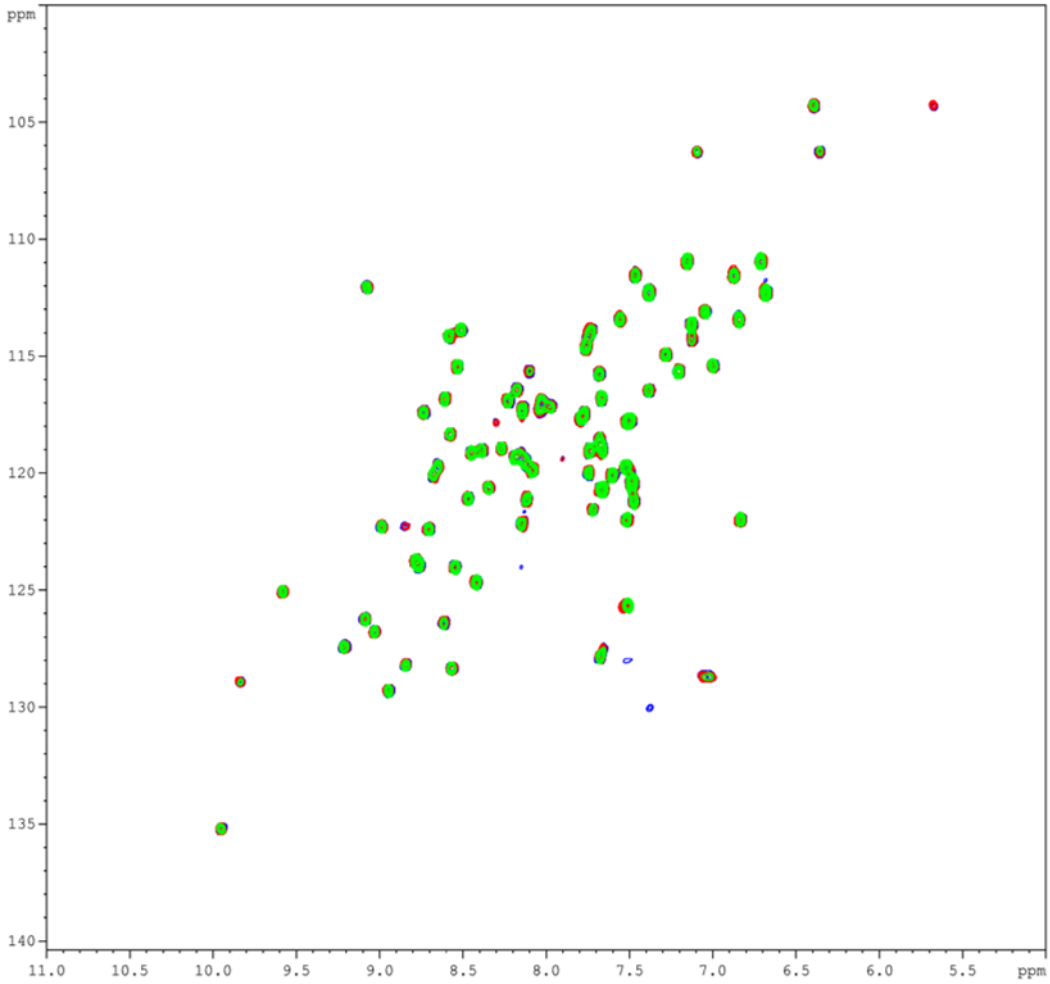

Fig. 9 - Superimposition of the ^{1}H-^{15}N HSQC spectra of 50 µM ^{15}N-labelled BOLA2 acquired in the absence (blue contours) and in the presence of: 100 µM $(NH_4)_2Fe(SO_4)_2$ (red contours) and 50 µM KH3 + 100 µM $(NH_4)_2Fe(SO_4)_2$ (green contours). Spectra were acquired at 900 MHz, at 298 K.

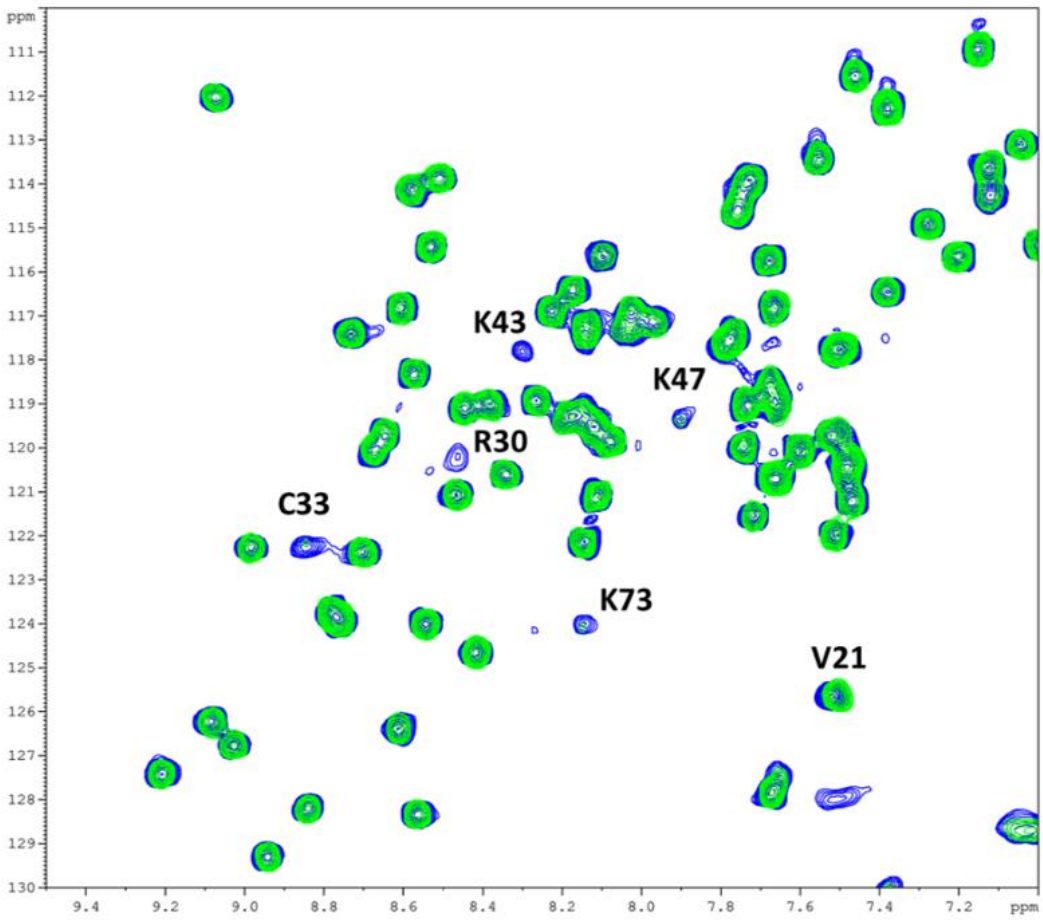

Fig. 10 - Zoom of the superimposition of the ^{1}H-^{15}N HSQC spectra of 50 µM ^{15}N-labelled BOLA2 acquired in the absence (blue contours) and in the presence of: 100 µM $(NH_4)_2Fe(SO_4)_2$ (red contours) and 50 µM KH3 + 100 µM $(NH_4)_2Fe(SO_4)_2$ (green contours). Spectra were acquired at 900 MHz, at 298 K.

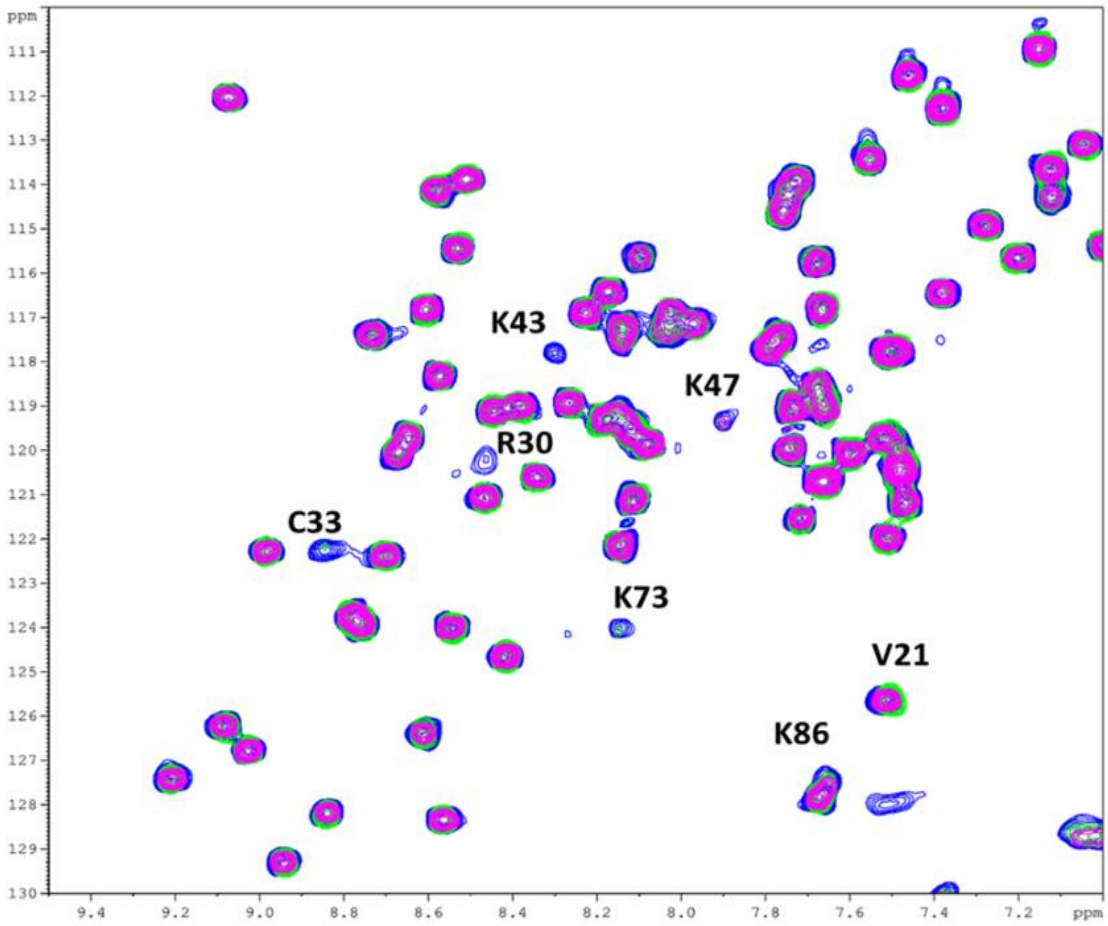

Fig. 11 - Superimposition of the ^{1}H-^{15}N HSQC spectra of 50 µM ^{15}N-labelled BOLA2 acquired in the absence (blue contours) and in the presence of: 50 µM unlabeled KH3 + 100 µM $(NH_4)_2Fe(SO_4)_2$ (green contours) and 50 µM unlabeled KH3 + 200 µM $(NH_4)_2Fe(SO_4)_2$ (violet contours). Spectra were acquired at 900 MHz, at 298 K.

3.5.7. Discussion of the preliminary results

The interaction between BOLA2 and KH3 in presence of Fe(II) and GSH was analyzed by NMR spectroscopy and size exclusion chromatography. Overall, the results showed a weak, aspecific interaction between the two proteins and the metal. Indeed, residues of BOLA2 affected by the presence of KH3 and $(NH_4)_2Fe(SO_4)_2$ do not identify a well-defined protein-protein recognition site on the structure of the apo protein (Fig. 12). On the contrary, they are distributed over the whole structure in a random way, including also some residues buried in the protein core. The changes observed in the HSQC spectra are likely due to an unspecific protein-protein recognition pattern, i.e. the two proteins are likely interacting, but with random relative orientations. Moreover, residues C31 and H68, that were reported in Philpott's paper as key residues for the interaction of BOLA2 with Fe(II) and KH3, are not affected. This indicates that they are not interacting with a Fe^{2+} ion. In conclusion, our data do not provide clear evidences for the formation of a BOLA2-Fe(II)-KH3 complex *in vitro*.

In the next steps of the study, different experimental conditions for the formation of the BOLA2-Fe(II)-KH3 complex will be tested, possibly mimicking more closely the cellular conditions in which the complex was observed by Philpott's group. Moreover, since the BOLA2 construct that we used in our NMR characterization was slightly different from that used by Philpott's group[7] (native vs Strep-II tagged protein, respectively), we will repeat the analysis using the same construct used in the paper, in order to assess whether local conformational changes due to the absence or to the presence of a StrepII-tag at the C-termini of BOLA2 might affect the interaction with KH3.

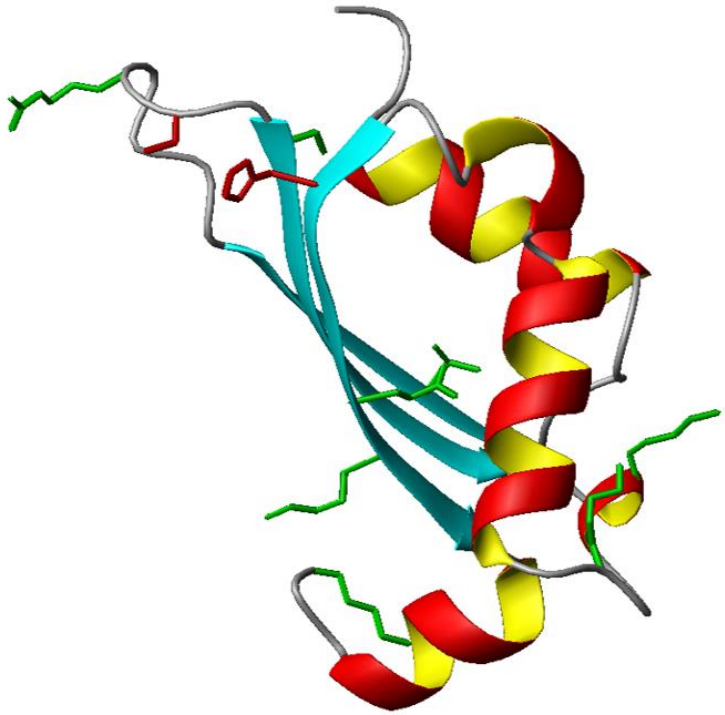

Fig. 12 - Mapping of the ^{15}N BOLA2 residues affected by the interaction with unlabeled KH3 and Fe(II) on the 3D model structure of apo BOLA2. The sidechains of V21, R30, C33, K43, K47 and K73 residues are mapped in green. The sidechains of C31 and H68 are in red.

CONCLUSION AND PERSPECTIVES

4. CONCLUSION AND PERSPECTIVES

The aim of my PhD project was to characterize iron-sulfur proteins and to perform cluster transfer experiments in order to obtain information about iron-sulfur cluster biogenesis in the cytosol. The results, obtained during my PhD, clarified structural aspects of cytosolic proteins and provided new models regarding the clusters maturation in the first step of CIA assembly machinery.

I focused my research activity on the anamorsin protein, a crucial member of the CIA machinery, and my studies clarified the type of Fe-S clusters bound to M1 and M2 motifs of anamorsin, ending the debate in the literature. I showed that *in cellulo* anamorsin binds two $[2Fe\text{-}2S]^{2+}$ clusters at both M1 and M2 motifs, and it is also consistent with the hypothesis that this holo form of anamorsin is the physiologically relevant species.

The studies also provided evidences for role of anamorsin as an electron donor in the GLRX3-dependent [4Fe-4S]-NUBP1 maturation process, giving for the first time evidence of the role of this human protein as an early constituent of the CIA machinery. I proposed that one molecule of $[2Fe\text{-}2S]_2$-$GLRX3_2$-GS_4 and two molecules of [2Fe-2S] anamorsin form a stable complex, that acts as a component of the CIA machinery at its early stage, by transferring two GLRX3-bound [2Fe-2S] clusters to NUBP1. The study clarified the function of the cluster bound to M1 motif, showing that only that cluster is able to act as electron donor for the reductive coupling of the two $[2Fe\text{-}2S]^{2+}$ clusters donated by $[2Fe\text{-}2S]_2$-$GLRX3_2$-GS_4.

I also focused my PhD activities on the structural characterization of the NUBP1-NUBP2 complex, a scaffold protein involved in the early step of CIA machinery, which contains two Fe-S cluster binding sites, at N-terminal and C-terminal motifs. My PhD work overcame the problems related to NUBP2 production, obtaining a stable heterocomplex for the spectroscopic and analytical gel filtration studies. The characterization of the NUBP1-NUBP2 complex showed the binding of a [4Fe-4S] cluster to the N-terminal site of the heterocomplex, while the studies performed on wild-type NUBP1-NUBP2 and on a mutant lacking the N-terminal binding motif in NUBP1, suggested that the C-terminal motif might bind a labile cluster, that thus could not be characterized.

In order to study of the *de novo* assembly of [4Fe-4S] clusters in cytosol, I investigated the ability of GLRX3, another protein involved in the early step of CIA pathway, to assemble [4Fe−4S] cluster(s) on NUBP1-NUBP2 heterocomplex. The GLRX3 protein acts as [2Fe-2S] clusters chaperone for NUBP1-NUBP2 complex, with the formation of a [4Fe-4S] cluster thanks to the electrons donated by GSH. Spectroscopic characterization of the wild type heterocomplex and of a mutant

hereocomplex containing only the C-terminal cluster binding site, did not allow to observe the cluster bound to the C-terminal motif and bridging the two subunits of the dimer. Whether GLRX3 can transfer its clusters to the C-terminal motif of NUBP1-NUBP2 complex, and more in general, whether the C-terminal motif of NUBP1-NUBP2 heterocomplex can bind a [4Fe-4S] cluster, remain an open question and requires further investigation. A possible strategy to assess whether a C-terminal [4Fe-4S] cluster is bound or not to the heterocomplex after the interaction with GLRX3, could be the investigation of the maturation of the late CIA components by the NUBP1-NUBP2 heterocomplex.

I focused the last part of my research on the characterization of the pathway in which the iron was pooled in the cytosol, at the beginning of CIA machinery. *In vivo* and *in vitro* experiments indicate that PCBP1–Fe–GSH–BOLA2 serves as an intermediate complex required for the assembly of [2Fe–2S] clusters on BOLA2–GLRX3. The interaction between BOLA2 and KH3 in presence of Fe(II) and GSH was analyzed by NMR spectroscopy and size exclusion chromatography. The research activities do not provide clear evidences for the formation of a BOLA2-Fe(II)-KH3 complex *in vitro*. The perspectives of the study will test some different experimental conditions for the formation of the BOLA2-Fe(II)-KH3 complex, and change the BOLA2 construct that we used in our NMR characterization because it was slightly different from that used by Philpott's group.

BIBLIOGRAPHY

5. BIBLIOGRAPHY

1. Handbook on Metalloproteins Edited by Ivano Bertini (University of Florence), Astrid Sigel, and Helmut Sigel (University of Basel). Marcel Dekker: New York, Basel. 2001. xxx + 1182 pp (plus 16 color plates). $265.00. ISBN: 0-8247-0520-3. *J. Am. Chem. Soc.* **123**, 12748–12748 (2001).
2. Görgülü, G. & Dede, B. *CATALASE, CATECHOLASE AND PHENOXAZINONE SYNTHASE-LIKE ACTIVITIES OF HOMODINUCLEAR Co(II), Ni(II), Cu(II) and Zn(II) COMPLEXES INCLUDING OXIME GROUP*. *J. Chil. Chem. Soc* vol. 63 (2018).
3. P Gupta, S. Roles of metals in human health. *MOJ Bioorganic Org. Chem.* **2**, 221–224 (2018).
4. Zhang, C., Zhang, F., Zhou, P. & Zhang, C. Functional role of metalloproteins in genome stability. doi:10.1007/s11515-016-1392-4.
5. A Netz, D. J. *et al.* Eukaryotic DNA polymerases require an iron-sulfur cluster for the formation of active complexes. *Nat. Chem. Biol.* (2011) doi:10.1038/nCHeMBIO.721.
6. Beilschmidt, L. K. & Puccio, H. M. Mammalian Fe-S cluster biogenesis and its implication in disease. *Biochimie* **100**, 48–60 (2014).
7. Ciofi-baffoni, S. & Banci, L. Interaction networks in human Fe-S protein maturation. 1–30.
8. Rouault, T. A. *Iron-sulfur proteins hiding in plain sight*. www.nature.com/naturechemicalbiology (2015) doi:10.1038/nchembio.1843.
9. Maio, N. & Rouault, T. A. Iron-sulfur cluster biogenesis in mammalian cells: New insights into the molecular mechanisms of cluster delivery ☆. (2014) doi:10.1016/j.bbamcr.2014.09.009.
10. Lill, R. & Mühlenhoff, U. Iron-sulfur-protein biogenesis in eukaryotes. *Trends Biochem. Sci.* **30**, 133–141 (2005).
11. Li, Y. & Ni, X. Molecular Evolution and Functional Analysis of Rubredoxin-Like Proteins in Plants. (2019) doi:10.1155/2019/2932585.
12. Reesbeck, M. E. *et al.* Oxidized and reduced [2Fe-2S] clusters from an iron(I) synthon. *J Biol Inorg Chem* **20**, 875–883 (2015).
13. Mühlenhoff, U. & Lill, R. Biogenesis of iron–sulfur proteins in eukaryotes: a novel task of mitochondria that is inherited from bacteria. *Biochim. Biophys. Acta - Bioenerg.* **1459**, 370–382 (2000).
14. Tanaka, N. *et al.* Identification of IscU residues critical for de novo iron-sulfur cluster assembly. *Mol. Microbiol.* **112**, 1769–1783 (2019).
15. Olive, J. A. & Cowan, J. A. Role of the HSPA9/HSC20 chaperone pair in promoting directional human iron-sulfur cluster exchange involving monothiol glutaredoxin 5. *J. Inorg. Biochem.* **184**, 100–107 (2018).
16. Nasta, V. *et al.* A pathway for assembling [4Fe-4S] 2+ clusters in mitochondrial iron-sulfur protein biogenesis. doi:10.1111/febs.15140.

17. Sheftel, A. D. *et al.* The human mitochondrial ISCA1, ISCA2, and IBA57 proteins are required for [4Fe-4S] protein maturation. **23**, (2012).

18. Brancaccio, D. *et al.* Formation of [4Fe-4S] Clusters in the Mitochondrial Iron−Sulfur Cluster Assembly Machinery. *J. Am. Chem. Soc* **136**, 46 (2014).

19. Suraci, D., Saudino, G., Nasta, V., Ciofi-Baffoni, S. & Banci, L. ISCA1 Orchestrates ISCA2 and NFU1 in the Maturation of Human Mitochondrial [4Fe-4S] Proteins. *J. Mol. Biol.* **433**, 166924 (2021).

20. Kispal, G., Csere, P., Prohl, C. & Lill, R. The mitochondrial proteins Atm1p and Nfs1p are essential for biogenesis of cytosolic Fe/S proteins. *EMBO J.* **18**, 3981–3989 (1999).

21. Qi, W. *et al.* Glutathione Complexed Fe−S Centers. *J. Am. Chem. Soc* **134**, 39 (2012).

22. Kumar, C. *et al.* Glutathione revisited: A vital function in iron metabolism and ancillary role in thiol-redox control. *EMBO J.* **30**, 2044–2056 (2011).

23. Srinivasan, V., Pierik, A. J. & Lill, † Roland. *Crystal Structures of Nucleotide-Free and Glutathione-Bound Mitochondrial ABC Transporter Atm1*. http://science.sciencemag.org/.

24. Philpott, C. C. & Jadhav, S. The ins and outs of iron: Escorting iron through the mammalian cytosol. *Free Radic. Biol. Med.* **133**, 112–117 (2019).

25. Banci, L., Camponeschi, F., Ciofi-Baffoni, S. & Muzzioli, R. Elucidating the Molecular Function of Human BOLA2 in GRX3-Dependent Anamorsin Maturation Pathway. *J. Am. Chem. Soc.* **137**, 16133–16143 (2015).

26. Frey, A. G., Palenchar, D. J., Wildemann, J. D. & Philpott, C. C. A glutaredoxin-BolA complex serves as an iron-sulfur cluster chaperone for the cytosolic cluster assembly machinery. *J. Biol. Chem.* **291**, 22344–22356 (2016).

27. Stehling, O. *et al.* Human CIA2A-FAM96A and CIA2B-FAM96B integrate iron homeostasis and maturation of different subsets of cytosolic-nuclear iron-sulfur proteins. *Cell Metab.* **18**, 187–198 (2013).

28. Okuno, T., Yamabayashi, H. & Kogure, K. Comparison of intracellular localization of Nubp1 and Nubp2 using GFP fusion proteins. *Mol. Biol. Rep.* **37**, 1165–1168 (2010).

29. Hausmann, A. *et al. The eukaryotic P loop NTPase Nbp35: An essential component of the cytosolic and nuclear iron-sulfur protein assembly machinery*. www.pnas.orgcgidoi10.1073pnas.0406447102 (2005).

30. Netz, D. J. A., Pierik, A. J., Stümpfig, M., Mühlenhoff, U. & Lill, R. The Cfd1-Nbp35 complex acts as a scaffold for iron-sulfur protein assembly in the yeast cytosol. *Nat. Chem. Biol.* **3**, (2007).

31. A Netz, D. J. *et al.* Tah18 transfers electrons to Dre2 in cytosolic iron-sulfur protein biogenesis. *Nat. Chem. Biol.* **6**, (2010).

32. Haunhorst, P. *et al.* Crucial function of vertebrate glutaredoxin 3 (PICOT) in iron homeostasis and hemoglobin maturation. **24**, (2013).

33. Camponeschi, F. *et al.* GLRX3 Acts as a [2Fe−2S] Cluster Chaperone in the Cytosolic Iron−Sulfur Assembly Machinery Transferring [2Fe−2S] Clusters to NUBP1. *J. Am. Chem. Soc* **142**, 10794–10805 (2020).

34. Gajda, K. *et al.* N-terminal domains mediate [2Fe-2S] cluster transfer from glutaredoxin-3 to

anamorsin. *Nat. Chem. Biol.* (2015) doi:10.1038/nchembio.1892.

35. Patel, S. J. *et al.* A PCBP1–BolA2 chaperone complex delivers iron for cytosolic [2Fe–2S] cluster assembly. *Nat. Chem. Biol.* doi:10.1038/s41589-019-0330-6.

36. Balk, J., Pierik, A. J., Aguilar Netz, D. J., Mühlenhoff, U. & Lill, R. The hydrogenase-like Nar1p is essential for maturation of cytosolic and nuclear iron-sulphur proteins. *EMBO J.* **23**, 2105–2115 (2004).

37. Banci, L. *et al.* Human anamorsin binds [2Fe-2S] clusters with unique electronic properties. doi:10.1007/s00775-013-1033-1.

38. Camponeschi, F., Ciofi-Baffoni, S. & Banci, L. Anamorsin/Ndor1 Complex Reduces [2Fe-2S]-MitoNEET via a Transient Protein-Protein Interaction. *J. Am. Chem. Soc.* **139**, 9479–9482 (2017).

39. Leidgens, S. *et al.* Each member of the poly-r(C)-binding protein 1 (PCBP) family exhibits iron chaperone activity toward ferritin. *J. Biol. Chem.* **288**, 17791–17802 (2013).

40. Hacker, D. L., Polytechnique, E. & Lausanne, F. De. *2.29 - Recombinant Technology*. *Comprehensive Biotechnology* vol. 1 (Elsevier B.V., 2011).

41. Dell, A., Danovaro, R. & Marco Luna, G. DNA extraction procedure: a critical issue for bacterial diversity assessment in marine sediments. *Environ. Microbiol.* **8**, 308–320 (2006).

42. Reece-Hoyes, J. S. & Walhout, A. J. M. Gateway Recombinational Cloning. (2018) doi:10.1101/pdb.top094912.

43. Edwards, A. M. *et al.* Protein production: Feeding the crystallographers and NMR spectroscopists. *Nat. Struct. Biol.* **7**, 970–972 (2000).

44. Kremer, W. & Kalbitzer, H. R. Physiological Conditions and Practicality for Protein Nuclear Magnetic Resonance Spectroscopy: Experimental Methodologies and Theoretical Background. *Methods Enzymol.* **339**, 3–19 (2001).

45. Stevens, R. C. Stevens(2000)Struc.F.D. 8,R177. 177–185 (2000).

46. Stehling, O. *et al.* Human Nbp35 Is Essential for both Cytosolic Iron-Sulfur Protein Assembly and Iron Homeostasis. *Mol. Cell. Biol.* **28**, 5517–5528 (2008).

47. Vitale, G., Fabre, E. & Hurt, E. C. NBP35 encodes an essential and evolutionary conserved protein in Saccharomyces cerevisiae with homology to a superfamily of bacterial ATPases. *Gene* **178**, 97–106 (1996).

48. Netz, D. J. A. *et al.* A bridging [4Fe-4S] cluster and nucleotide binding are essential for function of the Cfd1-Nbp35 complex as a scaffold in iron-sulfur protein maturation. *J. Biol. Chem.* **287**, 12365–12378 (2012).

49. Camire, E. J., Grossman, J. D., Thole, G. J., Fleischman, N. M. & Perlstein, D. L. The yeast Nbp35-Cfd1 cytosolic iron-sulfur cluster scaffold is an ATPase. *J. Biol. Chem.* **290**, 23793–23802 (2015).

50. Designed Research; O, R. L. S. Function and crystal structure of the dimeric P-loop ATPase CFD1 coordinating an exposed [4Fe-4S] cluster for transfer to apoproteins. (2021) doi:10.1073/pnas.1807762115.

51. Qi, W. *et al.* Glutathione complexed Fe-S centers. *J. Am. Chem. Soc.* **134**, 10745–10748 (2012).

52. Lane, D. J. R. *et al.* Cellular iron uptake, trafficking and metabolism: Key molecules and mechanisms and their roles in disease. *Biochim. Biophys. Acta - Mol. Cell Res.* **1853**, 1130–1144 (2015).

53. Sidiqi, M. *et al.* Structure and RNA binding of the third KH domain of poly (C) -binding protein 1. **33**, 1213–1221 (2005).